Graduate School ETD Form 9
(Revised 12/07)

# PURDUE UNIVERSITY
## GRADUATE SCHOOL
## Thesis/Dissertation Acceptance

By Nina Mahootcheian Asl

Entitled
Design of Multilayer Electrolyte for Next Generation Lithium Batteries

For the degree of Master of Science in Mechanical Engineering

Is approved by the final examining committee:

Youngsik Kim
Chair

Hazim El-Mounayri

Likun Zhu

To the best of my knowledge and as understood by the student in the *Research Integrity and Copyright Disclaimer (Graduate School Form 20)*, this thesis/dissertation adheres to the provisions of Purdue University's "Policy on Integrity in Research" and the use of copyrighted material.

Approved by Major Professor(s): Youngsik Kim

Approved by: Jie Chen 03/01/2013
Head of the Graduate Program Date

# DESIGN OF MULTILAYER ELECTROLYTE FOR NEXT GENERATION LITHIUM BATTERIES

A Thesis
Submitted to the Faculty
of
Purdue University
by
Nina Mahootcheian Asl

In Partial Fulfillment of the
Requirements for the Degree
of
Master of Science in Mechanical Engineering

May 2013
Purdue University
Indianapolis, Indiana

# ACKNOWLEDGMENTS

I would like to express my greatest gratitude to my advisor, Dr. Youngsik Kim, for his supervision, guidance and financial assistance throughout my Master's degree. Dr. Kim shared with me his knowledge and research experience even in my hardest time, for which I am always thankful.

I would like to thank my thesis committee members Dr. Hazim El-Mounayri and Dr. Likun Zhu for their time and participating in my thesis defense. Their advice and comments have further enriched the quality of this thesis. In addition, I extend thanks to Ms. Valerie Lim Diemer for assisting me with formatting my thesis.

Finally, and most importantly, will be my thanks and gratitude to my lovely parents Nahid and Ahad, and also my beloved brother Hesam. I am really blessed to have a great family like them that have given me priceless advice, support, and encouragement throughout my entire life. I would also like stretch out my thanks to my friends whom inspired me in this journey.

TABLE OF CONTENTS

Page

# LIST OF TABLES

# LIST OF FIGURES

Figure Page

Figure Page

Figure Page

Figure Page

# ABSTRACT

Mahootcheian Asl, Nina. M.S.M.E., Purdue University, May 2013. Design of Multilayer Electrolyte for Next Generation Lithium Batteries. Major Professor: Youngsik Kim.

Rechargeable lithium ion batteries are widely used in portable consumer electronics such as cellphones, laptops, etc. These batteries are capable to provide high energy density with no memory effect and they have small self-discharge when they are not in use, which increases their potential for future electric vehicles. Investigators are attempting to improve the performance of these cells by focusing on the energy density, cost, safety, and durability. The energy density improves with high operation voltage and high capacity. Before any further development of high voltage materials, safe electrolytes with high ionic conductivity, wide electrochemical window, and high stability with both electrodes need to be developed.

In this thesis a new strategy was investigated to develop electrolytes that can contribute to the further development of battery technology. The first study is focused on preparing a hybrid electrolyte, the combination of inorganic solid and organic liquid, for lithium based rechargeable batteries to illustrate the effect of electrode/electrolyte interfacing on electrochemical performance. This system behaves as a self-safety device at higher temperatures and provides better performance in comparison with the solid electrolyte cell, and it is also competitive with the pure liquid electrolyte cell. Then a multilayer electrolyte cell (MEC) was designed and developed as a new tool for investigating electrode/electrolyte interfacial reactions in a battery system. The MEC consists of two liquid electrolytes (L.E.) separated by a solid electrolyte (S.E.) which

prevents electrolyte crossover while selectively transporting $Li^+$ ions. The MEC successfully reproduced the performance of $LiFePO_4$ comparable with that obtained from coin cells. In addition, the origin of capacity fading in $LiNi_{0.5}Mn_{1.5}O_4$full-cell (with graphite negative electrode) was studied using the MEC. The performance of $LiNi_{0.5}Mn_{1.5}O_4$ MEC full-cell was superior to that of coin full-cell by eliminating the Mn dissolution problem on graphite negative electrode as evidenced by transmission electron microscopy (TEM) analysis. The MEC can be a strong tool for identifying the electrochemical performances of future high voltage positive electrode materials and their electrode/electrolyte interfacial reactions. Finally, by employing the multilayer electrolyte concept, a new application will be introduced to recycle the lithium. This study demonstrates the feasibility of using water and the contents of waste Li-ion batteries for the electrodes in a Li-liquid battery system. Li metal was collected electrochemically from a waste Li-ion battery containing Li-ion source materials from the battery's anode, cathode, and electrolyte, thereby recycling the Li contained in the waste battery at the room temperature.

# 1. INTRODUCTION

## 1.1. Introduction

Fossil fuels have been used as the main energy resources for years without considering the consequences. Over the last decades, the demand for and consequences of using coal and natural gases kept growing. Although these resources can be supplied for several more centuries, conservation is critical. Moreover, global warming is caused by the air pollution from consuming fossil fuels. Rising costs is another major factor, due to decreasing resources as well as economic instability due to dependency on foreign oil suppliers. All these concerns point to the necessity of replacing combustion engines with the electrical engines. Therefore, the alternative energy resources like solar radiation, wind, and wave become more attractive for investigators [1].

Developing a portable device with the ability of storing electrical energy gained from renewable and eco-friendly energy sources becomes a challenging topic for numerous inventors. An electrochemical power source is a device which utilizes the chemical reactions to store the energy and is capable to convert chemical energy directly to electrical energy and vice versa. The batteries are capable of converting energies at high efficiency without producing gases. Rechargeable lithium ion batteries are improving as an advanced technology for energy storage due to their high energy density and low self-discharge rates compared to the other types of batteries [2].

At present, Li-ion batteries are being widely used in portable electronic devices such as cell phones, PDAs, laptop computers, artificial hearts, or hybrid electric vehicles to address global warming. Moreover, they have been intensively studied as power

supplies in devices requiring high energy and high power densities such as electric vehicles (EVs) and hybrid electric vehicles (HEVs). Li-ion rechargeable batteries have received attention for intense research due to their high efficiency, light weight, and rechargeable properties. Sony company manufactured the first commercialized Lithium-ion battery in the 1990s [3]. Higher energy density batteries are demanded for further development of electrical vehicles and other applications. The need for clean and efficient energy storage is massive; however, the present Li-ion battery technology is limited due to low capacity compared to its anode [4].

Increments of specific capacity will be achieved with the development of higher voltage and higher capacity materials. Prior to further development of higher voltage materials, operational electrolytes at high voltages are required to be produced. In this thesis, a new strategy was investigated to develop electrolytes that can contribute to the further development of battery technology.

The first chapter includes the literature review and brief introduction to batteries and is mostly focused on rechargeable lithium ion batteries and their operation principles. The components of these cells were described relatively. Furthermore, the attempts for developing new electrolytes, improving the existing electrolyte, and producing new hybrid concept electrolytes were studied.

The second chapter of this thesis is focused on preparing a hybrid electrolyte, the combination of 90 wt% inorganic solid and 10 wt% organic liquid, for lithium based rechargeable batteries to illustrate the affect of electrode/electrolyte interface on electrochemical performance. The inorganic solid electrolyte selected is $Li_{1.3}Ti_{1.7}Al_{0.3}(PO_4)_3$, and the Li-ion conducting organic liquid electrolyte selected is 1M $LiPF_6$ in EC:DEC. Because of the addition of Li-ion conducting liquid between the solid electrode and solid electrolyte, the hybrid electrolyte cell minimizes the ineffective solid-on-solid interfaces common in all-solid-state cells. It is also expected that using a liquid electrolyte at the point of contact between the solid electrolyte and the electrode will

adjust for the volume change of the electrode during Li insertion/extraction. As a result, the electrochemical performance of the hybrid electrolyte cell is superior to that of a solid electrolyte cell and is also competitive to that of a pure liquid electrolyte coin cell. Another advantage of the hybrid electrolyte cell observed in this work is that this system behaves as a self-safety device when sudden, higher temperatures are applied.

The next chapter is focused on preparation of a multilayer electrolyte cell in a newly designed and developed device. High voltage $LiNi_{0.5}Mn_{1.5}O_4$ is one of the promising cathode materials for next generation rechargeable batteries for electric vehicles. This material operates at voltage of 4.7V. Dissolution of Manganese in liquid electrolyte, penetration of mixture through the cell, and finally reduction of Manganese on the surface of graphite will cause the capacity of this material to fade during cycling when it used in a full cell with graphite as an anode. The Li-ion-conducting glass ceramic plate, $Li_{1+x+y}Ti_{2-x}Al_xP_{3-y}Si_yO_{12}$ is used as a barrier to separate the cathode side from the anode side to provide an environment with a higher stability for the electrodes. Existence of 1M $LiPF_6$ in EC:DEC liquid electrolyte in both side of the solid electrolyte dissolves interface problems. Also, the separation of electrodes in a multi-layer electrolyte cell allows for more choices over existing electrolyte and electrode materials which may be capable to store the energy more efficiently and operate at the higher energy densities. The use of the multilayer electrolyte strategy in this battery system made it possible to increase cycle life of $LiNi_{0.5}Mn_{1.5}O_4$ and provides benefits from advantageous properties of different electrolytes.

Finally, in Chapter Four the new concepts and designs developed in previous studies were applied to perform a new application in this field. This study demonstrates the feasibility of using water and the contents of waste Li-ion batteries for the electrodes in a Li-liquid battery system. Li metal was collected electrochemically from a waste Li-ion battery containing Li-ion source materials from the battery's anode, cathode, and electrolyte, thereby recycling the Li contained in the waste battery at room temperature. The harvested Li metal in the battery system was discharged to produce electricity by

using water as the cathode. The discharge voltage of the water showed 2.7 V at 0.1 $mA/cm^2$ versus Li metal harvested from waste Li-ion batteries, compared to 2.8 V versus fresh Li metal at the same current rate. Since the electrodes for this proposed battery system are water and the contents of waste Li-ion batteries, the cost of the battery decreases, which is an attractive strategy for a large size energy storage application.

## 1.2. Electrochemical Principles of Cells

In general, chemical reaction in each cell is held in both electrode sides. If a load is applied to a cell by an external circuit connected to it during discharge, electrons will flow from the negative side to the positive side of the cell. This electrical circuit will be completed with the flow of anions or negative ions from the cathode and flow of cations or positive ions from the anode in the electrolyte medium. Reduction takes place in the cathode or positive side of the cell which is represented by the following equation in forward direction:

$$C + ne^- \rightleftharpoons C^{n-}$$

In this equation, n is the number of electrons which material C in the cathode will receive through an external circuit to be oxidized. At the other side, oxidation takes place in the anode or negative side of the battery cell, which is represented by the following equation in forward direction:

$$A \rightleftharpoons A^{n+} + ne^-$$

In this equation, n represents the number of electrons which material A in the anode will pass through the external circuit to be reduced. The overall chemical reaction in a cell can be written as the submission of these two half reaction equations:

$$A + C \rightleftharpoons A^{n+} + C^{n-}$$

For rechargeable batteries during recharge process, electrons flow reversibly from the cathode to the anode, so the anode will be the positive electrode and the cathode will

be the negative electrode. Through the charging process, reduction occurs in the negative electrode and oxidation takes place in the positive electrode in the cell, so these equations will be held in the backward direction. The operation of a cell during charging and discharging is shown schematically in Figure 1.1.

During the oxidation and reduction reactions, a battery converts the chemical energy held in its active material into electrical energy. The voltage of a galvanic cell in which reactants and products are in their standard states is determined by the Gibbs free energy of the chemical reaction that occurs inside the cell. The standard potential of a cell can be expressed with the change in a free energy of the system due to the reactions:

$$E° = -\frac{\Delta G°}{nF}$$

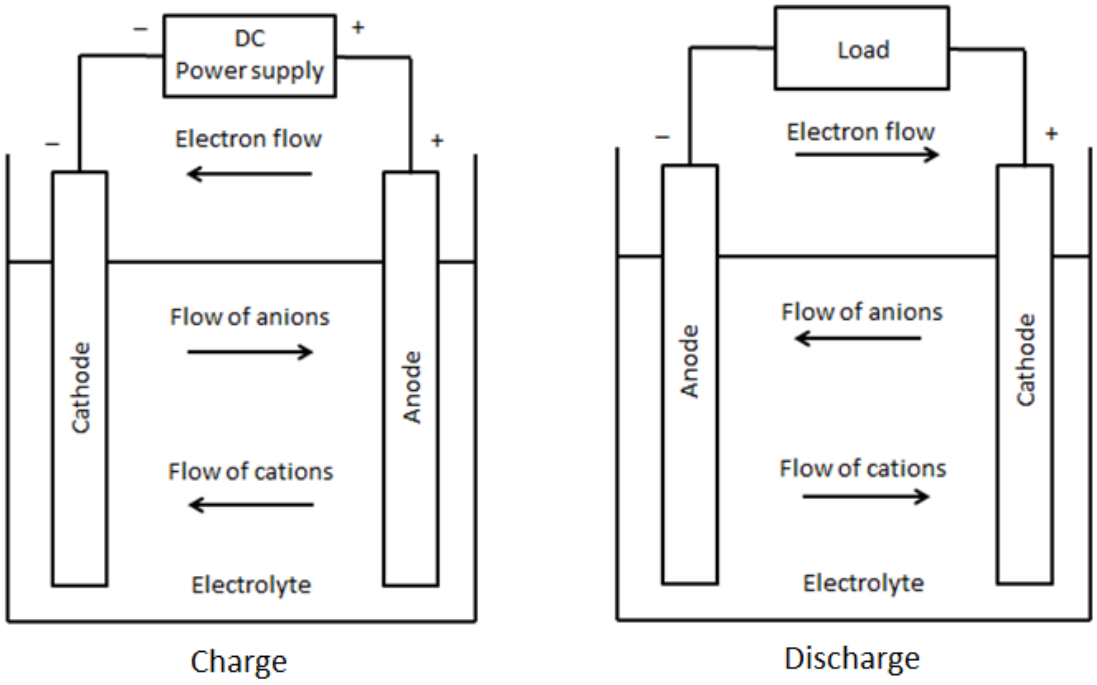


Figure 1.1 Electrochemical operation of a cell during charging and discharging [5]

where $\Delta G°$ is the standard Gibbs energy of the reaction, n is number of electrons involved in the reaction, F is a constant Faraday number ($\approx 96500C\ or\ 26.8Ah$), and $E°$ is the standard potential of the cell.

Under non-standard concentrations, temperatures, or pressure conditions, the voltage of the cell with following overall reaction:

$$aA + bB \rightarrow cC + dD$$

is determined by the following equation known as Nernst equation:

$$E = E° - \frac{RT}{nF} \ln \frac{C^c D^d}{A^a B^b}$$

where R is the gas constant, T is the absolute temperature, and A, B, C, and D are the activity of the reactants and products involved in the cell reaction.

A desired cell can convert all the stored chemical energy into electrical energy during discharge. This electrical energy, which is delivered by chemical energy stored in electrodes, depends on the change in Gibbs free energy $\Delta G$ of the electrochemical pairs. However, there is no device with one hundred percent efficiency. When a load current I is applied through the electrodes, the voltage of the cell will be different due to the polarization losses and internal impedance in the cell associated with the electrochemical reactions. The polarization losses include activation polarization and concentration polarization. The activation polarization is caused by overcoming the energy barrier of the slowest step, which determines the rate of the reaction, and to proceed it requires activation energy which is followed by a shift in potential of the cell. The concentration polarization is caused by the concentration difference of the species at the electrode surface and in the bulk due to the mass transfer. As the reactants and products were consumed by the reaction, higher variation in the voltage will be required to preserve the same load current.

The other significant loss which affects the performance and operation potential is internal impedance of the cell which is usually referred as Ohmic polarization. The Ohmic polarization is due to the ionic conductivity of the electrolyte, electronic resistance of the active materials and current collector, and the contact resistance of electrodes and current collectors. To maintain Ohm's law, which is the linear relationship between potential and current, the potential of the cell will drop to preserve the load current. The operation voltage of a cell connected to an external load R can be expressed as:

$$E = E_{\circ} - [(\eta_{ct})_a + (\eta_c)_a] - [(\eta_{ct})_c + (\eta_c)_c] - iR_i = iR$$

where $E_{\circ}$ is the open circuit of the cell, $(\eta_{ct})_a, (\eta_{ct})_c$ are activation polarization at anode and cathode, respectively, $(\eta_c)_a, (\eta_c)_c$ are concentration polarization at anode and cathode respectively, $i$ is the operating current of cell on load, and $R_i$ is the internal resistance of the cell. If a cell operates at a very low current, the cell voltage will be close to the open circuit voltage. Figure 1.2 shows the activation, concentration, and Ohmic polarizations of a cell as a function of operating current.

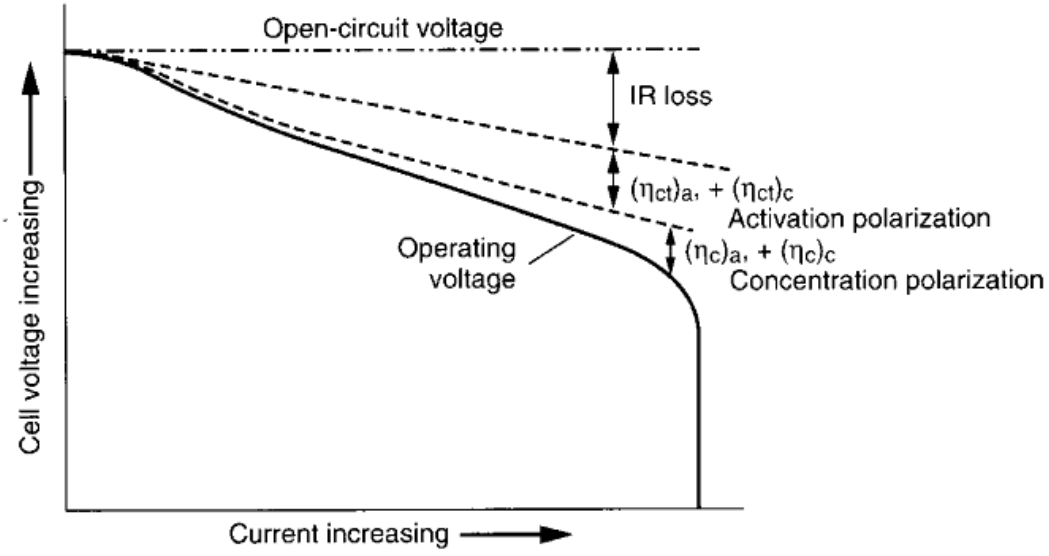


Figure 1.2 Voltage variations as a function of operating current due to the cell polarization [5]

## 1.3. Classification of Cells

Batteries are divided into two major categories of primary and secondary batteries. These two main subdivisions are distinguished with capability of being electrically recharged, which is specified for secondary or rechargeable batteries. Primary batteries cannot electrically recharge and they need to be discarded after discharging. The other classifications of the batteries are related to the structural and design identifications. In the following sections, examples of each one will be provided.

### 1.3.1. Primary Batteries

Primary batteries have studied for more than hundreds of years. The zinc-carbon primary battery was the only commercialized cell in 1940; this battery provided the capacity of 50Wh/kg at its early ages, and nowadays the capacity of 500Wh/kg is achieved in lithium primary cells. Various numbers of electrodes can be used for these systems, but only few of them become practical [5]. Table 1.1 shows characteristics and comparison of few major primary batteries.

Table 1.1 Characteristics of major Primary batteries [5]

| System | **Zinc-carbon (Leclanche´)** | **Zn / Alk. /MnO2** | **Zn /HgO** | **Zinc / air** | **Li /MnO2** |
|---|---|---|---|---|---|
| Anode | Zn | Zn | Zn | Zn | Li |
| Cathode | MnO2 | MnO2 | HgO | O2 (air) | MnO2 |
| Electrolyte | NH4Cl and ZnCl2 (aq) | KOH (aq) | KOH or NaOH (aq) | KOH (aq) | Organic solvent, salt solution |
| Cell voltage (V) | 1.5 | 1.5 | 1.35 | - | 3 |
| Specific Energy (Wh/ kg) | 85 | 145 | 100 | - | 230 |
| Energy Density (Wh/L) | 165 | 400 | 470 | - | 533 |

### 1.3.2. Secondary Batteries

Rechargeable batteries have the capability of continuous converting of chemical energy into electrical energy and vice versa. These processes should be practically reversible with minimum physical change to maintain desirable cycle life and minimum chemical side reactions, which can cause corrosion in components of the cell, as well as low efficiency. The requirements for compatible rechargeable batteries are high specific energy, good cycle life, low resistance, and the batteries should be applicable over broad range of temperature [5]. Characteristics and comparison of a few selected rechargeable batteries are presented in Table 1.2.

Table 1.2 Characteristics of major rechargeable batteries [5]

| System | **Lithium Ion** | **Nickel Metal-Hydride** | **Lead Acid** | **Nickel-Cadmium** | **Zinc / air** |
|---|---|---|---|---|---|
| Anode | Carbon (Graphite) | Metal-Hydride | Lead Alloy | Cadmium | Zn |
| Cathode | $LiCoO_2$ | Nickel oxyhydroxide | Lead dioxide | Nickel oxyhydroxide | O2 (air) |
| Electrolyte | Organic solvent, salt solution | Aqueous KOH, polypropylene | Aqueous $H_2SO_4$, polyethylene | Aqueous KOH, polypropylene | Aqueous KOH |
| Nominal voltage (V) | 3.6 | - | 2 | - | - |
| Energy density (Wh/ L) | 260 | 220 | 70 | 60-100 | 200 |
| Power Density (W/L) | 400-500 | 475 | ~400 | 220-360 | 190 |
| Cycle Life | 500-1000 | 300-600 | 250-500 | 300-700 | ~200 |

Lead-acid batteries were the first type of practical secondary batteries developed and they are popular due to their low cost, availability, ease to manufacture, and long

cycle life, but these batteries have low energy density and low specific energy. They are widely used in the automotive industry. The performance degrades if they are stored inactively for a long time especially in high temperatures. SLI batteries contain antimonial lead grids can lose up to 3% of their capacity every day. To stabilize performance these batteries are dry-charged by removing the electrolyte from the cell; the cells need to be activated before use by filling the cell with the electrolyte [6].

Nickel-Cadmium (Ni-Cd) and Nickel-metal hybrid (Ni-MH) batteries represent alkaline rechargeable batteries. Ni-Cd batteries are used in durable industrial applications such as diesel engine starting, mining vehicles, aircraft batteries, and emergency power applications. These batteries are characterized by excellent cycle life, high rate of discharging, operation at constant voltage, and the ability to operate at low temperatures. Unfortunately, they are suffering from memory effect, cost, maintenance requirement, and the Cd used as the negative electrode is not environmentally friendly. To achieve higher power and energy densities, nickel foam or plastic bonded electrodes are employed. Replacement of Cd with the metal alloy in the Nickel-metal hydride increases the energy density and produces more eco-friendly power sources. During charge, the metal alloy absorbs the hydrogen and forms metal hydride; hydrogen is produced during the discharge, so the metal alloy is capable to undergo this reversible process. These types of batteries are being applied in the aerospace devices which require good cycle life with low depth of charge; however, they have higher cost, lower rate capability, and lower tolerance for overcharges in compare with Ni-Cd batteries [7].

Rechargeable lithium ion batteries were commercialized by Sony Company in 1991 with LiCoO2 as the cathode and graphite as the anode. This type of battery has been widely studied and used in portable electronic devices. They provide high energy density which attracts investigators attention due to their potential for being used in large applications like hybrid electric vehicles (HEV). Lithium ion batteries will be presented in detail in the following sections [5, 8].

## 1.4. Rechargeable Lithium Ion Batteries

### 1.4.1. Operation Principles

The commercial rechargeable Lithium ion batteries do not contain lithium metal; the cell contains a carbon-based material as the anode which is oxidized by losing the electrons through the circuit. The lithium transition metal oxide as a cathode is reduced by receiving the electron from the circuit. A liquid electrolyte as an ionic conductor constructs a proper environment for movement of Lithium ions through the cell. Figure 1.3 illustrates a schematic of a lithium ion battery during the charge and discharge processes. During the charging process, graphite will be the host for lithium ions which are traveling through the electrolyte from the cathode side; electrons will be passing across the external circuit at the same time to maintain neutrality in the anode. During the discharge process cathode material will be the host to accept the Lithium ions deriving from the anode [1, 9].

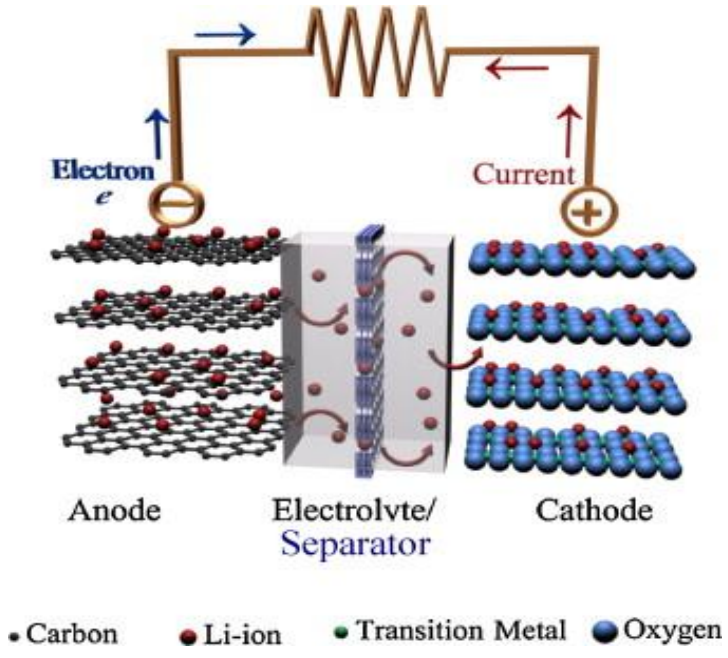


Figure 1.3 Schematic of a lithium ion battery during discharge process [5]

For further development of rechargeable lithium batteries, understanding and selecting the appropriate materials consistent in a system is quite challenging for researchers. Figure 1.4 shows an open circuit energy diagram for a thermodynamically stable non-aqueous electrolyte cell. The electrochemical window of the electrolyte $E_g$ is the band gap between the lowest unoccupied molecular orbital (LUMO), and the highest occupied molecular orbital (HOMO). The anode and cathode are electron conductors with electrochemical potentials of $\mu_A$ and $\mu_C$ respectively. The electrode potentials $\mu_A$ and $\mu_C$ are required to stay within the electrolyte electrochemical window. An anode with $\mu_A$ higher than LUMO level and a cathode with $\mu_C$ lower than HOMO level can decompose the electrolyte, unless a passivating solid electrolyte interface (SEI) layer preserve electron transfer from the anode to the LUMO or from the HOMO to the cathode. The open circuit voltage $V_{oc}$ of a battery cell is determined by the difference between the electrode electrochemical potentials:

$$V_{oc} = \frac{\mu_C - \mu_A}{e}$$

where e is representing the amount of electron charge [1].

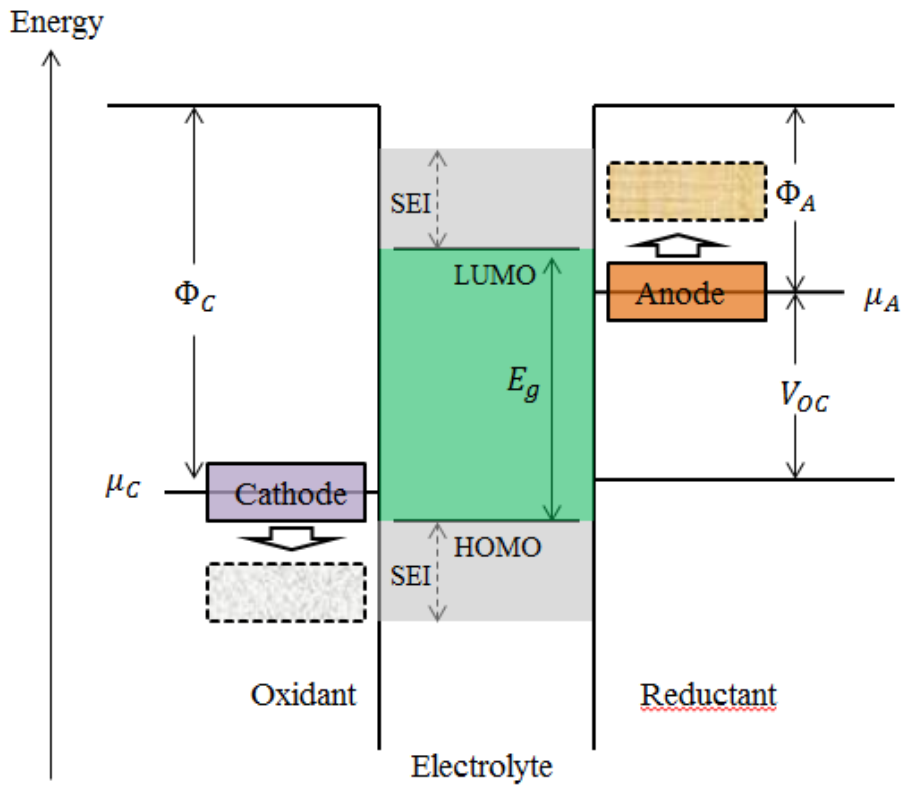


Figure 1.4 Open circuit energy diagram for a thermodynamically stable aqueous electrolyte cell [1]

The specific capacity $\Lambda$ of a rechargeable lithium ion battery is described as reversible charge transfer per unit weight (Ah/g) between the electrodes. Based on this value the energy density of the cell is defined as $\Lambda V_{oc}$. The specific capacity decreases as charge rate increases. The movement of lithium ions through the liquid electrolyte is proportional to electron transfer across the external circuit. During the charge/discharge process ions transfer across electrodes and the electrode/electrolyte interface, so ionic motion is smaller in comparison with electron transfer. Therefore, to maintain equilibrium in the charge distribution, the capacity will decrease as current density reduces. To retrieve the capacity loss, the charge rate needs to be decreased [1, 5].

High mobility of ions can be obtained through liquids or water. The electrochemical window of water is approximately 1.3eV which limits the open circuit voltage of the cell. To achieve higher energy density, requires using non-aqueous electrolytes with a larger electrochemical window. The LUMO and HOMO level of non-aqueous electrolytes should be obtained to design a cell where the electrodes potential lie within this gap. The lithium metal is a great nominated anode, but its electrochemical potential is located above the LUMO level. Formation of a passivating SEI layer can allow usage of lithium metal as an anode. During charge and discharge cycling, dendrites will be formed which can break the SEI layer inside the cell. Growth of dendrites through cycling will cause short circuiting in the cell which can be dangerous. Therefore, the potential of the anode and cathode must remain within the electrochemical window of the electrolyte, or broken passivating SEI layer due to the volume change through charge and discharge cycles must rapidly produce; moreover, the SEI layer should be capable of fast ionic conduction [1].

For more development of rechargeable lithium ion batteries researchers are challenged to find low cost, safe, and environmentally friendly materials for three major parts of a cell. A stable, high lithium ion conductive, non-aqueous electrolyte with a window capable of over 4V at applied temperature range of -40 to 60$°C$, and anodes and cathodes with a high reversible capacity comparable to the window of the electrolyte are required.

## 1.4.2. Components of the Lithium-ion Battery Cell

### 1.4.2.1. Electrodes

To design a battery system, electrodes need to be chemically stable with electrolyte; Proper selection of electrodes consist with electrochemical potential within LUMO or HOMO level of electrolyte is desired. The electrodes reported for rechargeable lithium ion batteries have the capability to host lithium ions, so they can intercalate reversibly. The first reported lithium ion battery was contained LiCoO2 and petroleum coke electrodes [10]. During the last 30 years of research, investigators were struggling to develop high energy density batteries. Figure 1.5 shows voltage and specific capacity of electrodes consist within electrochemical window of 1M $LiPF_6$ in EC/DEC organic liquid electrolyte [1]. In the following two sections, the most promising positive and negative electrodes will be reviewed.

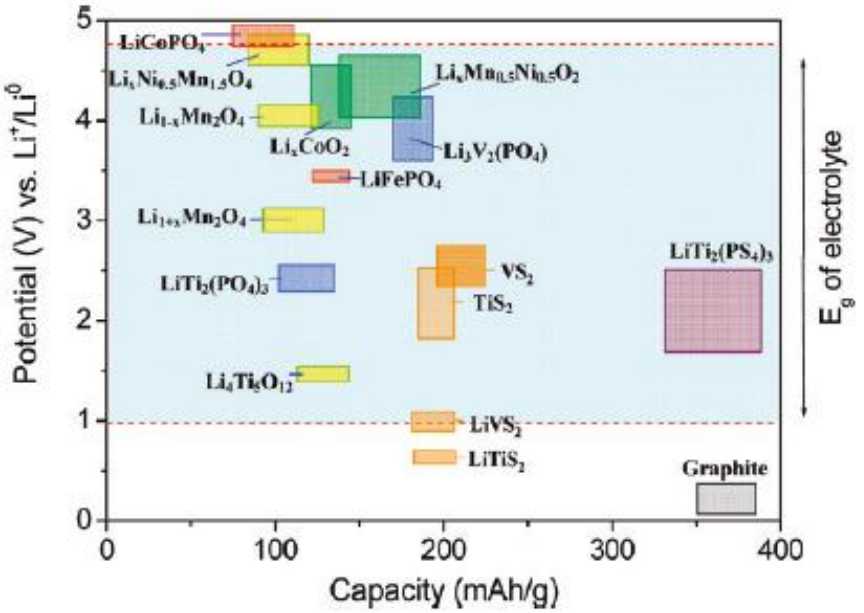


Figure 1.5 Voltage versus capacity of common electrode materials relative to electrochemical window of 1 M $LiPF_6$ in EC/DMC [1]

#### 1.4.2.1.1. Cathode

The most commonly used positive electrode in commercial rechargeable lithium ion batteries is LiCoO2. This nominated cathode material has flat operation voltage about 3.9V (all voltages presented in this paper are versus Lithium) with specific capacity approximately 140mAh/g which is half of the theoretical capacity; so, only half of the lithium ions can move reversibly. Also, it has high volumetric and gravimetric specific capacities. This material has layered structure which provides fast two dimensional diffusion of lithium ions as shown in Figure 1.6. For developing high energy density batteries, intensive research was done to develop materials with higher voltage and/or higher rechargeable capacities which can be compatible with $LiCoO_2$ [11]. Another layered structure cathode nominated material is $LiCo_{1/3}Ni_{1/3}Mn_{1/3}O_4$ with the capacity of 200mAh/g. The voltage of this material is lower than $LiCoO_2$; however, the high capacity can maintain energy density equal to or slightly higher than $LiCoO_2$ [12].

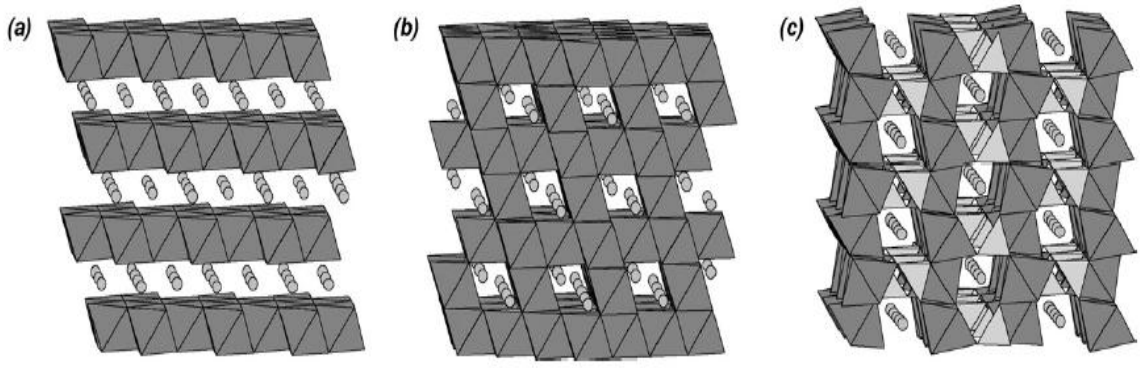


Figure 1.6 Schematic of crystal structures of (a) Layered structure ($LiCoO_2$), (b) Spinal structure ($LiMn_2O_4$), and (c) Olivine structure ($LiFePO_4$) [13]

Extensive studies were done on the spinal structure $LiMn_2O_4$ (Figure 1.6 (b)) due to the higher flat operation voltage of up to 4.1V. The theoretical capacity of this cathode material is 148mAh/g; however, it has a rechargeable capacity of 110mAh/g which gives lower energy density in comparison to $LiCoO_2$ [14]. In this regard, other Manganese-

based spinal structure materials with operation voltage of up to 5V were studied. The $LiNi_{0.5}Mn_{1.5}O_4$ with very flat operation voltage of 4.7V and practical capacity of 135mAh/g which offers higher energy density can be an alternative for advanced lithium ion battery systems [15].

The other nominated cathode material is $LiFePO_4$ with the olivine structure which is shown in Figure 1.6 (c). This material becomes more attractive due to the low cost and low toxicity of Fe in comparison with other materials used in lithium ion batteries as cathodes. A properly made $LiFePO_4$ has a rechargeable capacity of 160mAh/g with extremely flat operation voltage around 3.5V, which is slightly lower than layered oxide materials. This material is chemically stable and capable of being cycled over thousands of times without significant change in its capacity. Although $LiFePO_4$ has lower energy density due to lower operation voltage, they provide lower sensitivity in thermal variations and higher safety than batteries with $LiCoO_2$ cathodes. This material has low ionic and electronic conductivity at room temperature, so extensive studies were done to improve the conductivities. These studies involved decreasing the particle size and carbon coating. Nanosize particles coated with conductive carbon $LiFePO_4$ provides a capacity close to the theoretical one with better cycling performance [16-18]. Other high voltage cathode materials were introduced, but they are not applicable in lithium ion batteries due to instability with electrolyte and voltage over the LUMO layer of existing electrolytes. Figure 1.7 shows charge and discharge curves of a few selected cathode materials tested in non-aqueous liquid electrolytes [13].

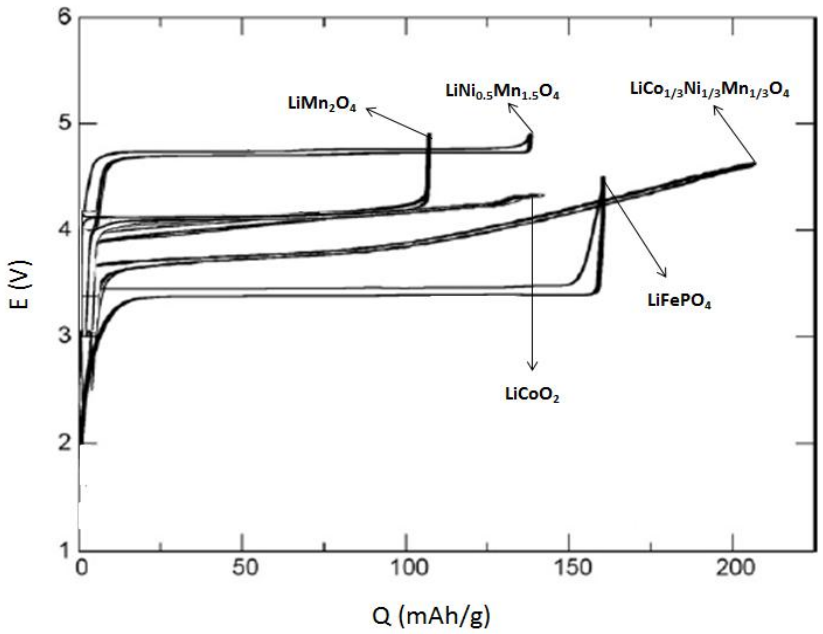


Figure 1.7 Charge and discharge graphs of $LiCoO_2$, $LiMn_2O_4$, $LiCo_{1/3}Ni_{1/3}Mn_{1/3}O_4$, $LiNi_{0.5}Mn_{1.5}O_4$, and $LiFePO_4$cathode materials tested in non-aqueous liquid electrolyte [13]

#### 1.4.2.1.2. Anode

The anode plays a significant role in lithium ion batteries, equal to other components of lithium ion batteries. As discussed in the previous section, to achieve an effective development for high energy density cells, employing electrode materials with high capacities is essential. For this reason, alkali metals can be good candidates as negative electrodes. The most promising anodes for currently used batteries are lithium based anodes. Lithium is the lightest metal and is the preferred material for anodes, with the most electropositive among other alkali metals. Higher voltage can be obtained with this metal, depending on the cathode material used in the system. Lithium has the high specific capacity of 3862mAh/g due to its low density. The systems consisting lithium metal are preferred for low weight and low volume portable devices. However, practical usage of lithium as an anode has been a challenge for researchers due to the safety issues. Formation of dendrites during the charge process breaks the separator and causes a short circuit; also, lithium metal can chemically react with the electrolytes, and they are

expensive and toxic. Hence, the hazard of using lithium and developing alternative anode materials becomes more interesting for researchers [19-21].

Carbonaceous materials with high lithium hosting reversibility, low electrochemical potential, high electronic conductivity, and high capacity are the best alternative candidates. Graphite, with the layered structure, allows intercalation of lithium within the layers. This material has low cost, high performance, and high specific capacity of 372mAh/g which makes it suitable to be used as an alternative anode material for advanced lithium ion batteries [22].

In comparison with lithium, graphite has low energy density, so attempts were continued to develop anode materials with lower voltage similar to lithium's and higher practical specific capacity. Silicon material is another alternative to replace the traditional graphite anodes. This material has the theoretical capacity of 4200mAh/g with operation voltage about 0.4V. Undesirably, Si has over 300% expansion and contraction for a full charge and discharge. Electrode cracking and loss of electronic inter particle contact are the consequences of this volume change which results in extremely poor cycle life. Fabricating the Si nanowires is one of the attempts for increasing the cell cycle performance, but it cannot be protected from interaction with electrolytes due to the formation of the SEI layer for this anode [23].

Another candidate for anode material is $Li_4Ti_5O_{12}$. This material provides flat operation voltage around 1.5V and theoretical specific capacity of 175mah/g. The advantage of this anode material is low variation of lattice parameter during lithium intercalation which is the reason it is called zero-strain material. Hence, it is suitable for long cycle life required application. However, usage of $Li_4Ti_5O_{12}$ as the anode material decreases the overall battery voltage, so lower energy density will be achieved with the same cathode material used in the system [24]. Table 1.3 contains theoretical specific capacity, theoretical charge density, volume change, and electrochemical potential of a few anode materials.

Table 1.3 comparison of selected anode materials [25]

| Materials | **Li** | **C** | **$Li_4Ti_5O_{12}$** | **Si** |
|---|---|---|---|---|
| Density ($g/cm^3$) | 0.53 | 2.25 | 3.5 | 2.33 |
| Lithiated phase | Li | $LiC_6$ | $Li_7Ti_5O_{12}$ | $Li_{4.4}Si$ |
| Theoretical specific capacity (mAh/g) | 3862 | 372 | 175 | 4200 |
| Theoretical charge density ($mAh/cm^3$) | 2047 | 837 | 613 | 9786 |
| Volume change (%) | 100 | 12 | 1 | 320 |
| Potential vs. Li (~V) | 0 | 0.05 | 1.6 | 0.4 |

### 1.4.2.2. Electrolyte

The electrolyte is the medium for the transfer of lithium ions which highly affects the performance of the cell. During charge and discharge cycling, the volume of electrode materials keeps changing, so the electrolyte is required to provide stable behavior for electrode/electrolyte interface, and the continuous ability to heal the broken passivating SEI layer. The ionic conductivity of the Li-ion needs to be higher than $10^{-4}$S/cm over the operation temperature of the cell, and electronic conductivity is desired to be smaller than $10^{-10}$S/cm. Lithium ion conductivity should be approximately equal to the total conductivity; total conductivity includes all the other ions' conductivity, electronic conductivity, and ionic conductivity. The electrolyte must be chemically stable with the anode and cathode, as well as low cost, nontoxic, and nonflammable due to the short circuiting. Offering a proportional electrolyte with a high electrochemical window and stability at the practical temperature, which meets all these factors, is the challenge for the investigators [1, 5].

Different types of electrolytes are being used based on the cell application. Table 1.4 is the collection of different types of electrolytes including an example of each one, the amount of ionic conductivity, and the electrochemical window.

Table 1.4 Non-aqueous Electrolytes for Li-Ion Batteries [1]

| Electrolytes | Example of electrolytes | Ionic conductivity ($\times 10^{-3}$ s/cm) at room temp | Electrochemical window (V) vs Li+/Li0 | | Property | Reference |
|---|---|---|---|---|---|---|
| | | | Reduction | Oxidation | | |
| Liquid organic | 1M $LiPF_6$ in EC:DEC (1:1) | 7 | 1.3 | 4.5 | Flammable | [26-28] |
| | 1M $LiPF_6$ in EC:DMC (1:1) | 10 | 1.3 | >5 | Flammable | [27, 28] |
| Ionic liquids | 1M LiTFSI in EMI-TFSI | 2 | 1 | 5.3 | Non-flammable | [2] |
| | 1M $LiBF_4$ in EMI-$BF_4$ | 8 | 0.9 | 5.3 | Non-flammable | [2, 8] |
| Inorganic liquid | $LiAlCl_4 + SO_2$ | 70 | - | 4.4 | Non-flammable | [6] |
| Inorganic solid | $Li_{3.25}Ge_{0.25}P_{0.75}S_4$ | 2.2 | <0.0 | >5 | Non-flammable | [20] |
| Polymer | LiTFSI-P(EO/MEEGE) | 0.1 | <0.0 | 4.7 | Flammable | [10] |
| | $LiClO_4$-$PEO_8$ + 10 wt % $TiO_2$ | 0.02 | <0.0 | 5 | Flammable | [19] |
| Liquid organic + Polymer | $LiClO_4$ + EC + PC + PVdF | 3 | | 5 | - | [21] |
| Ionic liquid + Polymer | 1M LiTFSI + $P_{13}$TFSI + PVdF-HFP | 0.18 | <0.0 | 5.8 | Less Flammable | [29] |
| onic liquid + Polymer + Liquid organic | 56 wt % LiTFSI-$Py_{24}$TFSI + 30 wt % PVdF-HFP + 14 wt % EC/PC | 0.81 | 1.5 | 4.2 | Less Flammable | [30] |
| Polymer + Inorganic solid | 2 vol % $LiClO_4$-TEC-19 + 98 vol% 95 ($0.6Li_2S + 0.4Li_2S$) + $5Li_4SiO_4$ | 0.03 | <0.0 | >4.5 | Non-flammable | [31] |
| Ionic liquid + Liquid organic | | - | - | - | Non-flammable | [7] |

#### 1.4.2.2.1. Liquid Electrolyte

Organic liquid electrolytes contain carbonate liquids in which lithium salts are soluble [27, 32], with an HOMO level at 4.7V [26, 33] and an LUMO level at 1.0V [28]. Another property of this type of electrolyte is the small activation energy of ion diffusion due to low viscosity. Common electrolytes are the mixture of two or fewer carbonates such as propylene carbonate (PC), ethylene carbonate (EC), diethyl carbonate (DEC), dimethyl carbonate (DMC), or ethylmethyl carbonate (EMC). Ethylene carbonate is capable to produce an SEI layer to prevent electrolyte decomposition; the electrolyte will be consumed to form an SEI layer which commonly causes nonreversible capacity loss [34, 35]. These types of solvents are very flammable, and favorable salt, $LiPF_6$, can decompose to LiF and $PF_6$ and produce toxic and hazardous material when it reacts with water. Researchers are continuously searching for good additives to increase the performance and safety [36].

No Room Temperature Ionic Liquids (RTILs) have been commercialized in the Lithium ion batteries yet, but recently they have been recommended as alternative liquid electrolytes over organic liquids. These types of electrolytes have an LUMO level at about 5.3V which offers the opportunity of using the cathodes with higher voltages. RTILs have better thermal stability when compared with Organic liquids; they are also nonflammable, lower vapor pressure, lower toxicity, and have higher boiling temperature. Lithium salts are highly soluble in ionic liquids, but these electrolytes have lower ionic conductivity due to their higher viscosity. Imidazolium cation constructed ionic liquids have the lowest viscosity and higher salt solubility among other Ionics at room temperature. Liquid Ionics decompose at voltages under 1.1V, so EC or VC additives increase their stability. By adding these additives the stability will increase by constructing a SEI layer for low voltage anodes [37, 38].

Inorganic liquid electrolytes are the other type of liquid electrolyte, for example, a nonflammable $LiAlCl_4$ and $SO_2$ electrolyte with high lithium conductivity about $7 \times$

$10^{-2}$ S/cm at room temperature. Unfortunately, inorganic liquids are not competitive with other liquids due to their low electrochemical window [6, 39].

#### 1.4.2.2.2. Solid Electrolyte

As mentioned previously, developing a safe, reliable, and durable electrolyte as an alternative substitution for currently used organic electrolytes in lithium ion batteries was investigated by researchers. Using a solid electrolyte, which is safer and can simplify the design of the cells, has been broadly studied by researchers; they can satisfy most of the electrolyte requirements with a wide electrochemical window. Ceramic and solid polymer electrolytes are the two most common types of solid electrolytes. Ceramics have higher elastic moduli, so they are more applicable for thin film devices which have a rigid design. Also, these types of solid electrolytes have higher conductivity at higher temperatures, and they are more stable in aggressive environments. In contrast, the low elastic moduli and light weight of polymers make them suitable for flexible designs; moreover, they can process easier which decreases the production costs. However, solid electrolytes or more general dry cells provide low ionic conductivity, especially at room temperature, which decreases the cell rate capability. Current studies in solid electrolytes are mostly focused in increasing the conductivity at room temperatures while efficient cycling is still improving. In this section, examples and a brief explanation of both electrolytes is provided [40].

Ceramic electrolytes are divided into three main subdivisions of sulfides, oxides, and phosphates. Movement of ions inside the ceramic electrolytes requires energy, so an increase in temperature causes an increase in ionic conductivity in this type of electrolyte. Therefore, they can be investigated for the applications at high temperatures. Their high mechanical strength can easily overcome the required energy for dendrite formation.

Glass or glass-ceramic $Li_2S$-$P_2S_5$ is an example of a sulfides ceramic electrolyte. In comparison with the amorphous phase, the crystalline phase has better ionic

conductivity and lower activation energy [41-43]. The $Li_{3.25}Ge_{0.25}P_{0.75}S_4$ lies in the thio-LISICON group and is another type of sulfide crystal reported in the literature [44, 45]. The perovskite (La,Li)TiO3 or LLTO is a promising lithium ion conducting oxide; changing concentration of La and Li in the structure improves the conductivity of this material [46-48]. Doping of LLTOs is the other approach to increase the conductivity and electrochemical window in oxide ceramics [49-51]. Finally, phosphates are the best nominated among the sulfides and oxides due to their higher conductivity. NASICON compounds are an example of this type of electrolyte. The $Li_{1+x}Al_xGe_{2-x}(PO_4)_3$ (LAGP) were observed to have the highest conductivities [52-54]. Like the others, proper amounts and concentration of additives and doping can increase the conductivity in them [55]. Extensive studies on LiPON with an ionic conductivity about $2 \times 10^{-6}$ S/cm illustrate that other properties of electrolytes beside conductivity play an important role. The LiPON is an amorphous ceramic with a high electrochemical window of 5.5V and with thermal stability about 300 ° C [56]. Ceramic electrolytes are brittle, so they can break due to the volume change resulting from lithium intercalations during cycling; moreover, studies show that poor performance of all solid state batteries is due to the solid electrolyte's inability to interface with the solid electrodes [57].

Solid polymer electrolytes are not only used as a separator between the electrodes, they can also preserve the interface between the electrodes and electrolyte during cycling caused by the electrodes' volume change. The advantages of this type of electrolyte over ceramic solid electrolytes are easily producible, flexible design, and dimensional stability; also, similar to ceramics, they are capable of preventing the formation of dendrite. The low ionic conductivity at room temperature is their main disadvantage.

In polymer electrolytes, lithium salts are solvent in the polymer chains; the crystallization structure of PEOs at room temperature decreases the ionic conductivity, so studies were done for increasing the amorphous structure to provide faster movement of ions. $LiPF_6$ or $LiAsF_6$ salts in polyethylene oxides (PEOs) are examples of solid polymer electrolytes with low cost, low toxicity, and high chemical stability. However, the ionic

conductivity of these materials is low at room temperature (approximately about $10^{-5}$ S/cm), so they are not applicable for high power systems. Substances with rapid non-conducting properties were added to block copolymer electrolytes to decouple mechanical properties and conductivity. For example, PS-block-PEO electrolytes were doped with LiTFSI salt which increased the ionic conductivity of electrolyte to $10^{-4}$ S/cm in the temperature of approximately 100°C. The mechanical properties improved dramatically, but ionic conductivity improved only slightly. Observations from stress analysis shows that wall boundaries have lower mobility due to the low concentration of ions. For fabricating PEOs applicable in rechargeable batteries, conductivity at room temperature needs to be improved [58, 59].

The ionic conductivities of $Li_2S$-$P_2S_5$ as the sulfide [43], (La,Li)TiO3 (LLTO) [48] and aluminum doped LLTO as the oxides [51], $Li_{3.25}Ge_{0.}25P_{0.75}S_4$ [44] and LAGP [53] as the phosphates inorganic ceramics, and LiTFSI salt in PEO as solid polymer electrolyte [55] at different temperatures in Fahrenheit and in Celsius are provided in Figure 1.8.

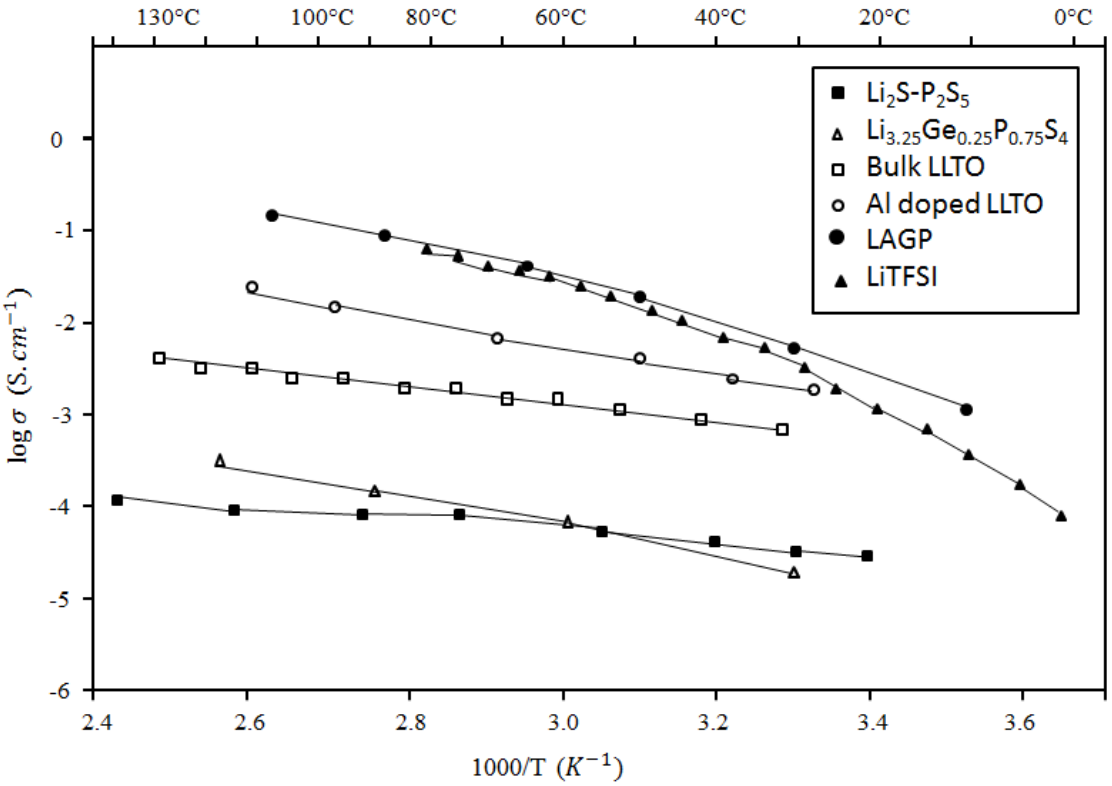


Figure 1.8 Ionic conductivity of solid electrolytes at different temperature [29]

1.4.2.2.3. Hybrid Electrolyte

In spite of all the advantages which solid electrolytes provide over liquid electrolytes, all solid state batteries were not considered for large scale production due to their instability to preserve the interface between the electrodes and electrolytes during cycling caused by electrodes' volume change. All these led to the point of investigation on the other type of electrolytes as hybrid electrolytes. Basically, a blend of two or more existing electrolytes was indicated as hybrid electrolytes. In this section, a few different types of these blends will be briefly reviewed.

A polymer-liquid electrolyte is another type of hybrid electrolyte system with the blend of organic liquid and polymer electrolytes, with or without ceramic particles. In

these types, mostly liquids provide conductivity and solids provide mechanical properties. Employing these electrolytes may omit the leakage of the cells and the need for separators. Poly vinylidene fluoride (PVdF) is an example of a polymer gel electrolyte; to decrease the crystallinity of the polymer, hexafluoropropylene (HFP) is added. In contrast with PEOs, the PVdF-HFP copolymers are chemically stable and they have the capability of dissolving organic liquids while preserving their specific properties; they have similar conductivity as organic liquids, but the safety is improved and they have flexible shape. To improve the conductivity in PVdF-HFP, the pore structure needs to be improve; to do this, ceramic particles like $BaTiO_3$ were added to the gel polymers [60-62].

An attempt to improve the ionic conductivity in amorphous polymer electrolytes typically causes loss in their mechanical integrity; softened electrolytes are not applicable in batteries maintained with lithium metal. To improve the mechanical properties of solid polymer electrolytes, two approaches are fabricating polymer ceramic composite and polymer ceramic hybrid electrolytes.

The polymer ceramic composite electrolytes (CPES) are the combination of ceramic nanoparticle additives like $Al_2O_3$, $TiO_2$, $SiO_2$, and S-$ZrO_2$ in polymer electrolytes in which improvement in ionic conductivity, electrochemical, and mechanical properties were observed; these additives can increase the salt solubility in PEOs by constraining chain crystallization which increases the amorphous polymer matrix. These composite particles provide an electrostatic surrounding which supports more in conduction between particles. Existence of these composite impurities in PEOs can cause undesirable side reactions with electrodes; however, they reduce formation of an SEI layer which stabilizes the interface, and they also reduce the dendrites formation in lithium metal base anodes. Although additives can improve the ionic conductivity, the conductivity is too small to be competitive with organic liquid electrolytes [63-67].

The polymer ceramic hybrid electrolytes are the blend of organic and inorganic ingredients with the goal of achieving proper chemical reactions, which make them soluble in each other without losing their specific properties. The most common type of these electrolytes, which are synthesized by the sol-gel method, are organic compositions cross linked with a molecular range of inorganic components. Self-assembly of triblock copolymer, poly (ethylene oxide), poly (propyleneoxide), and poly (ethylene oxide) (PEO–PPO–PEO), is an example of polymer ceramic hybrid electrolytes with conductivity in the range of $10^{-4}$ to $10^{-6}$ S/cm at the room temperature; however, the mechanical properties and strength of this electrolyte requires it to be characterized and compared with the pure polymer and composite polymer electrolytes [68]. Another example of an inorganic-organic hybrid electrolyte is the short chain polymer which is densely functionalized with nanosize ceramic particles. Change in the length of polymer, density, and particle size and ratio of inorganic substance can change the mechanical property of the electrolyte. The ionic conductivity of these electrolytes lies in the range of $10^{-3}$ to $10^{-6}$ S/cm at the room temperature. Polymer chains make nanosize particles capable of forming a homogeneous organic–inorganic phase among the film with Young's modulus above 0.1 GPa at room temperature. Also, in films doped with the 1 Mole solution of LiTFSI in TEGDME, the tensile moduli decreased approximately to 10 MPa with the conductivity of 2×10-5 S/cm at room temperature [69, 70].

The gel electrolyte blended with organic liquids has low thermal stability, low stability with cathodes, low vaporization temperature, flammability, and unsatisfactory module of elasticity to avoid formation of dendrites in the lithium metal anode; therefore, adding room temperature ionic liquids instead of organic liquids attracted the investigators to achieve higher performance of hybrid electrolyte systems. Ionic liquids are nonflammable and nonvolatile, which increases the safety of the batteries. N-n-butyl-N-ethylpyrrolidinium N,N-bis (trifluoromethane) sulfonimide ($Py_{24}TFSI$) is an example of ionic liquid dissolved in PVdF-HFP. Although the conductivity of these types of electrolytes is similar to the organic liquid polymer gels, they suffer from the other issues

like a low transference number. The movement of ions, other than the lithium ion, will not provide electrical power across the external circuit. Undesired movements of these ions carry charge in ionic liquids and decrease lithium ion movement. Mixing the ionic liquids with EC or ceramic particles can increase the transference number [30, 71-73].

Figure 1.9 shows the ionic conductivities at different temperatures of PEO with $SiO_2$ nanoparticle additive as polymer ceramic composite electrolytes [64], PVdF-HFP as gel electrolytes blended with the lithium salt LiPF6 [60], carbonate solvents (EC, PC) dimethyl carbonate (DMC), and ethyl methyl carbonate (EMC), BaTiO3 doped PVdF-HFP as doped polymer-liquid electrolyte [60], $Py_{24}$TFSI as gel electrolyte blended with ionic liquids, and $Py_{24}$TFSI-EC-PC as gel electrolyte blended with ionic and organic liquids [30].

Also, a proper ratio of organic liquids, which preserves the nonflammable property of electrolytes, can be added to ionic liquids to decrease the HOMO level for anode material can also be considered as another hybrid electrolyte systems [74].

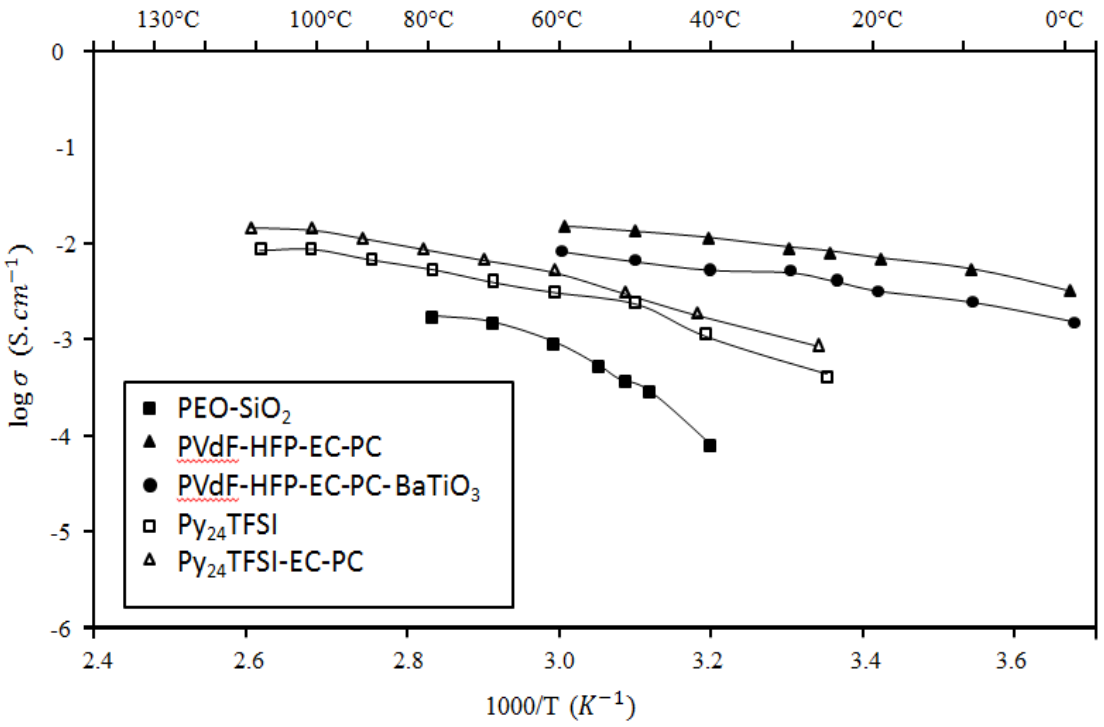


Figure 1.9 Ionic conductivity of polymer electrolytes at different temperature [29]

### 1.4.2.3. Separator

The separator protects the cell from internal short circuiting caused by direct contact of electrodes inside the cell and is capable of inactivating the cell in overcharge conditions. Polyethylene (PE) and Polypropylene (PP) are examples of microporous membrane separators which are commercially being used. These separators can be cycled hundreds of times without losing their properties. If a battery is overcharged, materials inside the cell start to exothermically react with each other which causes self-heating; the separators' shutdown mechanism prevents this thermal behavior in lithium ion batteries. At the temperature of the separator reaches to the shutdown point, the porous polyolefin separator switches to the nonporous insulator between the electrodes. The PE separators have a shutdown point at temperatures around 130 to 140°C. After the separator becomes

an insulator, the temperature inside the cell continues to increase. The desirable separators require maintaining their mechanical properties after the shutdown point to protect against safety hazards due to internal short circuiting. The meltdown point is the temperature at which the separator can preserve its mechanical property. PE and PP have meltdown temperatures close to their shutdown temperatures. The shutdown temperature of the PP separator is around 170°C [75, 76]. Investigators in this field are attempting to develop separators with meltdown temperatures higher than their shutdown temperature. One approach was the layered PP and PE separators, in which PE provides a lower shutdown temperature and PP provides a higher meltdown temperature [77].

# 2. INORGANIC SOLID/ORGANIC LIQUID HYBRID ELECTROLYTE

## 2.4. Introduction

Extensive research has been done to find ways to progress current Li-ion battery technology by addressing concerns with organic liquid electrolytes. Organic liquid electrolytes are problematic due to their flammable liquid characteristics, solvent leakage, and tight electrochemical window. In an effort to combat those issues, many Li-ion conducting materials such as polymer, polymer-gel, ionic-liquid, and inorganic solids have been investigated as alternative electrolytes for Li-ion batteries [1]. Within the category of inorganic solids, fast Li-ion conducting inorganic solid materials are considered to be superior candidates over liquid and polymer electrolytes due to their following advantages [78]: (1) high Li-ion conductivity over $10^{-4}$ S/cm, (2) a wide electrochemical window (0 – 7 V vs. $Li^+/Li^0$), and (3) good chemical stability with highly reducing and oxidizing electrodes.

These benefits have led to the development of many fast Li-ion conducting solid types such as sulfide glass, glass-ceramics, and oxy-sulfide glass [43, 79-81]. Due to the high polarizability of sulfur, Li-ion conductivity has been observed to be higher in sulfide compounds rather than oxide compounds. Many fast Li-ion conducting sulfide compounds such as $Li_{3.325}P_{0.935}S_4$ [82], $Li_{3.25}Ge_{0.25}P_{0.75}S_4$ [83], and LiI-$Li_2S$-$GeS_2$-$Ga_2S_3$ [84] glasses have been tested as electrolytes in a Li-ion battery. However, such compounds are generally very unstable in air which makes them more difficult to handle. On the other hand, there are a few oxide compounds that give a high Li-ion conductivity up to $10^{-3}$ S/cm which include the NASICON type: $Li_{1.3}Ti_{1.7}Al_{0.3}(PO_4)_3$ [85, 86], the

Garnet type: $Li_7La_3Zr_2O_{12}$ [87], and the LLTO type: $Li_{3x}La_{(2/3)-x()(1/3)-2x}TiO_3$ [78] as used in our research.

Using these fast Li-ion conducting inorganic solid materials as electrolytes has been intensively and extensively studied in the design of all-solid-state electrolyte cells that use solid materials for anode, cathode, and electrolyte [57, 88-93]. However, even with the highly ion-conductive solid electrolytes, it has been a struggle for a solid electrolyte battery to obtain a similar specific capacity, rate capability, and cycle life to those of a liquid electrolyte battery. A common problem noted with a solid electrolyte battery is the large capacity decay after the first charge (or discharge) of the cell and poor cycle life even at a very small current rate ($<0.07 mA/cm^2$) [57, 94]. Studies conclude that such complications arise from the solid electrolyte's inability to interface with the solid electrodes rather than from a failure of the solid electrolyte itself [57]. Proponents of the solid electrolyte battery attempted to apply a coating of ceramic onto the surface of electrode particles in an effort to minimize the electrode/electrolyte interface resistance [88, 95-98]. However, the electrochemical performance remained lower than that of the liquid electrolyte battery. This may be due to the fact that the coating materials are not flexible enough to match the volume change of the electrode materials during Li insertion/extraction, which occurs during cycling of the cell.

Therefore, the question has been raised as how to minimize the issues related to solid-on-solid interfaces while retaining the solid electrolyte cell attributes and making the electrochemical performance competitive with that of liquid electrolyte cells. As a result, this study focuses on preparing a solid/liquid hybrid electrolyte cell to illustrate the effect of interfacing on electrochemical performance. The hybrid electrolyte cell will minimize the ineffective solid-on-solid interface by addition of a Li-ion conducting liquid between the solid electrode and solid electrolyte.

The use of liquid at the point of contact between solid electrolyte and solid electrode is also expected to adjust to the volume change of the electrode during Li

insertion/extraction. Similar concept of a solid/liquid hybrid electrolyte was reported in literature [99], where hybrid solid glass electrolytes were fabricated by $LiPF_6$ liquid electrolyte infiltration into nano-porous oxide glass membrane. Since their Li-ion mobility was only provided by the liquid electrolyte located in the interconnected channels of the glass membrane, the interface resistance between the glass membrane and solid electrodes caused a poor electrochemical performance.

For relatively easy handling and synthesis, $Li_{1.3}Ti_{1.7}Al_{0.3}(PO_4)_3$ was selected as the solid electrolyte for this study. The Li-ion conducting liquid is 1M $LiPF_6$ in ethylene carbonate: diethyl carbonate (EC:DEC), which is commonly used as an organic liquid electrolyte. With the use of $Li_{1.3}Ti_{1.7}Al_{0.3}(PO_4)_3$ as the solid electrolyte and 1M $LiPF_6$ in EC:DEC as the liquid electrolyte, the stable electrochemical window of the hybrid electrolyte becomes only 2.5 – 4.5 eV vs. $Li^+/Li^0$ as shown in Figure 2.1. The organic liquid electrolyte is reduced above 1eV and oxidized below 4.5 eV vs. $Li^+/Li^0$, respectively. The solid electrolyte is reduced above 2.5 eV vs. $Li^+/Li^0$ by reducing $Ti^{4+}$ to $Ti^{3+}$ in the $Li_{1.3}Ti_{1.7}Al_{0.3}(PO_4)_3$.

To remove any other side effects, such as the decomposition of liquid and solid electrolyte, $LiMn_2O_4$ was chosen as the material composition for both positive and negative electrodes. Figure 2.1 shows that the Fermi energy of $Li_2Mn_2O_4$ and $Mn_2O_4$ are located in the stable window of both the liquid and solid electrolytes. Hence, the charged and discharged shape of this material will not overlap the electrochemical intersection of the solid and liquid electrolyte.

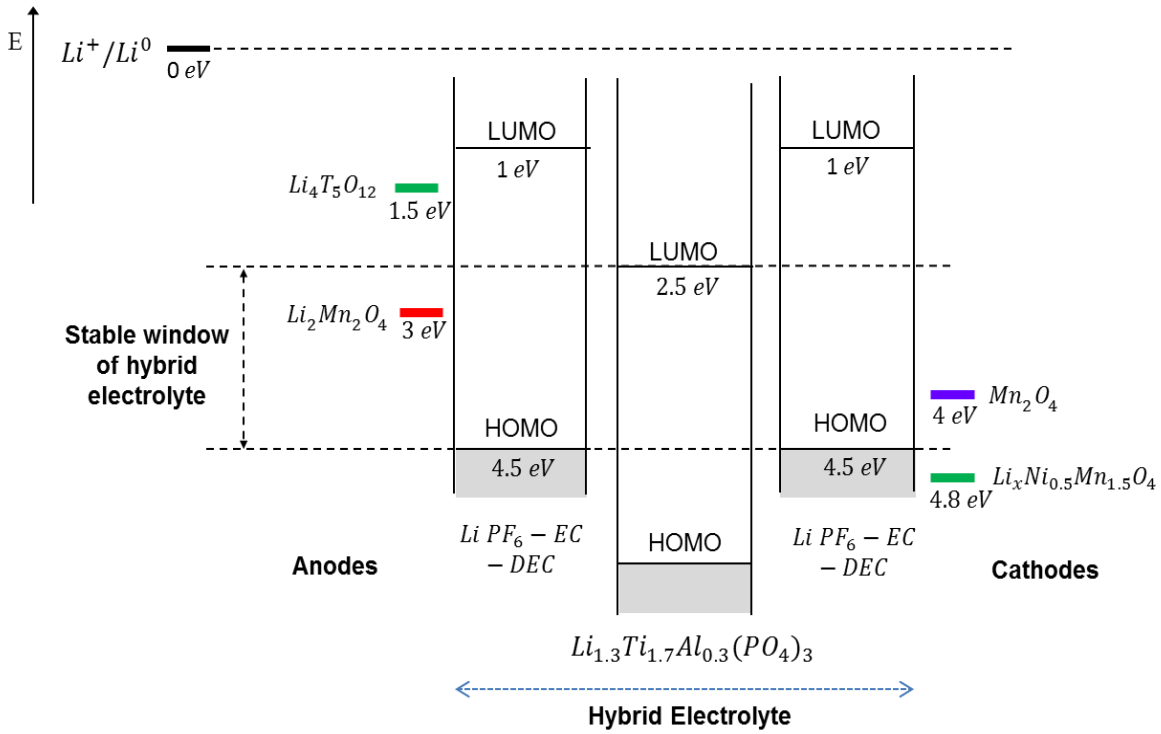


Figure 2.1 Schematic open-circuit energy diagram of the hybrid electrolyte. The stable electrochemical window of the hybrid electrolyte becomes 2.5 – 4.5 eV vs. $Li^+/Li^0$. The Fermi energy of $Li_2Mn_2O_4$ and $Mn_2O_4$ are located in the stable window of both the liquid and solid electrolytes.

## 2.5. Experimental Methods

### 2.5.1. Synthesis of Electrolytes and Electrodes

Preparation of the $Li_{1.3}Ti_{1.7}Al_{0.3}(PO_4)_3$ was modified based on the literature [100]. A stoichiometric mixture of $Li_2CO_3$, $Al_2O_3$, $TiO_2$ and $(NH_4)_2PO_4$ was ground and heated in a platinum crucible at 300°C for 2h and 900°C for 2h. The material was then reground into a fine powder using a ball mill for 5h using a wet process. The dried powder was reheated at 900°C for 2h and then ball milled again for 5h. Next, the powder was pressed into pellets. The pellets were heated at 1050°C for 5h and cooled to room temperature.

The ionic conductivity of the prepared pellets is $1.03 \times 10^{-3}$ S/cm. Preparation of the $LiMn_2O_4$ was also modified based on the literature [101]. A stoichiometric mixture of $Li_2CO_3$ and $MnO_4$ was ground and heated at 350°C for 2h and then heated at 850°C for 24 h, followed by naturally cooling the sample. The Li-ion conducting liquid, 1M $LiPF_6$ in EC:DEC (1:1volume ratio), was purchased from Novolyte Technologies.

### 2.5.2. Assembly of the Solid and Hybrid Electrolyte Cells

The negative and positive electrodes for the pure solid electrolyte cell and hybrid electrolyte cell were fabricated from a 47:47:6 (wt%) mixture of 47% $LiMn_2O_4$ as active material, 47% $Li_{1.3}Ti_{1.7}Al_{0.3}(PO_4)_3$ as Li-ion conductor, and 6% Super P carbon (Cnergy) as electron conductor. The three materials were thoroughly mixed by using agate mortar and pestle for 1h.

The schematic of the solid electrolyte cell is depicted in Figure 2.2. The solid electrolyte powder of 20 mg was placed inside the $Al_2O_3$ tube (6.4 mm inside and 12.6 mm outside diameters and 20 mm length) and pressed under a desired 2 tone. An electrode powder of 10 mg for each side was added to the pelletized electrolyte layer and pressed under the same pressure one by one. The three layers were sandwiched by two stainless steel cylinders with a 6.4-mm-diameter. The total thickness of the three layers is measured to be around 1 mm.

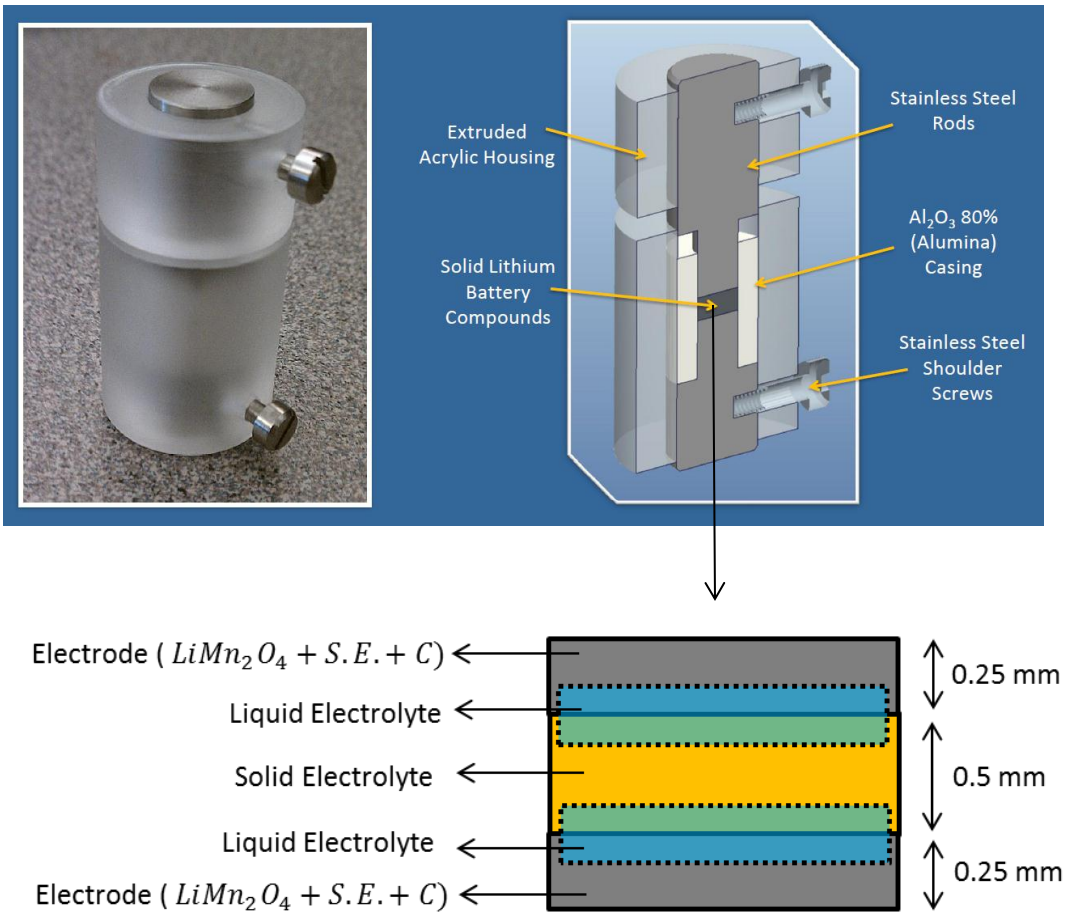


Figure 2.2 Schematic diagram of the battery testing cell with a solid electrolyte and hybrid electrolyte. The electrode is a mixture of $LiMn_2O_4$ powder (25 wt%), the solid electrolyte (25 wt%), and Super P carbon (3 wt%)

For the hybrid electrolyte cell, after the solid electrolyte powder (20 mg) was pelletized, 2 mg of Li-ion conducting liquid, 1M $LiPF_6$ in EC:DEC, was added between each electrode (10 mg) and solid electrolyte layer. Then those layers were sandwiched by two stainless steel cylinders roads and pressed together at 2 tones inside the $Al_2O_3$ tube. The space between the $Al_2O_3$ tube and the stainless steel bar was sealed by vacuum grease (Dow Corning Corporation) followed by the use of Parafilm to prevent the Li-ion conducting liquid from vaporizing while taking electrochemical measurements. The

preparation and electrochemical measurements of the hybrid electrolyte cells were done inside the argon filled glove box because the 1M $LiPF_6$ in EC:DEC used as Li-ion conducting liquid for this experiment can be chemically contaminated when exposed to any moisture.

The laboratory press located inside glove box was used to prepare the solid and hybrid electrolyte cells and also used to maintain the desired pressure during the electrochemical measurements.

### 2.5.3. Assembly of the Liquid Electrolyte Cell

The electrodes for the pure liquid electrolyte cell were fabricated from a 70:20:10 (wt%) mixture of active material, Super P carbon (Cnergy) as current conductor, and polytetrafluoroethylene (G-580, ICI) as binder. The active material and conductor were mixed completely, and then the polytetrafluoroethylene was added to the mass and mixed again. The mixture was rolled into thin sheets and punched into 7mm diameter circular disks as electrodes. The typical electrode mass and thickness were 5–10 mg and 0.03–0.08 mm, respectively. The electrochemical cells were prepared in standard 2016 coin-cell hardware with lithium metal foil used as both the counter and reference electrodes. The electrode disks and cells were prepared in an argon glove box along with the electrolyte used for analysis, 1M $LiPF_6$ in a 1:1 EC:DEC.

### 2.5.4. Testing of the Cell

All of the cells were placed in the battery testing system, a Solartron 1470, to perform charge and discharge tests. Electrochemical Impedance Spectroscopy (EIS) experiments were performed using a Solartron 1260 workstation. The complex impedance of the samples was measured at frequencies from 0.1 Hz to $10^6$ Hz. Impedance measurements were made by using an amplitude voltage of 0.05 V across the sample.

## 2.6. Results and Discussion

### 2.6.1. Solid Electrolyte Cell

Assembly of laboratory sized pure solid electrolyte cells have been reported in many journal articles [57, 88, 90-93]. Their electrochemical performances, especially capacity and cycle life, are generally poor and not competitive with the electrochemical performance of those measured in pure liquid electrolyte cells. In addition, the reported electrochemical performances of the solid electrolyte cell are not consistent in terms of how the cells are prepared and in terms of the weight ratio of the electrode, the thickness of the electrode and electrolyte layer, and the pressure applied to the cells. In order to compare the hybrid electrolyte cell with a pure solid electrolyte cell, a solid electrolyte cell is also assembled in this experiment under the same conditions that the hybrid electrolyte cell is prepared.

Figure 2.3 shows the EIS of the solid electrolyte cell composed of $LiMn_2O_4$ electrode / $Li_{1.3}Ti_{1.7}Al_{0.3}(PO_4)_3$ electrolyte / $LiMn_2O_4$ electrode under the pressures of 350, 700, and 1300 psi, respectively. Any pressure higher than 1300 psi breaks the $Al_2O_3$ tube. Only one semicircle is observed for all samples. The left intercept of the semicircle with real axis corresponds to the solid electrolyte resistance ($R_{SE}$) [102-104]. The size of the semicircle reflects the interface resistance ($R_{IR}$) between solid electrolyte particles or electrolyte/electrode particles. The EIS clearly shows that both of the bulk ($R_{SE}$) and interface resistance ($R_{IR}$) resistances decrease with an increase in pressure. This is because higher pressure provides better contact between the solid electrolyte particles (reducing $R_{SE}$) and between the electrolyte/electrode (reducing $R_{IR}$).

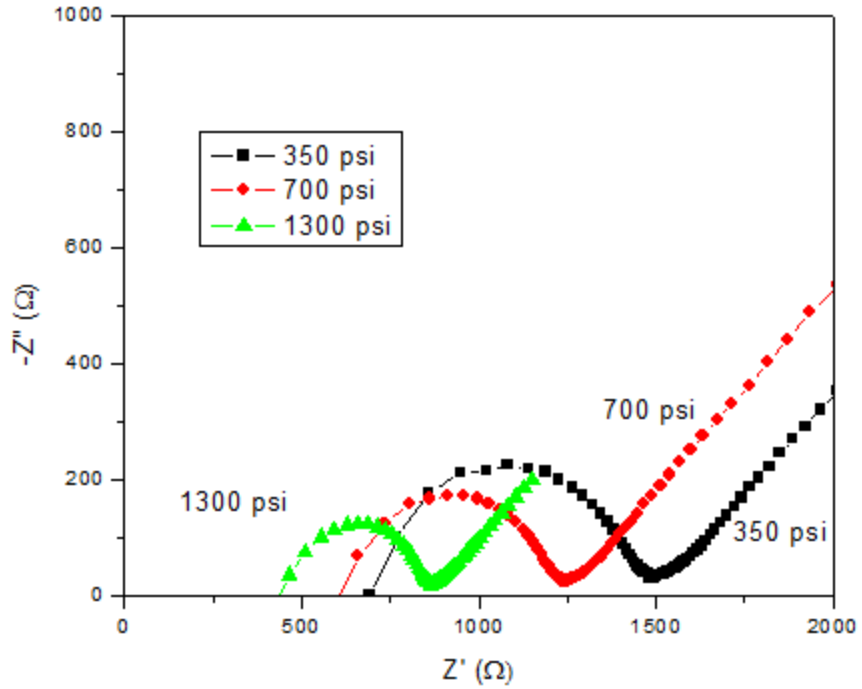


Figure 2.3 Electrochemical Impedance Spectroscopy (EIS) of the solid electrolyte cell composed of $LiMn_2O_4$ electrode / $Li_{1.3}Ti_{1.7}Al_{0.3}(PO_4)_3$ electrolyte / $LiMn_2O_4$ electrode under 350, 700, and 1300 psi, respectively.

Figure 2.4 shows the SEM images of the pure solid electrolyte cells that consist of three layers of anode, electrolyte, and cathode. Each layer is observed to be much denser when pressed under 1300 psi compared with their respective densities under 500 psi as shown in Figure 2.4 (a) and (b). Figure 2.4 (c) and (d) shows that the solid electrolyte particles seem to be more packed under higher pressure. Since the electrode is a mixture of $LiMn_2O_4$, $Li_{1.3}Ti_{1.7}Al_{0.3}(PO_4)_3$, and carbon particles, clear boundaries between the electrode and electrolyte layers are observed even at the high pressure of 1300 psi. This boundary may provide a main interface resistance of the solid electrolyte cell, which corresponds to the size of the semicircle in the impedance spectra shown in Figure 2.3.

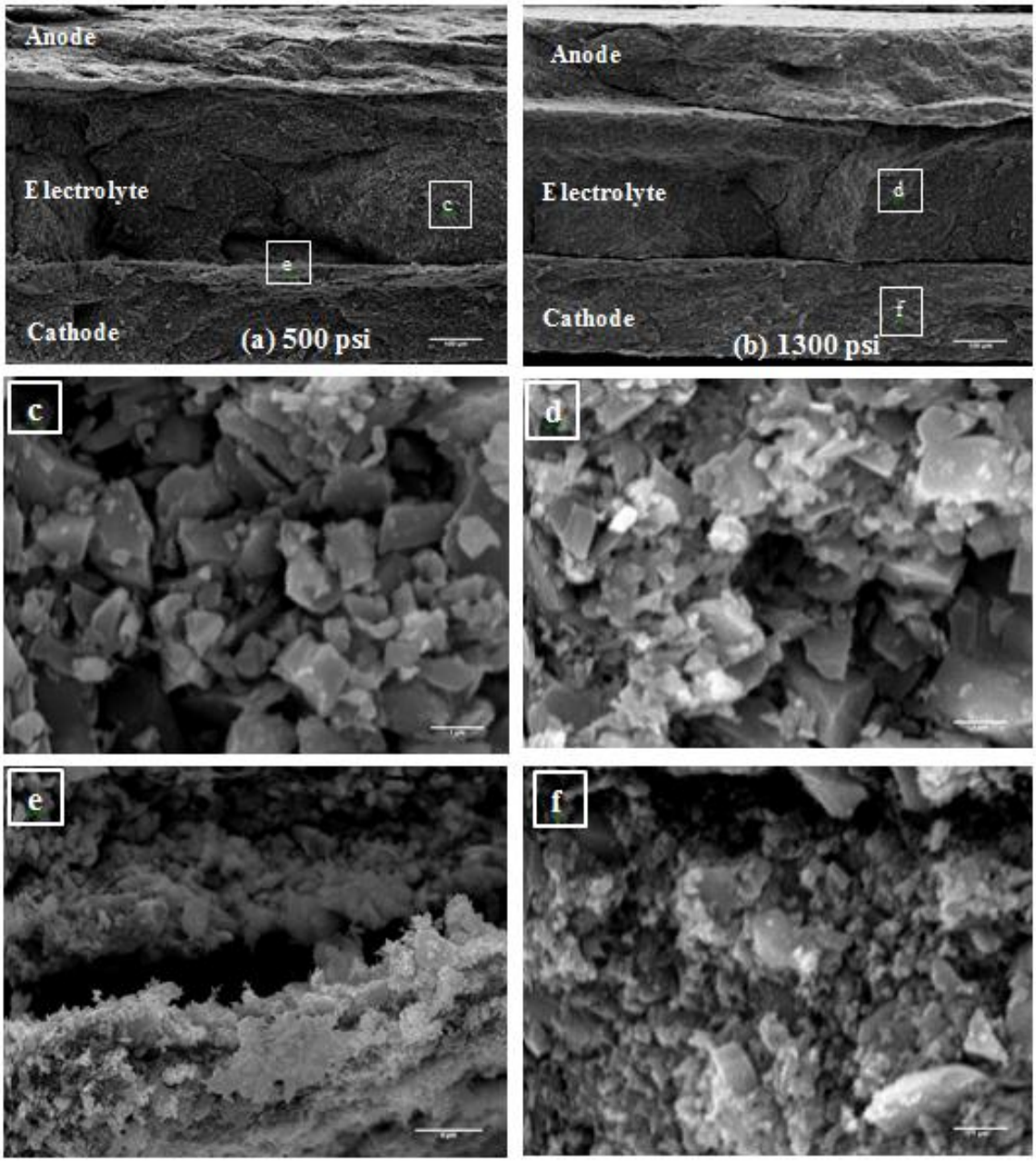


Figure 2.4 SEM of the solid electrolyte cell composed of $LiMn_2O_4$ electrode / $Li_{1.3}Ti_{1.7}Al_{0.3}(PO_4)_3$ electrolyte / $LiMn_2O_4$ electrode under (a) 500 and (b) 1300 psi, respectively. The solid particles in the solid electrolyte layer under (c) 500 and (d) 1300 psi, respectively. (e) the interface boundary of the electrolyte/cathode layer under 500 psi. (f) the solid particles in the cathode layer under 1300 psi.

The electrochemical performance of the solid electrolyte cell is measured under the pressure of 1300 psi to minimize the internal resistance of the cell. Figure 2.5 (a) shows the charge and discharge voltage test for the solid electrolyte cell prepared under the pressure of 1300 psi. The figure shows a smooth charge voltage curve during the first charge of the cell. The first charge capacity reaches 60 mAh/g at the slow current rate of 0.1 $mA/cm^2$ that corresponds to 0.1C rate. It is noted that the same current rate of 0.1 $mA/cm^2$ was applied for hybrid and liquid electrolyte cells in this study. When a current higher than 0.1 $mA/cm^2$ is applied to the solid electrolyte cell, a proper charge voltage curve could not be obtained. Using small current rates is common when testing solid electrolyte cells due to their large internal resistances [57, 88-93]. However, the second discharge and charge capacity after the first charge is not acceptable at the current rate of 0.1 $mA/cm^2$ and even at the lower current rate of 0.04 $mA/cm^2$.

Figure 2.5 (b) shows impedance profiles of the as-prepared solid electrolyte cell after charging to 1.6 V. There is a dramatic change in the impedance spectra after the first charging to 1.6 V – two semicircles were observed. However, the left intercept of the high frequency semicircle with real axis is the same as that of the initial state of the sample, which indicates that the solid electrolyte resistance ($R_{SE}$) was not affected by the charge of the cell.

Thus, it is believed that two semicircles and their increased sizes can be related to the increased interface resistances of the electrode/electrolyte, which are created by the volume change of $LiMn_2O_4$ during charging of the cell. Li-ions are extracted from the $Li_{1-x}Mn_2O_4$ cathode electrode during the charging process, and at the same time Li-ions are inserted into the $Li_{1+x}Mn_2O_4$ anode electrode. The extraction/insertion of the Li ions out of and into a solid solution compound occurs with the volume change of the solid solution compound. It is reported that the extraction of Li from $LiMn_2O_4$ slightly changes the lattice parameter from 8.245 Å in $LiMn_2O_4$ to 8.029 Å in $Mn_2O_4$, decreasing the unit cell by 7.6 % [105, 106]. On the other hand, Li insertion into $Li_{1+x}Mn_2O_4$ yields a severe crystallographic change with a 16% increase in the c/a ratio [105, 106].

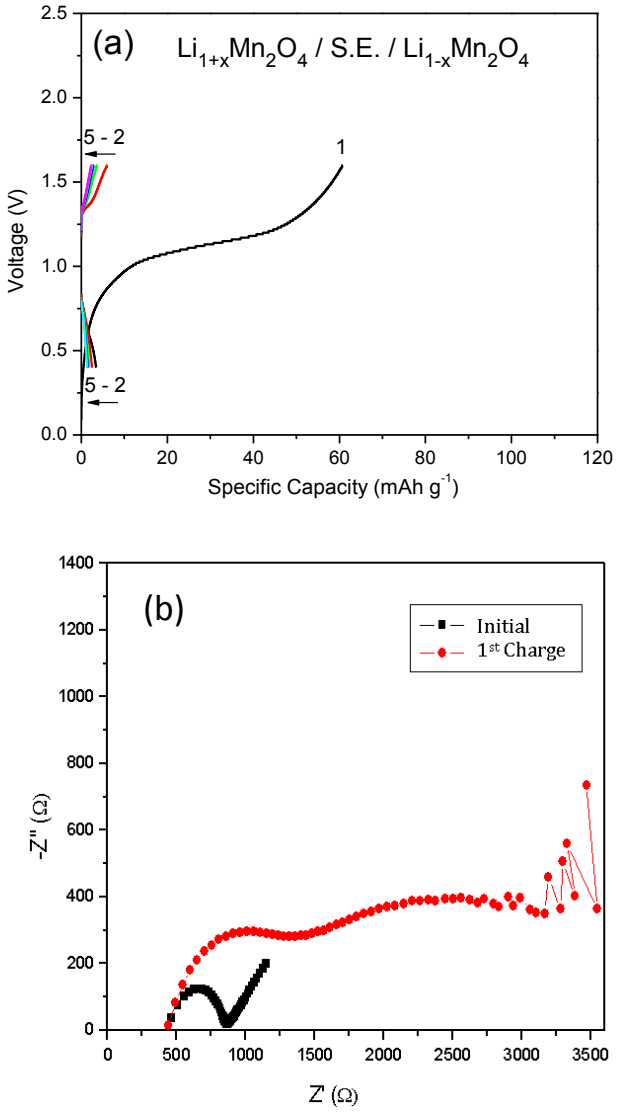


Figure 2.5 (a) Charge and discharge voltage curves measured at 0.1 mA/$cm^2$ for the solid electrolyte cell prepared under 1300 psi. (b) Impedance profiles of the solid electrolyte cell before and after the first charging.

It is believed that the volume change of the electrode creates an empty space (or cracks) in the electrode/electrolyte interface, which hinders Li-ion mobility between electrode and electrolyte. Figure 2.6 shows a schematic diagram of the volume change of the electrode during cycling. As a result, the two semicircle regions can be regarded as

the resistances at the interface of the $Li_2Mn_2O_4$/solid electrolyte and $Mn_2O_4$/solid electrolyte. It is also reported that there is a large interface resistance between the intercalation electrode and solid electrolyte [96]. Therefore, the interface resistance caused by the volume change of the electrode is the major cause of the dramatic capacity drop at the following discharge and charge cycles of the cell.

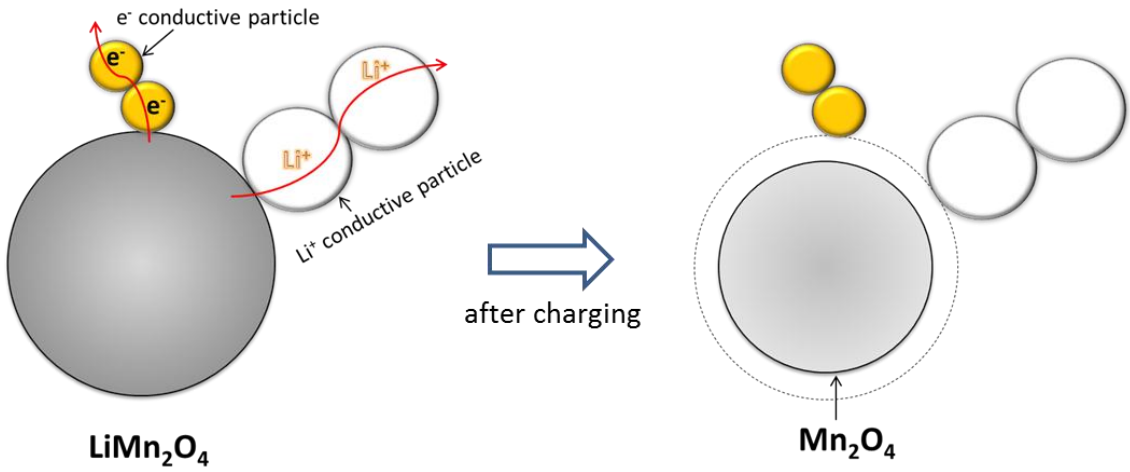


Figure 2.6 Schematic diagram of the electrode mixture. Each $LiMn_2O_4$ particle should contact both electronic conductive and Li-ion conductive particles to provide electron and Li-ion pathways. Carbon and solid electrolyte particles next to $LiMn_2O_4$ particles would be disconnected from the cathode particles when their volume shrinks after Li-ions leave the particles upon charging of the cell.

In addition to the volume change of the electrode materials, the design of the electrode for pure solid electrolyte cells would be challenging because it has to provide an electron pathway as well as a Li-ion pathway. For example, during the charging process, the electrons should leave the $LiMn_2O_4$ while simultaneously Li-ions leave the $LiMn_2O_4$ to balance the charge of the material. So, each $LiMn_2O_4$ particle should contact both electronic conductive and Li-ion conductive particles, respectively, to provide electron and Li-ion pathways as shown in Figure 2.6. If a $LiMn_2O_4$ particle is surrounded

by too many carbon particles or solid electrolyte particles, the proper electrochemical performances cannot be obtained due to poor electronic or Li-ion conductivities in the electrode matrix. In addition, the carbon and solid electrolyte particles next to $LiMn_2O_4$ particles would be disconnected from the cathode particle when its volume shrinks after Li-ions leave the particle upon charging as shown in Figure 2.6. This fundamental design problem of the electrodes will have to be considered if further developments of pure solid electrolyte batteries are desired. There are a few literature sources showing that putting coatings of ceramic on the surface of an electrode has been attempted to minimize this problem [88, 95-97]. However, this would not be an optimal solution in terms of handling the volume change of the solid electrode.

### 2.6.2. Hybrid Electrolyte Cell

In order to solve the solid/solid interface problem in the pure solid electrolyte cell, a Li-ion conducting liquid is used as an additive in the hybrid electrolyte cell to provide better ion-conductivity at the solid/solid interface. As shown in Figure 2.2, when 20 mg of solid electrolyte and 10 mg of each electrode are used, 1 mg of liquid electrolyte is used between each electrode and electrolyte, and the cell is pressed under 1300 psi. Figure 2.7 shows the impedance spectra at the initial state of the hybrid electrolyte cell compared with the solid electrolyte cell. The whole impedance spectrum of the hybrid electrolyte cell dramatically shifts to the lower impedance range. The size of the semicircle corresponding to the interface resistance decreases in the hybrid electrolyte cell. The solid electrolyte resistance indicated by the left intercept of the semicircle with real axis also decreases to 80 ohm compared to the 420 ohm of the solid electrolyte cell.

In the pure solid electrolyte cell, there is always the possibility of having space or cracks between solid/solid electrolyte particles, solid/solid electrode particles, and solid electrolyte/solid electrode particles even under higher pressure, as shown in the SEM image in Figure 2.4. Each solid particle must be connected together from the cathode to the anode side through the electrolyte to provide a continuous Li-ion mobility between

the two electrodes. Figure 2.7 (b) shows the path way of Li-ions in both a solid electrolyte and hybrid cell. The addition of liquid electrolyte fills the gaps between any of these solid particles, improving Li-ion mobility by creating a direct path for Li ions to travel between electrodes.

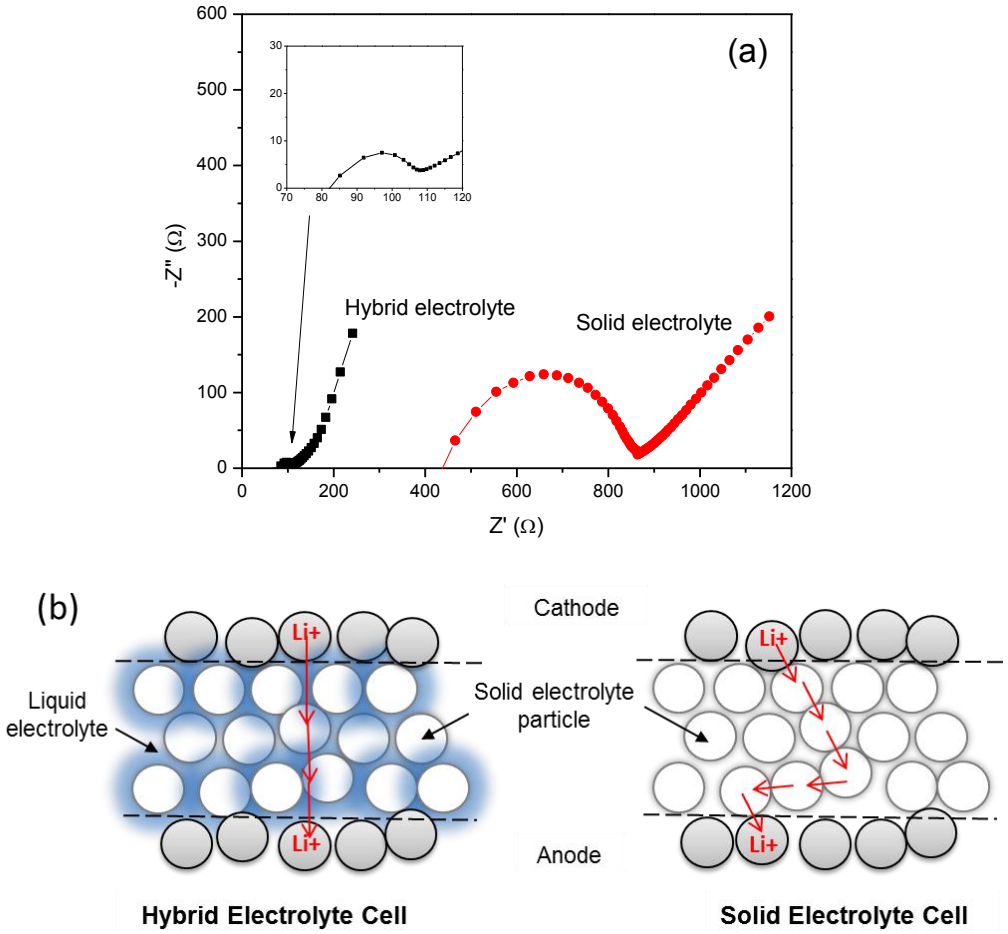


Figure 2.7 (a) Impedance profiles of a solid electrolyte cell and hybrid electrolyte cell at initial state. (b) Schematic diagrams showing the path of Li-ion movement in a solid electrolyte cell and a hybrid electrolyte cell.

Figure 2.8 (a) and (b) shows the cycles of charge and discharge voltage curves of the hybrid electrolyte cell at the rate of 0.1 $mA/cm^2$ that corresponds to 0.1C rate. Compared with the pure solid electrolyte cell of Figure 2.5 (a), there is a dramatic improvement in the first discharge capacity, 100 mAh/g. In addition, the following discharge and charge capacities are repeatable with a gradual loss. This improvement is believed to be due to the decrease in electrode/electrolyte interface resistance caused by adding the Li-ion conducting liquid. Figure 2.8 (c) shows the impedance spectra of the hybrid electrolyte cell measured at the end of charge on each cycle, and Figure 2.8 (d) shows the impedance spectra of the pure solid electrolyte cell. The size of the semicircle observed in the hybrid electrolyte cell, which corresponds to the interface resistance, slightly increases during cycling, but their sizes are much smaller than those observed in the solid electrolyte cells. In addition, only one semicircle remains in the hybrid electrolyte cell during cycling while more than two semicircles appear in the pure solid electrolyte cell. This suggests that the additional interface resistances in the solid electrolyte cell, which are caused by the volume change of the electrode, would be eliminated by the addition of liquid into the solid/solid interface of the solid electrolyte cell.

Even though less than 10 wt% of liquid electrolyte was used for this experiment, it was necessary to make absolutely sure that the electrochemical performance is from the hybrid electrolyte combination (of solid and liquid electrolyte) and not just from the liquid electrolyte. Therefore, the hybrid electrolyte cell was prepared with non-Li-ion conductive $Al_2O_3$ solid particles instead of $Li_{1.3}Ti_{1.7}Al_{0.3}(PO_4)_3$ solid particles The switch in materials did not produce any useable impedance data other than noise. It was not even possible to charge or discharge the hybrid electrolyte cell with $Al_2O_3$ solid particles even at a very low current rate of 0.005 $mA/cm^2$. This comparison supports the idea that the observed electrochemical performances are from the correct combination of solid and liquid electrolytes and not from the liquid electrolyte alone.

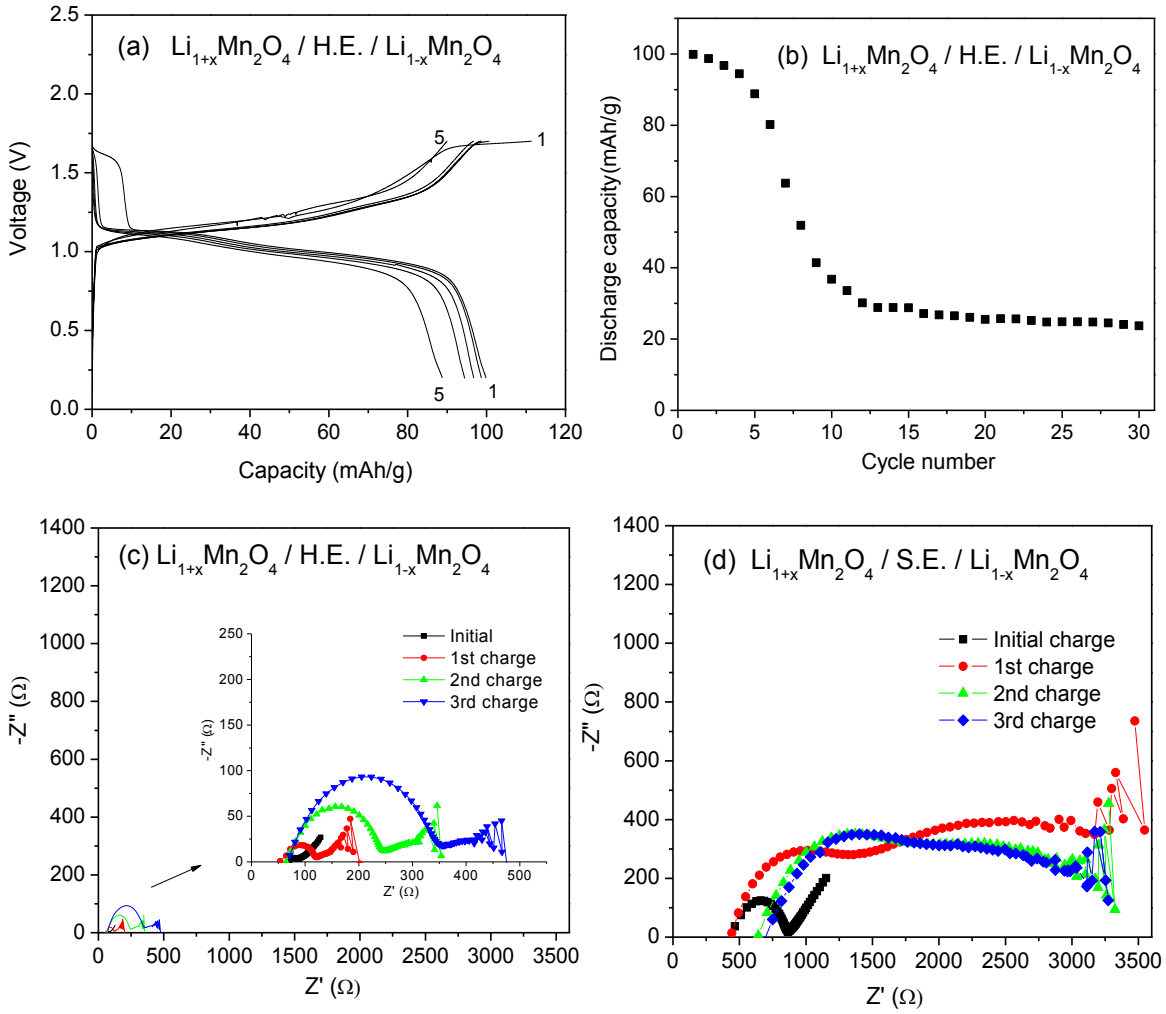


Figure 2.8 (a) The first five charge and discharge curves for a hybrid electrolyte (H.E.) cell and (b) the cycle number measured at 0.1 mA/cm$^2$. Impedance profiles at and after initial charging of (c) a hybrid electrolyte cell and (d) a solid electrolyte (S.E.) cell.

### 2.6.3. Electrochemical Performance of the Hybrid Electrolyte Cell Versus Liquid Electrolyte Cell

A full cell of $Li_{1+x}Mn_2O_4$ / liquid electrolyte / $Li_{1-x}Mn_2O_4$ is prepared to compare its electrochemical performance with that observed of the hybrid electrolyte cell. Interestingly, the capacity of the hybrid electrolyte cell is observed to be higher than that of the pure liquid electrolyte cell during the first five cycles at the same current rate of 0.1 $mA/cm^2$. Figure 2.9 (a) and (b) shows that the full cell assembled by the liquid electrolyte, $Li_{1+x}Mn_2O_4$ / L.E. / $Li_{1-x}Mn_2O_4$, gives a low capacity of ~60 mAh/g at the first cycle, and it gradually decreases for 30 cycles. The $Li_{1-x}Mn_2O_4$ is a common cathode material that provides a good cycle life by extracting Li ions from the $Li_{1-x}Mn_2O_4$. Our half-cell, Li/L.E./$Li_{1-x}Mn_2O_4$, measurement also shows the good reversibility of Li extraction from the $Li_{1-x}Mn_2O_4$, Figure 2.9 (c). Hence, the poor cycle life of the full cell, $Li_{1+x}Mn_2O_4$ / L.E. / $Li_{1-x}Mn_2O_4$, is related to the Li insertion into the $Li_{1+x}Mn_2O_4$ electrode. It is known that Li insertion into $Li_{1+x}Mn_2O_4$ at 3 V produces a large volume change by the phase change from the cubic-spinel $LiMn_2O_4$ to tetragonal $Li_2Mn_2O_4$ with a severe crystallographic Jahn-Teller distortion [105, 106]. In addition, a disproportionate reaction occurred on the $Li_2Mn_2O_4$ surface, which contains a high $Mn^{3+}$ concentration according to the reaction [5, 107, 108]:

$$2Mn^{3+}\,(\text{solid}) \rightarrow Mn^{4+}\,(\text{solid}) + Mn^{2+}\,(\text{solution})$$

Together with a volume change, the dissolution of $Mn^{2+}$ in the liquid electrolyte was known to be the major cause for poor capacity and cycle life of the $Li_{1+x}Mn_2O_4$ electrode [96, 107, 109]. The poor capacity and reversibility of Li insertion into the $Li_{1+x}Mn_2O_4$ is also observed in our experiment as shown in Figure 2.9 (d).

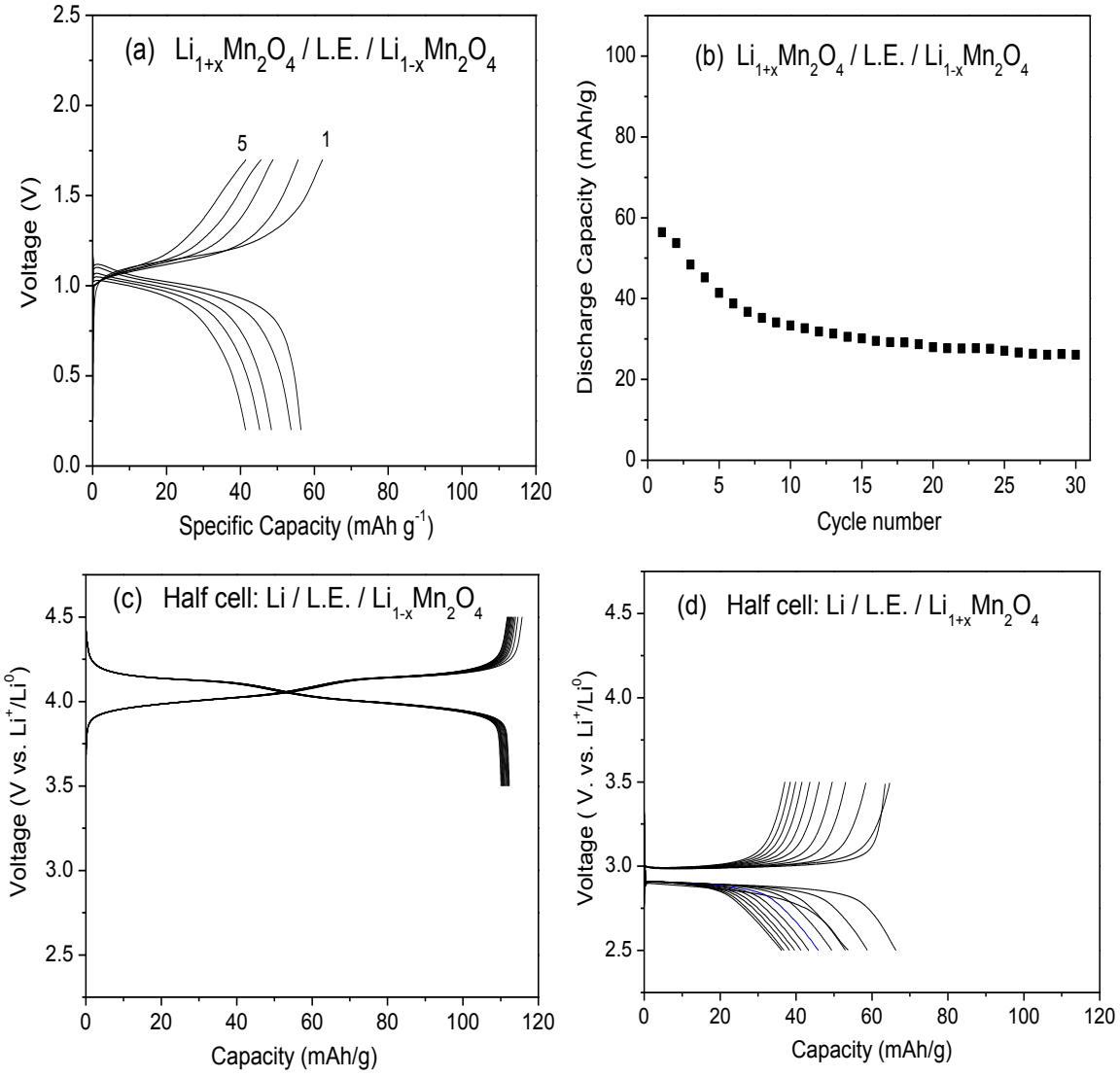


Figure 2.9 (a) The first five charge and discharge curves for the full cell, $Li_{1+x}Mn_2O_4$ / L.E. / $Li_{1-x}Mn_2O_4$ and (b) its cycle life performance. The half cells, (c) Li / L.E. / $Li_{1-x}Mn_2O_4$ and (d) Li / L.E. / $Li_{1+x}Mn_2O_4$ were also prepared to compare their electrochemical performances with those of the full cell. All cells were measured at the rate of 0.1mA/$cm^2$.

Interestingly, the capacities observed in the hybrid electrolyte cell, Figure 2.8 (a), are 40% higher than those observed in the pure liquid electrolyte cell, Figure 2.9 (a), during the first five cycles. This is believed to happen because the manganese dissolution in the hybrid electrolyte is alleviated due to its low content of the liquid electrolyte; the hybrid electrolyte contains 10 wt% of the liquid electrolyte and 90 wt% of the solid electrolyte. However, after five cycles, the capacity of the hybrid electrolyte cell drops quickly and is saturated at ~30 mAh/g, which is similar to the saturated capacity of the liquid electrolyte cell. It has been demonstrated that the dissolution of $Mn^{2+}$ in the liquid electrolyte produces by-products on the surface of the $Li_{1+x}Mn_2O_4$ [110, 111]. When the electrode is fully covered by the by-products (or surface layers), it produces a dramatic effect on the Li-ion diffusion paths, which leads to poor capacity and reversibility. Hence, it is believed that in the hybrid cell, the dissolution may have slowed down due to the small content of the liquid electrolyte. However, after having the electrode fully covered by the surface layer (after five cycles), the capacity drops quickly as indicated in Figure 2.9 (b). This could be an advantage of using a hybrid electrolyte rather than a pure liquid electrolyte as one search for new electrode materials that are chemically unstable with a highly soluble liquid electrolyte.

### 2.6.4. Safety Advantage of the Hybrid Electrolyte Cell

Another advantage the hybrid electrolyte offers is battery safety. In the hybrid electrolyte, the solid electrolyte constitutes the majority of the electrolyte and is utilized to improve safety of the battery, while the liquid electrolyte constitutes a small portion of the electrolyte and is only utilized to provide better interface between the solid electrode and solid electrolyte. Because using solid electrolytes is safer than using liquid electrolytes at high temperatures, the hybrid electrolyte cell – made mostly of solid electrolyte – increases safe operation when sudden high temperatures are applied. Figure 2.10 shows the charge voltage behaviors of both hybrid and liquid electrolyte cells when the temperature of the cell increases to 80°C during the charge process. The charge voltage of the pure liquid electrolyte cell drops to 0.2 V at 80°C, and the continuous

discharge curve appears below 1V even after discharging for 40h. This would indicate a reaction occurred between the electrode and electrolyte, which if not stopped, would cause catastrophic failure of the battery producing gas then fire. The inserted picture in Figure 2.10 shows that the transparent electrolyte turns black after reacting with electrode materials.

However for the hybrid electrolyte cell, when the temperature increases to 80°C, the voltage drops to 0.9 V from 1.0 V, and then the cell continues to gain charge up to 1.6 V followed by the cell halt. After a short reaction time between the electrode and the liquid portion of the hybrid electrolyte, the cells continuously operate with the solid portion of the hybrid electrolyte during charging. It was found that the cell using the hybrid electrolyte has a discharge behavior similar to that measured when using a pure solid electrolyte, Figure 2.5 (a). Thus, this experiment shows that using a hybrid electrolyte is safer than using a pure liquid electrolyte.

This experiment shows the advantage of using a hybrid electrolyte rather than pure liquid electrolyte that is highly soluble and flammable. The relatively smaller Li-ion conductivity of a solid electrolyte compared to that of liquid can be a problem for high current rate battery applications. However, recently some solid compounds show better Li-ion conductivity than that of liquid [112], which gives hope for further developments of this hybrid system.

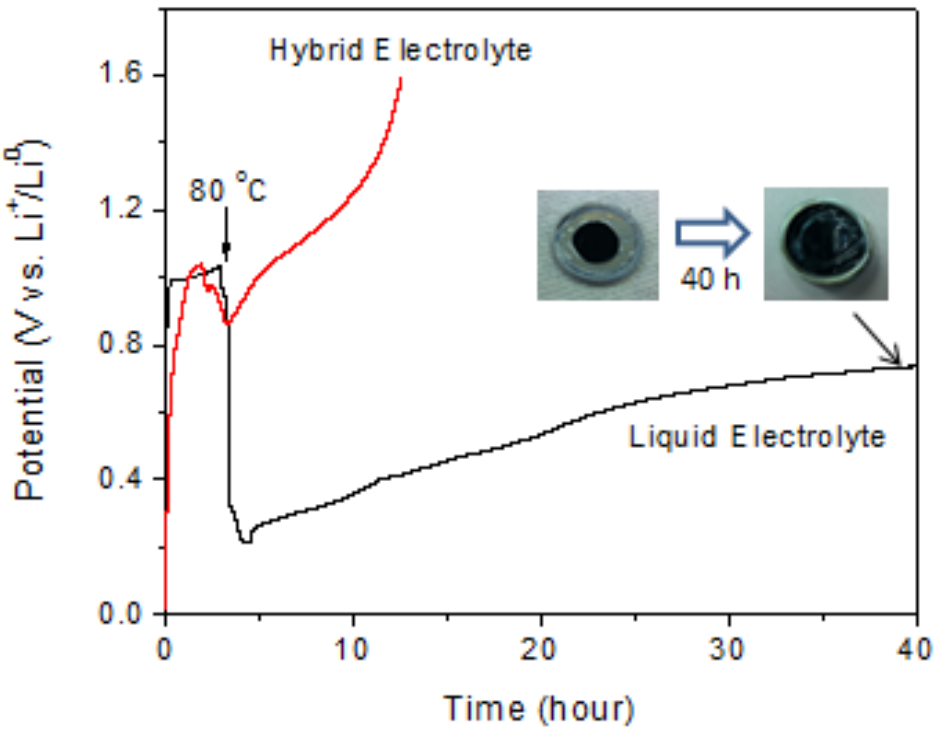


Figure 2.10 Charge voltage curves for a hybrid electrolyte cell and an organic liquid electrolyte during the heat test. As temperature increases to 80°C, the voltage of the hybrid electrolyte cell drops from 1.0 V to 0.9 V, and then the cell continues to be charged to 1.6 V followed by the cell stop. The liquid electrolyte cell shows a continuous discharge voltage from 0.2 V to below 0.8 V for 40 hours after the voltage drops to 0.2 V. The inserted figure shows the color of the transparent liquid electrolyte changes after reacting with electrode materials at 80 °C.

## 2.7. Conclusion

The interface resistance between solid electrode and solid electrolyte is quite a challenge for all-solid-state Li-ion rechargeable batteries. Although initially the interface may have good contact under high pressure, the volume change of the electrode during $Li^+$ insertion/extraction during cycling of the cell creates a large resistance at solid electrodes/solid electrolyte interface. Therefore constructing a hybrid electrolyte by adding a very small amount of liquid electrolyte, just enough to make good contact between the solid electrolyte and the solid electrode, adjusts for the volume change

during cycling of the cell. The addition of the liquid electrolyte fills the gaps between these solid particles and also provides better Li-ion mobility in the hybrid electrolyte. The hybrid electrolyte cell has a larger first charge capacity and loses less of its capacity in the following discharge when compared to pure solid electrolyte and liquid electrolyte cells. The hybrid electrolyte cell also improves safety when high temperature is introduced.

This study was performed solely to test the electrochemical performance and safety of using a hybrid electrolyte for a Li-ion rechargeable battery by using the $Li_{1.3}Ti_{1.7}Al_{0.3}(PO_4)_3$ solid electrolyte, 1M $LiPF_6$ in EC:DEC liquid electrolyte, and $LiMn_2O_4$ electrodes. Many types of hybrid electrolytes can be built from a combination of Li-ion conducting inorganic solids and liquids, which could be an alternative to the one-phase electrolyte that struggles to enhance the electrochemical performance of current Li battery technology.

# 3. MULTILAYER ELECTROCHEMICAL CELL

## 3.1. Introduction

The high operation voltage of the positive electrode can be beneficial for electric vehicle (EV) applications because it can reduce the number of cells in a pack and thereby lower overall costs. The $LiNi_{0.5}Mn_{1.5}O_4$ spinel (~ 4.7 $V_{vs.Li}$) is one of the promising high voltage positive electrode materials for next generation Li-ion batteries with a good power performance. However, a major challenge for the implementation of $LiNi_{0.5}Mn_{1.5}O_4$ for EV applications is the instability of standard electrolytes at high voltages (> 4.5 $V_{vs.Li}$) [27]. In addition, $LiNi_{0.5}Mn_{1.5}O_4$ spinel suffers from the "Mn dissolution" problem that is detrimental to the cycle life of full-cells with graphite negative electrodes [107, 109, 113, 114]. The poor cycle life observed in full-cells has been understood to occur by the loss of active $Li^+$ through continuous SEI formation (electrolyte reduction) promoted by Mn reduced on top of the graphite's surface [113, 115, 116]. Unfortunately, the impact of Mn dissolution on the overall capacity fading in the full-cell has not been gauged properly because it is difficult to separate the influence of reductive and oxidative electrolyte decomposition using traditional cell designs (i.e. coin cells).

In this study, a MEC was designed and developed as a new tool for investigating electrode/electrolyte interfacial reactions in a battery system. The MEC consists of two liquid electrolytes (L.E.) separated by a solid electrolyte (S.E.) which selectively transports $Li^+$ ions illustrated in Figure 3.1 (a). This design offers the benefit of isolating the individual positive and negative electrode/electrolyte interfacial reactions in a single cell which cannot be realized by conventional cell designs (i.e. coin cell). Here, the

stability of battery performance using the MEC was examined using $LiFePO_4$ as the positive electrode material. In addition, attempts to identify the origin of capacity fading and the impact of Mn dissolution in a $LiNi_{0.5}Mn_{1.5}O_4$/graphite full cell were studied and the potential applications for MEC were demonstrated. Finally, we identify the benefits of MEC as a tool for future electrode/electrolyte interface or materials studies.

The previous study showed that a small amount of liquid electrolyte improves the electrode/electrolyte interface. In this study, a new device was designed and developed to apply the same concept but with the different approach. Introducing a new single electrolyte which is stable with high voltage electrodes is quite challenging, but gathering different electrolytes with different properties can simply make it possible to be benefited from all those singular advantageous properties together. This device might be capable to improve the performance of existing electrolytes. Existence of solid electrolyte as a barrier within the cell allows using the liquid electrolyte only stable with the consistent electrode rather than the both electrodes. So basically, separation of electrodes in multi-layer electrolyte cell allows for more choices over existence materials to satisfy the required conditions. Moreover, it is expected that high volume change of some electrodes adjusted by using this device.

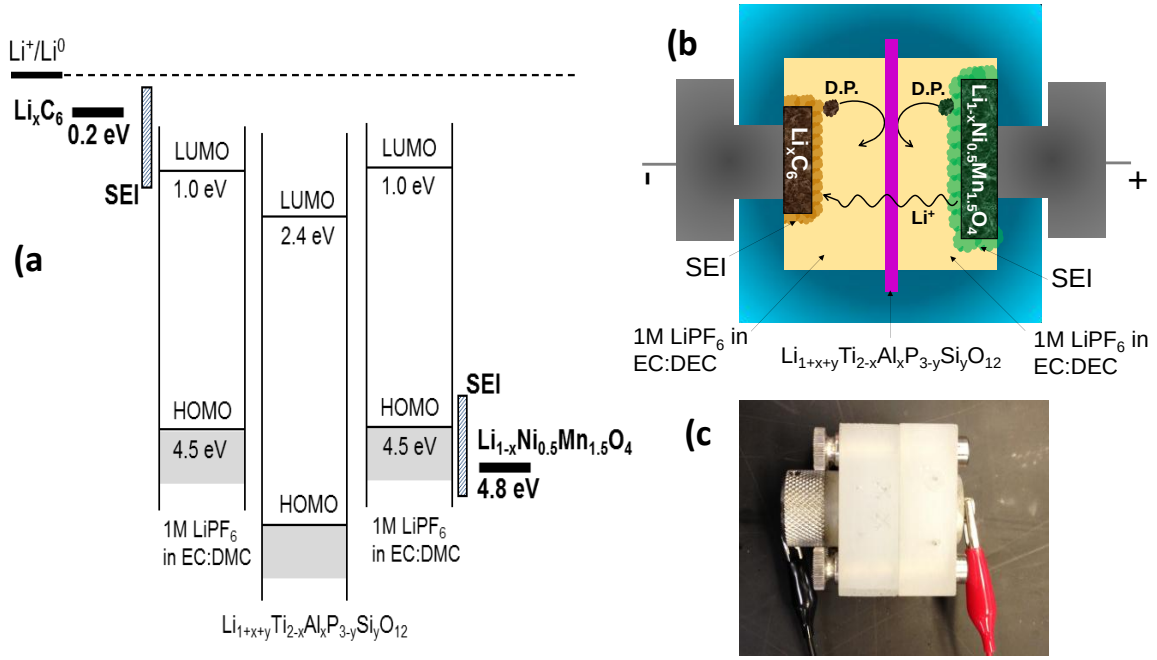


Figure 3.1 (a) Schematic open-circuit energy diagram of the multilayer electrolytes with the $Li_xC_6$ negative electrode and the $Li_{1-x}Ni_{0.5}Mn_{1.5}O_4$ cathode. (b) Conceptual illustration demonstrating a selective $Li^+$ transport through the solid electrolytes while blocking decomposed products (DP). (c) Picture of the assembled MEC under testing.

## 3.2 Experimental Methods

### 3.2.1 Chemicals

A lithium ribbon (99.9%) of 0.38 mm thickness was purchased from Sigma Aldrich were punched into 0.8 cm diameter disks for use as the anode. 1 M LiPF6 in ethylene carbonate (EC)–dimethyl carbonate (DMC) (1 : 1 volume ratio) as an organic nonaqueous liquid electrolyte was purchased from Novolyte Corporation; 1 M $LiNO_3$ in DI water was used as aqueous electrolyte and 1M LiTFSI in EMI-TFSI as an ionic liquid. The Li-ion conducting glass ceramic plate, $Li_{1+x+y}Ti_{22x}Al_xP_{32y}Si_yO_{12}$ (LTAP), with a

diameter of 19 mm, the thickness of 150 mm, and the ionic conductivity about $10^{-4}$ S/cm at room temperature was purchased from OHARA, Inc. SUPER P carbon black (TIMCAL) was used as the electronic conductive powder for the electrodes. The common cathode material of LiFePO4 and high voltage material of LiNi0.5Mn1.5O4 were used as positive electrodes.

### 3.2.2 Fabrication of the Multilayer Electrochemical Cell

Figure 3.2 shows a schematic diagram of the MEC. The cell was made with a polypropylene body which contains L.E., electrodes, and current collectors (stainless steel rods at each side). A dense ceramic S.E. , $Li_{1+x+y}Ti_{2-x}Al_xP_{3-y}Si_yO_{12}$ (LTAP, OHARA, Inc.), with a thickness of 150 μm was placed between the L.E.s and completely sealed in order to prevent any electrolyte and any potential reduction or oxidation products to crossover while selectively transporting $Li^+$ ions. Both regions of L.E. used 1 M $LiPF_6$ in EC:DMC (1:1 vol., Novolyte Corp.). For $LiFePO_4$ MEC half-cells, Li metal (99.9%, Sigma Aldrich) with a thickness of 0.38 mm was employed as the negative electrode. For the $LiNi_{0.5}Mn_{1.5}O_4$ MEC full-cells, mesoporous carbon microbeads graphite (MCMB, Osaka Gas Co.) was employed as the negative electrode. The charge and discharge tests of the battery cells were performed using a Solartron 1470 cell tester. The cycled graphite negative electrodes were analyzed using an aberration-corrected transmission electron microscope (TEM, JEOL JEM-2001F) with energy dispersive X-ray (EDX). TEM samples were prepared by scraping powder material off the electrode surfaces and dusting it onto carbon-supported copper TEM grids.

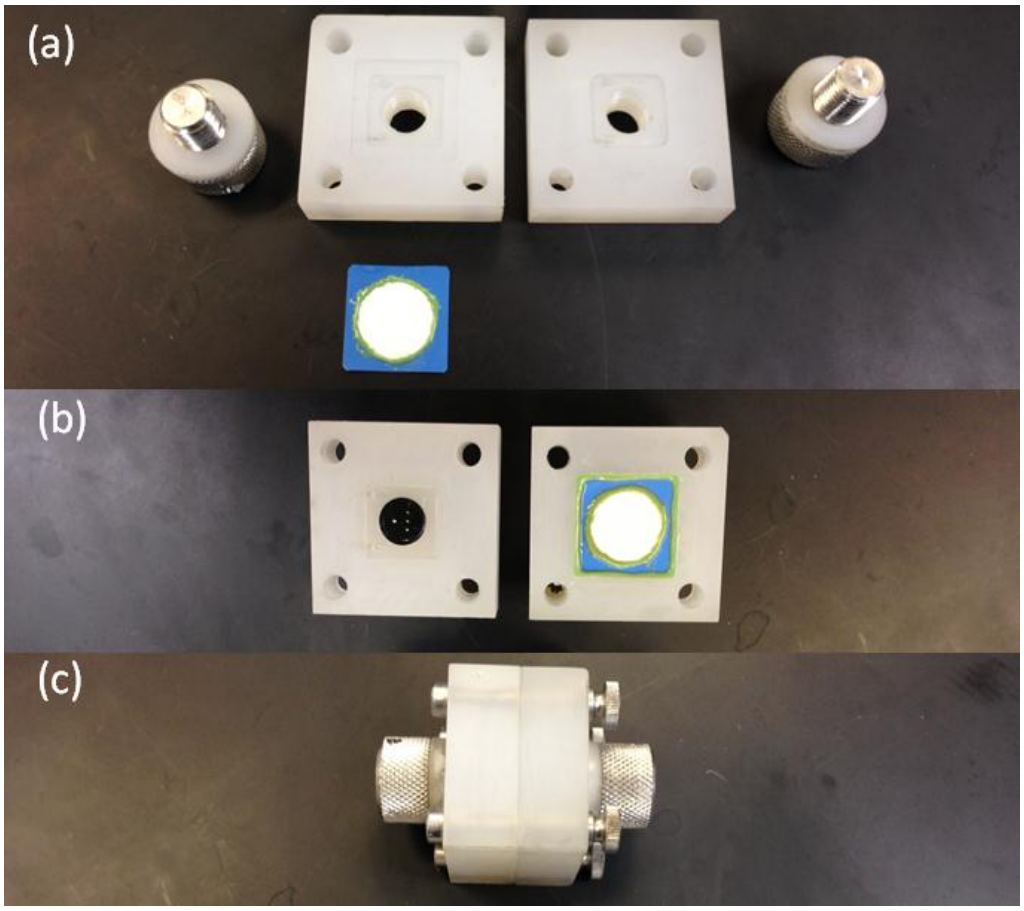


Figure 3.2 Assembly process of the home made multilayer electrochemical cell

### 3.2.3 Assembly of the Pouch Multilayer Electrochemical Cell

Figure 3.3 shows an image of fully assembled pouch multilayer electrochemical cell and its exploded view. The cell consists of two layers which were separated with the LTAP solid electrolyte assembled in the middle of 4.5 × 4.5 cm aluminum laminated film with epoxy. The electrodes were located in each layer and then the liquid electrolyte was filled in each side inside the argon filled glove box. Finally, layers were sealed individually to prevent penetrating of electrolyte to each side. Also, a layer of Celgard separator was placed between each layer to protect the solid electrolyte and epoxy from being directly contacted with the electrodes and current collectors.

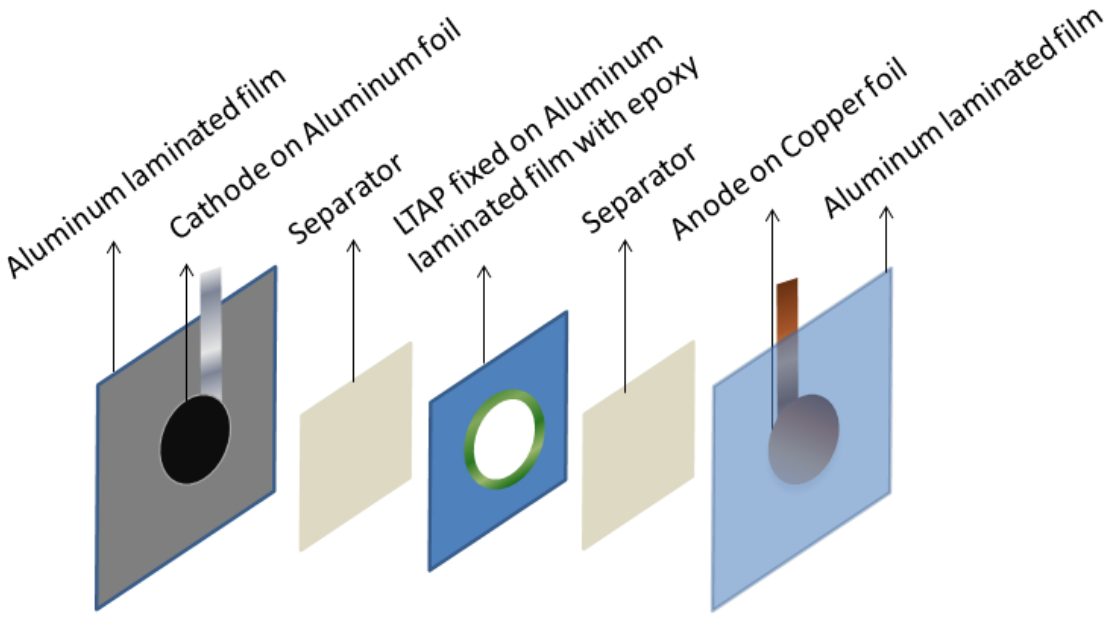


Figure 3.3 Exploded view of the pouch multilayer electrochemical cell

### 3.2.4 Assembly of the Coin Cell

The electrodes for the coin cell were fabricated from a 70 : 20 : 10 (wt%) mixture of active material, Super P carbon (purchased from Cnergy) as the current conductor, and polytetrafluoroethylene (G-580, ICI) as the binder. The active material and conductor were mixed completely, and then the polytetrafluoroethylene was added in, and all three were mixed together. The mixture was rolled on the aluminum foil (for cathode materials) or cupper foil (for anode materials) into thin sheets and punched into 7 mm-diameter circular disks as electrodes. The typical electrode mass and thickness were about 5–10 mg and 0.03–0.08 mm, respectively. The electrochemical cells were prepared in standard 2016 coin-cell hardware with lithium metal foil used as both the counter and reference electrodes or graphite. The electrode disks and cells were prepared in an argon glove box along with the electrolyte used for analysis, 1 M LiPF6 in a 1 : 1 EC–DMC. A Solartron 1470 cell tester was used to perform the charge and discharge tests.

## 3.3 Results and Discussion

Figure 3.1 illustrates a schematic diagram and design of the MEC. In Figure 3.1(a), traditional L.E.s have their highest occupied molecular orbital (HOMO) located above the electrochemical potential of the $LiNi_{0.5}Mn_{1.5}O_4$spinel positive electrode. They also have their lowest unoccupied molecular orbital (LUMO) located below the potential of graphite. As a result, both electrolyte oxidation and reduction will occur in the $LiNi_{0.5}Mn_{1.5}O_4$/L.E./graphite full-cell. However, the passivation layer (SEI) formed on the graphite surface as a product of the electrolyte reduction will impede the electron transfer toward electrolyte, and in turn suppress further decomposition. In contrast, any sustainable or useful SEI has not yet been reported for $LiNi_{0.5}Mn_{1.5}O_4$ positive electrodes. The HOMO of the S.E. is located below that of $LiNi_{0.5}Mn_{1.5}O_4$ indicating its stability at high voltages. Each side of L.E. was sealed with S.E. preventing any electrolyte mixing. Therefore, decomposition species on each side of L.E. cannot migrate to the other side because the S.E. only selectively transports $Li^+$ ion as illustrated in Figure 3.1(b).

The performance of MEC was examined by using a $LiFePO_4$/L.E./S.E./L.E./Li half-cell. In comparison with coin half-cells, the MEC exhibited a larger voltage difference between the charge and discharge curves, especially at higher current rates as shown in Figure 3.4 (a) [117, 118]. This voltage difference is believed to be due to the low Li-ion conductivity (~$10^{-4}$ S/cm) of the solid electrolyte. The voltage difference between charge and discharge voltage curves can be minimized by applying low current rates during cycling. For example, Figure 3.4 (b) shows excellent capacity (~140 mAh/g after 5 cycles) and cycle life for $LiFePO_4$ at 0.05 mA/$cm^2$. This result is comparable to that of $LiFePO_4$/L.E./Li coin half-cells indicating that the MEC successfully reproduces the performance of coin-cells by cycling at low C-rates. The MEC design will be further improved by decreasing the distance between electrodes and by adopting L.E. and S.E. with higher ionic conductivities in the near future.

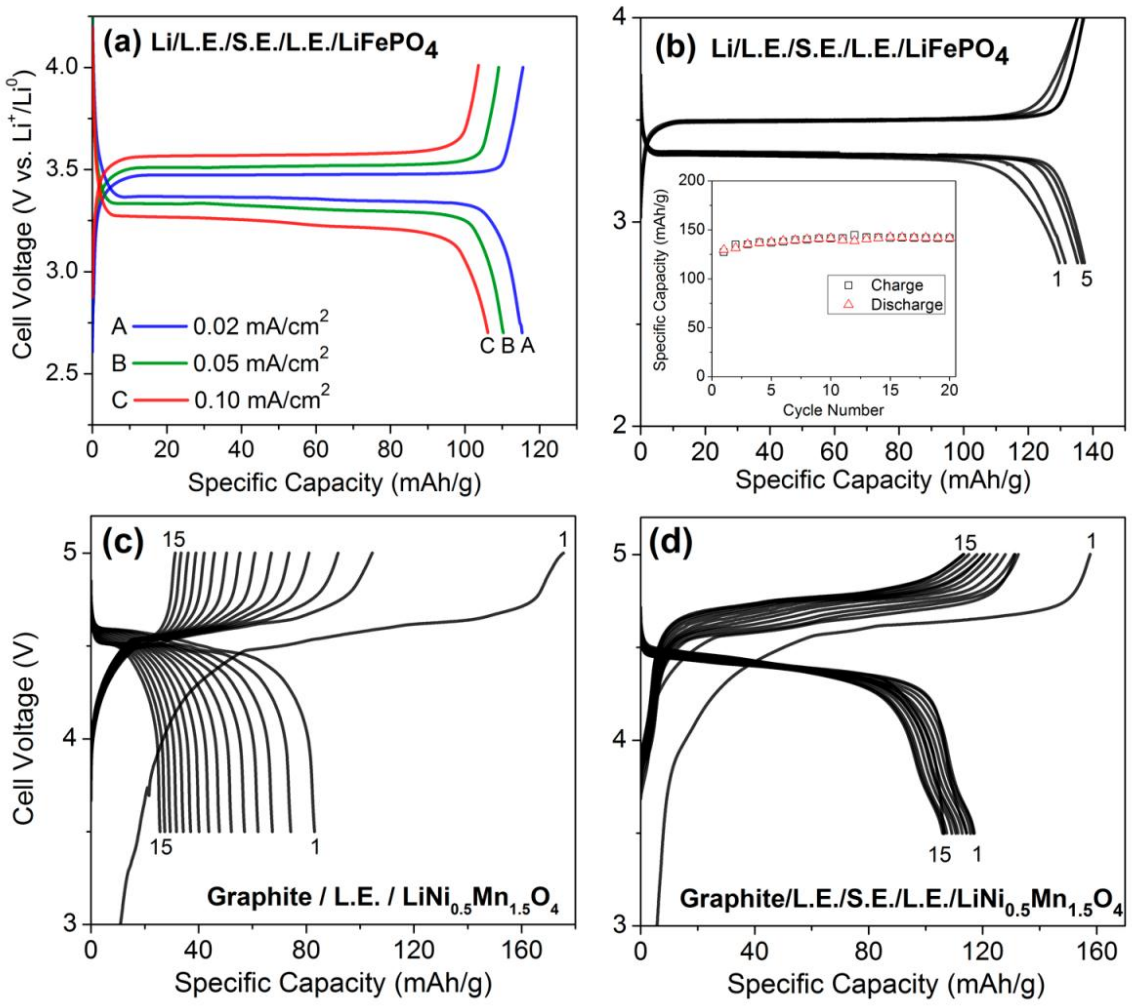


Figure 3.4 The charge-discharge voltage curves of $LiFePO_4$ MEC half-cells at 25°C: (a) voltage profiles at different current densities and (b) voltage profiles and cycle life (inset) at 0.05 mA/cm$^2$. The charge-discharge voltage curves of $LiNi_{0.5}Mn_{1.5}O_4$ full-cells (graphite as negative electrode) with C/20-rate at 25°C: (c) measured by coin cell and (d) measured by MEC.

Encouraged by the good reproducibility of the performance of $LiFePO_4$ using the MEC, the electrochemical performance of the $LiNi_{0.5}Mn_{1.5}O_4$/graphite full-cell was also explored. Unlike the $LiFePO_4$, the operation voltage of the $LiNi_{0.5}Mn_{1.5}O_4$ exceeds the stability limit of standard electrolytes, which results in the oxidative decomposition of the electrolyte. In addition, dissolved $Mn^{2+}$ ions from the $LiNi_{0.5}Mn_{1.5}O_4$ reduces on top of graphite, which in turn results in severe capacity fading due to the catalytic decomposition of electrolyte and the resulting loss of active $Li^+$ in the cell [113]. It is important to understand all the individual degradation factors which contribute to the capacity fading encountered in a full-cell cycling. Unraveling their respective impacts will serve as a foundation to determine effective mitigation strategies. However, a standard cell configuration does not allow the isolation of such degradation mechanisms. From this perspective, the MEC was employed to identify each degradation factors because the solid electrolyte blocks the migration of $Mn^{2+}$ ions by confining liquid electrolytes to their respective electrode sides.

The MEC full-cell ($LiNi_{0.5}Mn_{1.5}O_4$/L.E./S.E./L.E./graphite) was cycled at C/20-rate in a voltage range of 3.5 – 5 V. For comparison, $LiNi_{0.5}Mn_{1.5}O_4$/L.E./graphite coin full-cell was cycled using the same conditions. In Figure 3.4 (c), the coin full-cell delivered 83 mAh/g at the first discharge process and exhibited rapid capacity fading during 15 cycles. The cycle life of the $LiNi_{0.5}Mn_{1.5}O_4$/L.E./graphite full-cell was strongly impacted by the C-rates used. At a given cycle number, full-cells cycled at lower C-rates exhibited poor cycle lives compared with those obtained at higher C-rates (data not shown here). This can be understood by the acceleration of electrolyte decomposition during cycling at low C-rates; For example, electrolyte will be exposed to either high (> 4.5 V vs. Li) or low (< 1 V vs. Li) voltage regions for longer period of time with decreasing C-rate. The capacity fading of the full-cell has been understood in the literature to be caused by the following sources of degradation: i) oxidative decomposition of electrolyte at high voltages [1], ii) Mn loss from the $LiNi_{0.5}Mn_{1.5}O_4$ positive electrode [119, 120], iii) $Li^+$ loss by the forming of normal SEI on graphite [121, 122], iv) $Li^+$ loss during the reduction of $Mn^{2+}$ on graphite ($Mn^{2+} + 2\ LiC_6 \rightarrow Mn + 2\ Li^+$

+ graphite) [123], v) catalytic reduction of electrolyte by Mn on graphite, consuming additional $Li^+$ [113].

In contrast, the MEC delivered much improved performance compared with that of the coin cell. The MEC delivered capacity retention of 90% after 15 cycles, which is superior to that of the coin cell (25%). In addition, the MEC also showed higher coulombic efficiency compared with that of the coin cells achieving > 90% while the coin cell stayed ~ 80% after 5 cycles. This result clearly indicates that the MEC successfully suppressed some of critical degradation sources. Since the S.E. selectively conducts $Li^+$ while blocking the migration of $Mn^{2+}$, it was believed that the MEC would eliminate the iv) and v) among the listed sources of degradation. This hypothesis can be supported if the cycled graphite from the MEC does not contain any Mn particles on its surface. In this regards, TEM analysis was performed for the cycled graphite from both the coin cell and MECs. In Figure 3.5 (a), the surface of cycled graphite revealed the presence of nanoparticles on its surface with different sizes. The EDS measurement of these nanoparticles showed that most particles consisted of Mn (inset in Figure 3.5(a)). Occasionally, particles contained both Mn and Ni (not shown here). In contrast, cycled graphite from MEC showed clean surfaces without any Mn nanoparticles as can be seen in Figure 3.5(b). This result confirms that the S.E. in MEC effectively blocks the $Mn^{2+}$ migration towards the graphite negative electrode.

Figure 3.5(c) illustrates the origin of capacity loss from the full-cells. The difference of capacities between MEC and coin cells is directly related to the $Li^+$ loss as a result of the Mn dissolution problem (iv and v in listed sources). Although the other sources still degrade the cell performance in either positive (i and ii) or negative (iii) electrode sides, their impacts on the capacity fading is much less than that from the Mn dissolution (iv and v). This result clearly indicates that Mn dissolution is the main degradation factor for the $LiNi_{0.5}Mn_{1.5}O_4$/graphite full-cells using standard electrolytes.

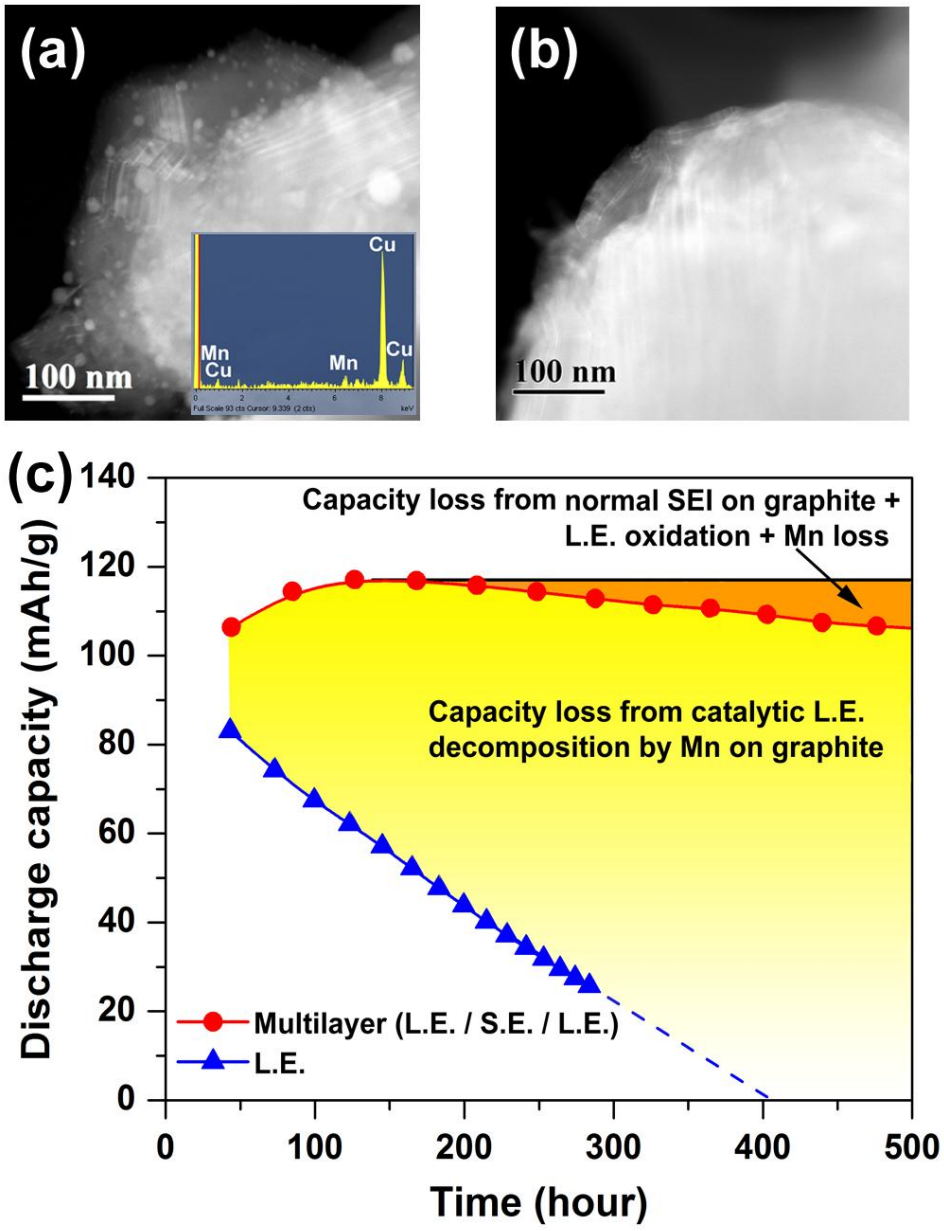


Figure 3.5 (a) TEM image of cycled graphite electrode using normal L.E. showing Mn particles on its surface. Inset is an EDS spectrum of nanoparticle contains Mn (The Cu signal is from a sample grid) (b) TEM image of cycled graphite electrodes using MEC revealing clean surface. (c) Origin of capacity loss in $LiNi_{0.5}Mn_{1.5}O_4$ / graphite full-cells. The MEC full-cell (L.E./S.E./L.E.) delivers improved cycle life compared with that obtained from normal liquid electrolyte (L.E.) by blocking migration of $Mn^{2+}$ ion from the $LiNi_{0.5}Mn_{1.5}O_4$ to the graphite electrodes.

## 3.4 Conclusion

The MEC successfully demonstrated its capability of blocking the migration of $Mn^{2+}$ ions and eliminating the effect of the "Mn dissolution" problem on the cell's electrochemical performances. This result instructs that incorporation of a S.E. in the Li-ion battery cell may solve the Mn dissolution problem. In addition, the MEC can provide many benefits as a tool for future electrode/electrolyte interface studies. The following two examples illustrate the potential benefits: a) Control and analyze the oxidative or reductive interfacial reactions separately in a single battery cell; As the cell is capable of employing different electrolytes at each electrode side with the S.E. barrier, one can examine the effect of electrolyte compositions or additives on the electrode/electrolyte interface for one side while maintaining the other side as a control sample. b) Investigation of high voltage positive electrode materials such as $LiCoPO_4$ and $LiNiPO_4$. As these positive electrodes possess even higher operation voltages than that of $LiNi_{0.5}Mn_{1.5}O_4$, it has been difficult to fully characterize the potential of these positive electrodes due to present electrolyte limitations. From this perspective, ionic liquid or their composite with polymer electrolyte can support such high voltages, but it again suffers below 1.1 $V_{vs.Li}$ due to the failure in generating a stable SEI formation on graphite [121, 122]. The MEC will be a useful tool again because it can adopt the ionic liquid electrolyte or its polymer composite on the positive electrode side while keeping conventional liquid electrolyte on the negative electrode side. As a result, the MEC can contribute to the understanding and improvement of the electrode/electrolyte interfaces through various types of Li-ion battery researches. In addition, the separation of electrodes in multi-layer electrolyte cell allows more choices over existing materials which will be capable of storing the energy more efficiently and producing a higher energy density.

# 4. LITHIUM-LIQUID BATTERY: HARVESTING LITHIUM FROM WASTE LI-ION BATTERIES AND DISCHARGING WITH WATER

## 4.1. Introduction

The increased interest in using renewable energy such as solar and wind has prompted the need to find energy storage systems, to make such energy sources reliable. Many types of energy storage [124-126] systems have been considered such as pumped hydroelectric storage, compressed air energy storage (CAES), flywheels, and electrochemical storage. Depending on the application of the system, each storage design is more suitable either in efficiency, lifetime, discharge time, or in weight or mobility of the system. Among these various energy storage systems, electrochemical storage such as batteries has the advantage of being more efficient compared to pumped hydroelectric and CAES storage [3]. A battery works by directly converting chemical energy to electrical energy by employing different chemistries. A varied combination of anode, cathode and electrolyte materials produces numerous types of batteries such as the Li-ion, Lead-acid, Na-S, and vanadium redox batteries.

Presently, the lithium (Li)-ion rechargeable battery is the most common type of battery used in consumer portable electronics due to its high energy density per weight or volume and its good recharge efficiency. However, the Li-ion battery for use in stationary energy storage applications is limited by cost and safety concerns. The cheapest rechargeable batteries are lead-acid batteries. Their efficiency is somewhere between 75-85% with a 15-25% loss of DC electric current from recharge to discharge [126, 127]. Sodium-sulfur (NaS) batteries are not well-known, but they have a high energy density and efficiency around 76% [126, 128]. However, NaS batteries are not

feasible for portable electric devices because they do not come in smaller sizes and only operate efficiently at high temperatures. However, the NaS batteries are economical and efficient for large installations. Another type of rechargeable battery for stationary energy storage applications is the flow battery. It stores electrolytes in tanks, therefore having a flexible energy capacity depending on how many electrolyte tanks one connects to the power input/output unit. The best known and widely applied flow battery is the vanadium redox battery (VRB) [129]. Even though the efficiency of the battery is relatively better than other types of energy storage devices, current battery technology is still considered too expensive for stationary storage. For renewable energy to be stored without government subsidy, the storage process must be kept below $200 per kilowatt [130]. Thus, to meet the increasing demand to store large amounts of electric energy for stationary applications, one must develop a viable battery technology that, as the battery increases in size, it decreases in cost per unit energy and amount of power stored.

Here, we propose the use of waste Li-ion batteries and water for both electrodes in a Li-liquid battery system. This study shows that the Li metal can be harvested from the waste Li-ion batteries, and the harvested Li metal can be discharged with the use of water as the cathode to produce electric energy. This concept can be extended to a Li-liquid flow battery for a large energy storage system (see Figure 4.1) where the discharge and charge parts are separated (via multi-layer electrolyte strategy) to allow for more choices of materials to efficiently store and produce the energy at a low cost. In the charging system, the Li metal is harvested by charging the cell and drawing from one of the following three sources: (a) using waste Li-ion battery materials containing Li ions such as the graphite anode $Li_xC_6$, cathodes made of $Li_xFePO_4$ or $Li_xCoO_2$, or the organic liquid electrolyte, 1M $LiPF_6$ in EC:DEC, (b) using the discharged products such as LiOH (aq) created by discharging the battery, or (c) collecting Li from both sources simultaneously. Charging the cell using renewable energy sources such as wind and solar power, the renewable energies are stored by the formation of the Li metal. As for the discharging system, water and other liquid solutions containing aqueous or non-aqueous solvents can be used as cathodes with the harvested lithium metal as the anode.

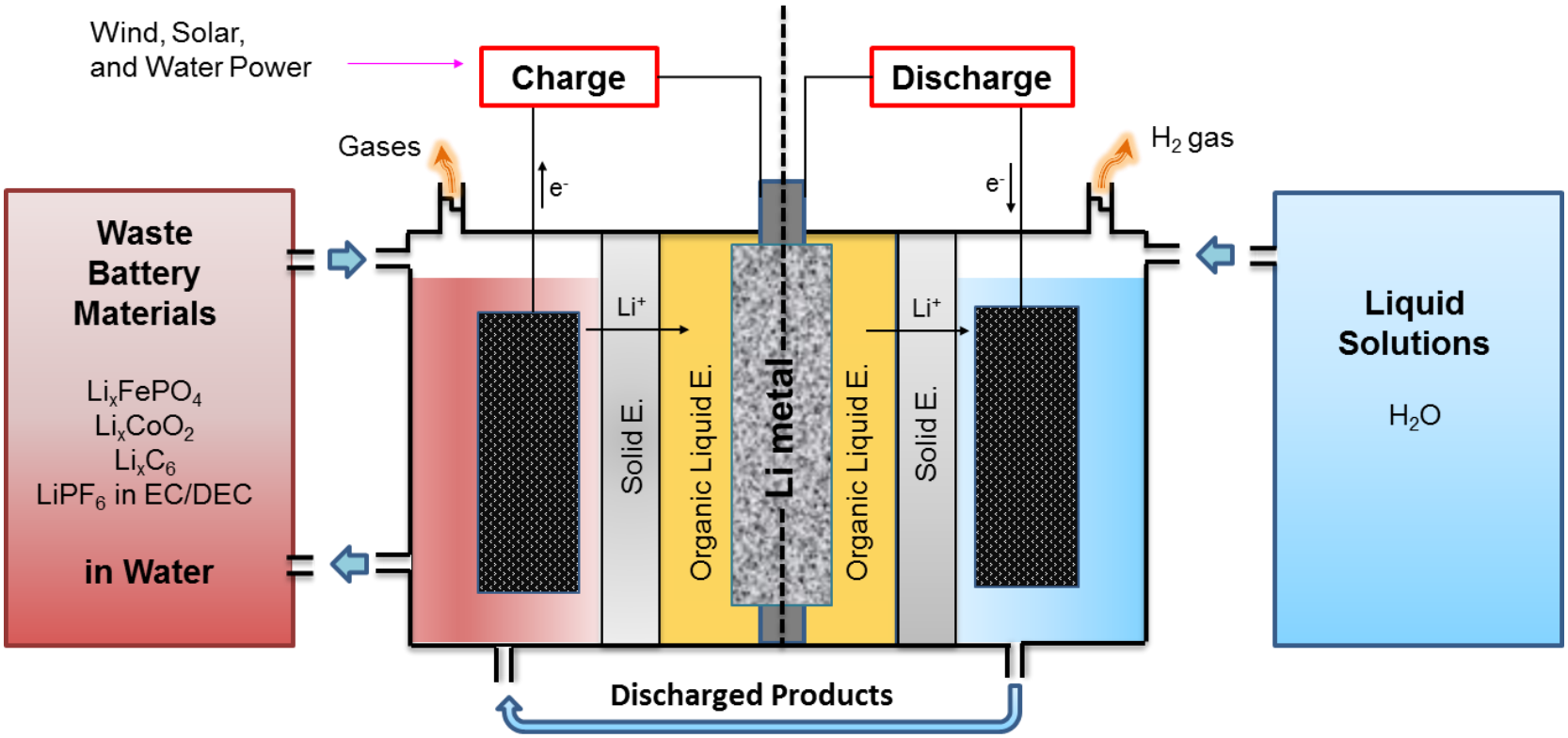


Figure 4.1 Schematic diagram of a Li-liquid battery system that uses waste battery materials and water as both electrodes. Li metal can be harvested electrochemically from a waste Li-ion battery containing Li-ion source materials from the battery's anode, cathode, and electrolyte. The harvested Li metal in the battery system can be discharged to produce the electricity by using water as the cathode. With further development of other technologies including the solid electrolyte and overall system design, this concept of the battery system could possibly be used as a stationary energy storage device. If the system is charged from renewable energy sources, the renewable energy sources are stored by this formation of Li metal in the system.

## 4.2. Experimental Methods

### 4.2.1. Chemicals

A Lithium ribbon (99.9%) with 0.38 mm thickness was purchased from Sigma Aldrich, and disks, each with a 0.8 cm diameter, were cut for use as the anode. 1M $LiPF_6$ in ethylene carbonate (EC): dimethyl carbonate (DMC) (1:1 volume ratio) was purchased from Novolyte Corp for use as an organic non-aqueous liquid electrolyte. As a solid electrolyte, the Li-ion-conducting glass ceramic plate, $Li_{1+x+y}Ti_{2-x}Al_xP_{3-y}Si_yO_{12}$ (LTAP), measuring 1 inch × 1 inch with a 150 μm thickness and a $\sigma_{Li} \approx 10^{-4}$ S/cm at room temperature, was purchased from OHARA, Inc. The solid electrode powders used in this study such as $LiFePO_4$, and $C_6$ were purchased from MTI Corporation. SUPER P carbon black (TIMCAL) was used as the electronic conductive powders for the solid and liquid electrodes. The carbon paper with 280 μm thickness purchased from Fuel Cell Store, Inc. was used as the current collector for liquid solutions.

### 4.2.2. Fabrication of the Multilayer Electrochemical Cell

Figure 4.2 shows a schematic diagram of the laboratory-sized battery cell that is designed for testing a small amount (≤ 5 mL) of liquids as cathodes. In order to prevent the two liquids from mixing, the open side of the polypropylene bar containing the Li metal anode and 1M $LiPF_6$ in EC:DMC liquid electrolyte is completely sealed from the cathode compartment by a dense ceramic solid electrolyte. The solid electrolyte plate was first placed on the top of the anode part of the cell and sealed by epoxy. The sealing of the anode part by the solid electrolyte must be done carefully to protect the Li metal from exposure to a highly oxidizing cathode environment. Otherwise, proper data cannot be obtained from the samples being investigated.

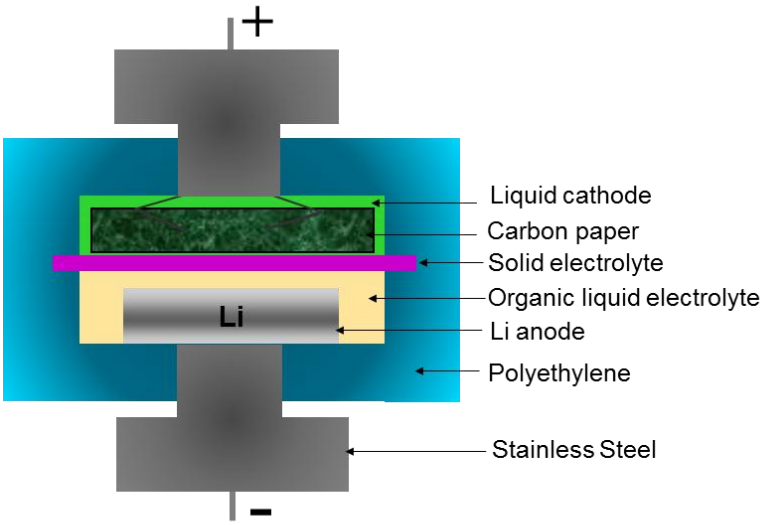


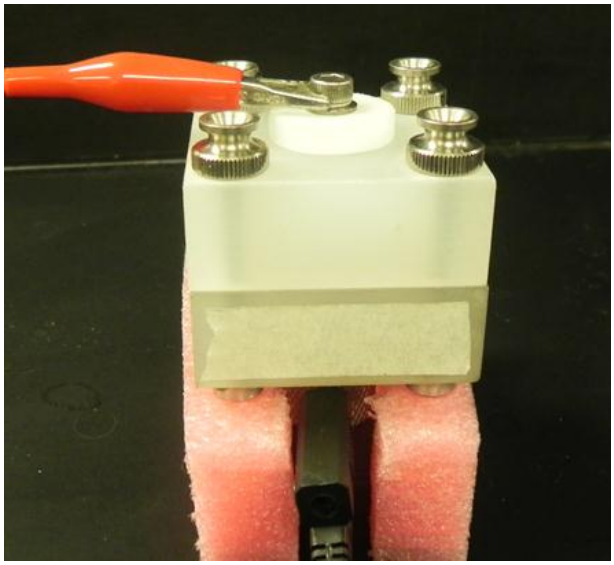

Figure 4.2 Schematic diagram of the cell designed for testing a liquid as the cathode with Li metal as the anode. The image shows the fully assembled cell under test

Then the sealed anode part was placed in an argon filled glove box where the water and oxygen concentrations were maintained at less than 4 ppm. The Li metal disk and a non-aqueous electrolyte, 1 M $LiPF_6$ in EC:DMC, were loaded into the anode part inside the glove box. After assembling the anode part, the assemblage was moved out of the glove box. The liquid cathode was poured into the cathode part of the cell. Then the carbon paper to be used as the current collector was placed over the liquid. The assembled battery cell was then connected to the testing station. A Solartron 1470 cell tester was used to perform the charge and discharge tests.

### 4.2.3. Assembly of the Liquid Electrolyte Cell

The electrodes for the pure liquid electrolyte cell were fabricated from a 70:20:10 (wt%) mixture of active material, Super P carbon (Cnergy) as current conductor, and polytetrafluoroethylene (G-580, ICI) as binder. The active material and conductor were mixed completely, and then the polytetrafluoroethylene was added in, and all three were mixed together. The mixture was rolled into thin sheets and punched into 7-mm-diameter circular disks as electrodes. The typical electrode mass and thickness were 5–10 mg and 0.03–0.08 mm. The electrochemical cells were prepared in standard 2016 coin-cell hardware with lithium metal foil used as both the counter and reference electrodes. The electrode disks and cells were prepared in an argon glove box along with the electrolyte used for analysis, 1M $LiPF_6$ in a 1:1 EC:DMC. A Solartron 1470 cell tester was used to perform the charge and discharge tests.

## 4.3. Results and Discussion

### 4.3.1. Multilayer Electrolyte Strategy

The key strategy in this research lies in the use of a multi-layer electrolyte. The multi-layer electrolyte consists of one liquid electrolyte and one solid electrolyte as shown in Figure 4.3. The organic, liquid electrolyte is used because, as a liquid, it creates close physical contact with the solid lithium anode. Although the lithium metal reduces the 1M $LiPF_6$ in EC:DEC liquid electrolyte by the direct contact, the formation of a solid electrolyte interface (SEI) layer on the surface of the Li metal allows Li to be used as the anode with the organic liquid electrolyte. The solid electrolyte is an inorganic solid that separates the two liquids (liquid electrolyte and liquid cathode), and prevents mixing of the liquids while also making it possible to use a cathode in all three phases (solid, liquid, and gas). The solid electrolyte, $Li_{1+x+y}Ti_{2-x}Al_xP_{3-y}Si_yO_{12}$ (from OHARA), is commercially available with an area of 1 inch × 1 inch, 150 μm thickness, and $\sigma_{Li} \approx 10^{-4}$ S/cm at room temperature. The relatively low Li-ion conductivity of the solid electrolyte can limit the electrochemical performance of the liquid cathodes when a high current discharge or charge is applied. Hence, in this experiment, a low current rate of 0.1 $mA/cm^2$ was applied to minimize the effect of the cell resistance on the voltage of materials being investigated.

The $Li_{1+x+y}Ti_{2-x}Al_xP_{3-y}Si_yO_{12}$ solid electrolyte is not stable at a low voltage range because the $Ti^{4+}$ in its structure can be reduced to $Ti^{3+}$ at 2.4 V versus $Li^+/Li^0$ by accepting electrons from the current collector. Figure 4.3(a) shows that the discharge voltage curve of the Li insertion into the $Li_{1+x+y}Ti_{2-x}Al_xP_{3-y}Si_yO_{12}$ sample was observed at 2.4 V vs. $Li^+/Li^0$ at the rate of 0.05 $mA/cm^2$, where it is compared to the discharge voltage curve of the $LiTi_2(PO_4)_3$ sample. The voltage relative to Li metal of Li intercalation solid compounds corresponds to the energy relative to $Li^+/Li^0$ of the redox couple energy of a transition-metal cation [1]. Hence, it is believed that the energy band

of the $Ti^{4+}/Ti^{3+}$ redox couple in the $Li_{1+x+y}Ti_{2-x}Al_xP_{3-y}Si_yO_{12}$ sample is located at 2.4 eV below the Fermi energy $E_F$ of Li metal, which also corresponds to the Lowest Unoccupied Molecular Orbital (LUMO) of the solid electrolyte as shown in Figure 4.3(b). However, the use of a polyanion $(PO_4)^{3-}$ in place of an oxide ion in the phosphate materials can lower the top of the O-2p bands to below 5.0 eV below $E_F$ of $Li^0$ [1], which corresponds to the Highest Occupied Molecular Orbital (HOMO) of the solid electrolyte.

By using a solid electrolyte with a lower HOMO in the cathode side, there is greater flexibility in choosing cathodes that produce voltages above 4.5 V. This will be an improvement over the small electrochemical window of liquid electrolytes, which are presently used and cannot produce a range beyond 1.0 – 4.5 V vs. $Li^+/Li^0$. In addition, when the anode part of the cell composed of Li metal and the organic liquid electrolyte are completely separated and sealed by the dense solid electrolyte – only providing Li-ion mobility [131, 132], the choices for cathode will be dramatically widened to include solid, liquid, and gas phases. Applying this concept, solid and liquid phases as well as gas phases have been used as cathodes to create different battery systems such as the Li-Ni [133], Li-liquid [132, 134-138], and Li-air [25, 132, 139-141] batteries. Based on these reports, we hypothesized that, by charging the cell, Li metal could be electrochemically collected from any material containing Li-ions. This idea extended to harvesting Li metal from waste Li-ion batteries, in both solid and liquid phases, that contain Li-ion sources such as the $Li_xC_6$ anode, $Li_xFePO_4$ cathode, and $LiPF_6$ in the EC:DEC electrolyte. The harvested Li metal could then be an anode Li-Liquid flow batteries by using water as the cathode.

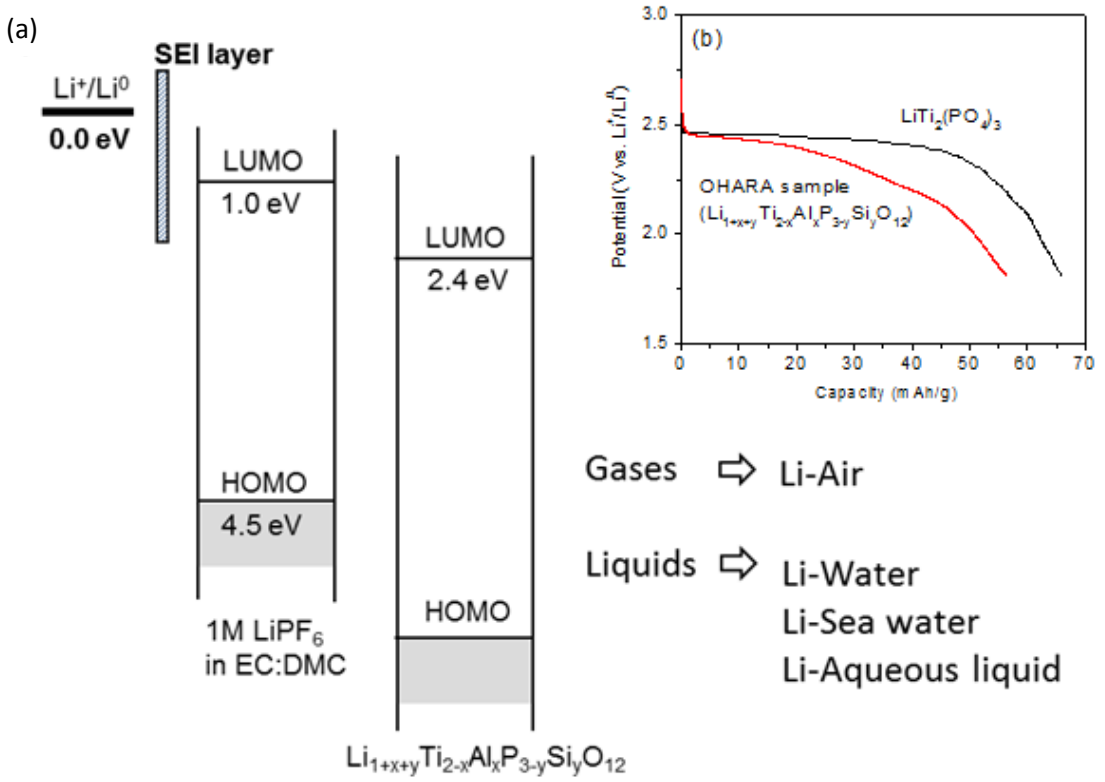


Figure 4.3 This figure represents electrochemical potentials of the multi-layer electrolyte of 1M $LiPF_6$ in EC:DMC / $Li_{1+x+y}Ti_{2-x}Al_xP_{3-y}Si_yO_{12}$. With this electrolyte strategy, the air and liquid phases such as water, sea water, and other liquid solutions can be selected as the cathodes. SEI layer: Solid Electrolyte Interface layer. LUMO: Lowest Unoccupied Molecular Orbital. HOMO: Highest Occupied Molecular Orbital. The inserted figure 3(b) shows the discharge voltages of the solid electrolytes vs. $Li^+/Li^0$ corresponding to 2.4 eV of the LUMO.

### 4.3.2. Li Metal Harvesting from Li Solid and Liquid Phases in Water

Experiments were performed during the charging of the cell to test whether Li-ions could be extracted from lithium solid and liquid phase compounds that were placed in water. Water was selected as a liquid matrix in which the lithium phases were placed (or dissolved) and delivered into the charge section of the proposed Li-Liquid flow battery system (see Figure 4.1). Water was a good choice in this experiment because it is a non-pollutant and inexpensive in most areas.

Solid cathode particles of the $LiFePO_4$ were mixed with carbon black powder, and the mixture was placed in water and ultrasonicated for one hour to produce a homogenous mixture with the water. Then the liquid solution was placed on the carbon paper in the cathode part where the carbon paper absorbed the solution and used it as the current collector. In the anode side, there was no Li metal attached at the initial state of the cell. This means that stainless steel (SS) was used as a negative electrode at the initial state. Figure 4.4 shows the charge curve of the $LiFePO_4$, which were placed in water and mixed with super P powders.

The open circuit voltage was observed to be around 0.4 V vs. stainless steel (SS) electrode for the $LiFePO_4$. When the cell began to charge at 0.1 $mA/cm^2$, the slope curve was observed to start around 0.4 - 3.5 V. This slope could be a result of the activation polarization that arises from kinetics hindrances of charge-transfer reaction taking place at the cathode/electrolyte interface (Li-ions leaving from the cathode particles) and the anode/electrolyte interface (Li forming on the SS electrode). At 3.50 V, after the slope curve, a flat charge voltage appears for the $LiFePO_4$ cathode, which corresponds to the Li extraction from the $Li_{1-x}FePO_4$. This flat voltage is similar in voltage range to that (3.47 V) of the $LiFePO_4$ measured in the coin cell with a Li metal anode and an organic liquid electrolyte, 1M$LiPF_6$ in EC:DMC as shown in Figure 4.4. This result indicates that the charge voltage curve of the cathode particle is not affected by the use of the solid electrolyte when a low current rate of the 0.1 $mA/cm^2$ is applied. The Li extraction from the $LiFePO_4$ particles in aqueous electrolytes were reported in the literature [142], but $LiTi_2(PO_4)_3$ was used as the anode for the $LiFePO_4$ cathode due to the small electrochemical window of aqueous electrolytes.

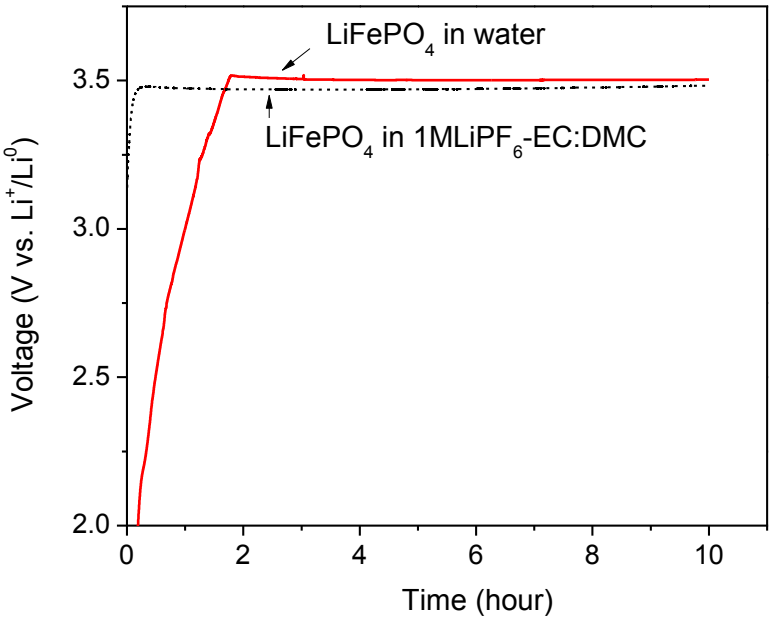


Figure 4.4 (a) Charge voltage curve of the $LiFePO_4$ in the pure DI water and compared with the charge voltage curve of the $LiFePO_4$ tested in the coin cell where the Li metal anode and the organic liquid electrolyte, 1M $LiPF_6$ in EC:DMC are used. They are measured at the current rate of 0.1 $mA/cm^2$.

Graphite ($C_6$) is the most common anode for present Li-ion batteries. When a waste Li-ion battery contains a lithiated graphite ($Li_xC_6$) anode, it would be another potential Li-ion source for the Li metal harvesting system. $Li_xC_6$ is prepared by electrochemical insertion of Li-ions into the $C_6$ inside the coin cell that uses Li metal as the negative electrode. Figure 4.5(a) shows the typical discharge and charge curves of the graphite versus Li metal electrode. When the graphite is fully discharged, it becomes $LiC_6$. After disassembling the cell, the $LiC_6$ powder (0.016 mg) is collected and transferred into the water (1.9 g). The aggressive exothermal reaction with the production of gas is observed, similar to that of Li metal in water (see equation (2)). Because the Fermi energy of the $LiC_6$ is only 0.2 eV below the Fermi energy of Li metal [1], the $LiC_6$ is also a very reducing agent. This means that the $LiC_6$ would decompose $H_2O$ and subsequently form LiOH when it is added to water. After the addition of the

$LiC_6$ into the pure DI water, the pH increases to ~12 from 7, which indicates that the pure DI water becomes a strong alkali aqueous solution due to the formation of the LiOH. This reaction is also supported by the literature [143], which reports that LiOH forms on the surface of the $LiC_6$ anode by adding $H_2O$ into the $LiClO_4$ in PC electrolyte in the battery cell.

Figure 4.5(b) shows the charge voltage curve of the $LiC_6$ placed in water. The flat voltage curve is observed at 3.8 V. This corresponds to the Li extraction from LiOH (aq) formed by the reaction of $Li_xC_6$ with water. To support this hypothesis, 0.1M LiOH aqueous liquid solution was prepared and charged at the same experimental condition as shown in Figure 4.5(b). The flat charge voltage curve appeared at 4.0 V with the chemical reaction below.

$$4LiOH\ (aq) \rightarrow 4Li\ (s) + 2H_2O\ (l) + O_2\ (g)$$

This is similar to what was observed (3.8 V) when the $LiC_6$ was placed in water. The slight voltage difference could be due to the difference of the LiOH mole concentration or chemical compounds formed in the liquid solution, which could affect Li-ion and electron conductivity of the liquid matrix.

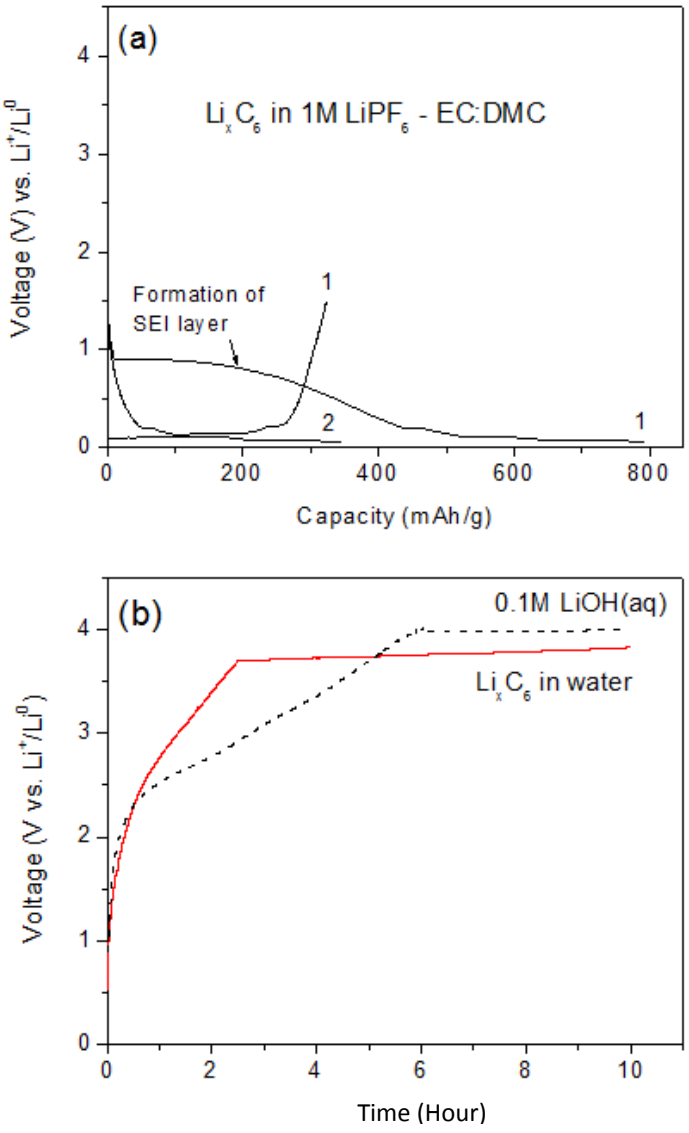


Figure 4.5 (a) Discharge and charge voltage curves of the $Li_xC_6$ in the 1M $LiPF_6$ in EC:DMC and (b) Charge voltage curves of $Li_xC_6$ in the pure DI water and compared with that of 0.1M LiOH (aq). They are measured at the current rate of 0.1 mA/cm$^2$.

In addition to the anode and cathode materials, electrolytes could be another Li-ion source for the Li metal harvesting system. Li-ions can be collected from a pure organic liquid electrolyte by charging the cell at voltage higher than 4.5 V vs. $Li^+/Li^0$. The oxidation voltage of the pure organic liquid electrolytes was reported at >4.5 V vs. $Li^+/Li^0$ in the literature [32]. Our measurement (Figure 4.6) also showed that pure liquid

electrolyte 1M $LiPF_6$ in EC:DMC is oxidized at 5.3 V vs. $Li^+/Li^0$ at the current rate of 0.1 $mA/cm^2$, where Li-ions are transferred into the anode side and form Li metal. Interestingly, when the organic liquid electrolyte 1M $LiPF_6$ in EC:DMC was mixed with water in a volume ratio of 1:1, the charge voltage curve was observed at about 3.7 V vs. $Li^+/Li^0$ at 0.1 $mA/cm^2$ as shown in Figure 4.6. This charge voltage is significantly lower than 5.3 V of the pure liquid electrolyte. Since the redox reaction in the liquid solution is affected by the chemistry of solvents and salts [144], the new chemical compounds formed by the reaction of the liquid electrolyte with water would be responsible for the low charge voltage of 3.7 V.

Indeed, the reaction of the $LiPF_6$ organic electrolyte with water has been intensively investigated [145-147] because water content in the liquid electrolyte is detrimental to the Li-ion battery. However, it is impossible to completely eliminate water from the liquid electrolyte. The mechanism for the reaction between the organic $LiPF_6$ liquid electrolyte and water is very complex and has not been clearly identified yet. This reaction was reported to occur with the formation of many chemicals compounds such as LiF, HF, $PF_5$, $POF_3$, $POF_2(OH)$, and LiOH [145-147]. In addition, the degree of electrolytic dissociation must be considered during the reaction between the $LiPF_6$ liquid electrolyte and water [147]. It would be challenging to identify the precise Li extraction mechanism of the mixed liquid solution (water + non-aqueous liquid electrolyte) that corresponds to the charged voltage of 3.7 V observed in this experiment at this moment.

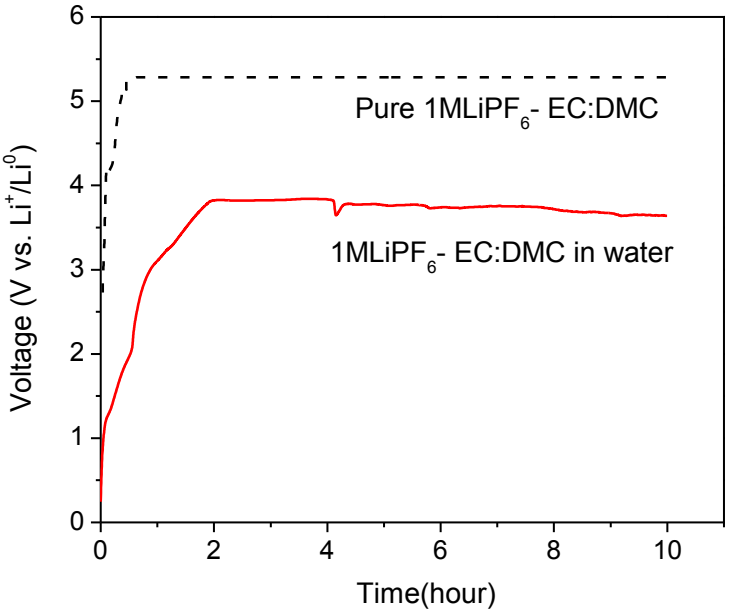


Figure 4.6 Charge voltage curves of 1M $LiPF_6$ -EC:DMC in the pure DI water and compared with that of the pure 1M $LiPF_6$ -EC:DMC. They are measured at the current rate of 0.1 $mA/cm^2$.

Due to the low oxidation voltage of organic liquid electrolytes with moisture content, tremendous efforts have been made in the research laboratory and battery company to keep the organic liquid electrolyte in a water free atmosphere. In contrast, this low oxidation voltage of the mixed liquid or water contaminated organic liquid electrolyte will be advantage for the Li metal harvesting system because a less energy is needed to collect Li metal from the liquid electrolytes that undergo changes in their chemical compositions and phases in the presence of water.

### 4.3.3. Li Harvesting from Waste Li-ion Batteries

We tested the harvesting of Li metal from waste Li-ion batteries by attempting to collect Li metal from a Li-ion battery that uses the graphite anode, $LiFePO_4$ cathode, and organic liquid electrolytes. The Li-ion battery was disassembled. Then the whole

disassembled battery including the anode, cathode, polymer separator, and organic liquid electrolytes were placed in water and stirred or ultrasonicated to collect electrode powders and electrolytes containing Li-ions. After removing the current collector and separator, only the liquid solution containing electrode powders and the liquid electrolyte remained as shown in Figure 4.7(a). That liquid solution was then placed on carbon paper in the cathode part (see Figure 4.2) and charged with a bare stainless steel (SS) electrode (instead of using a Li metal electrode). Figure 4.7(b) shows the charge voltage curves of the liquid solution containing all of the $Li_xC_6$, $Li_xFePO_4$, and organic liquid electrolyte at once. Li metal was observed on the surface of the SS electrode as shown in Figure 4.7(c) after disassembling the cell. The aggressive reaction producing exothermal heat was observed when the SS electrode was placed in the water, which is another confirmation of the formation of Li metal.

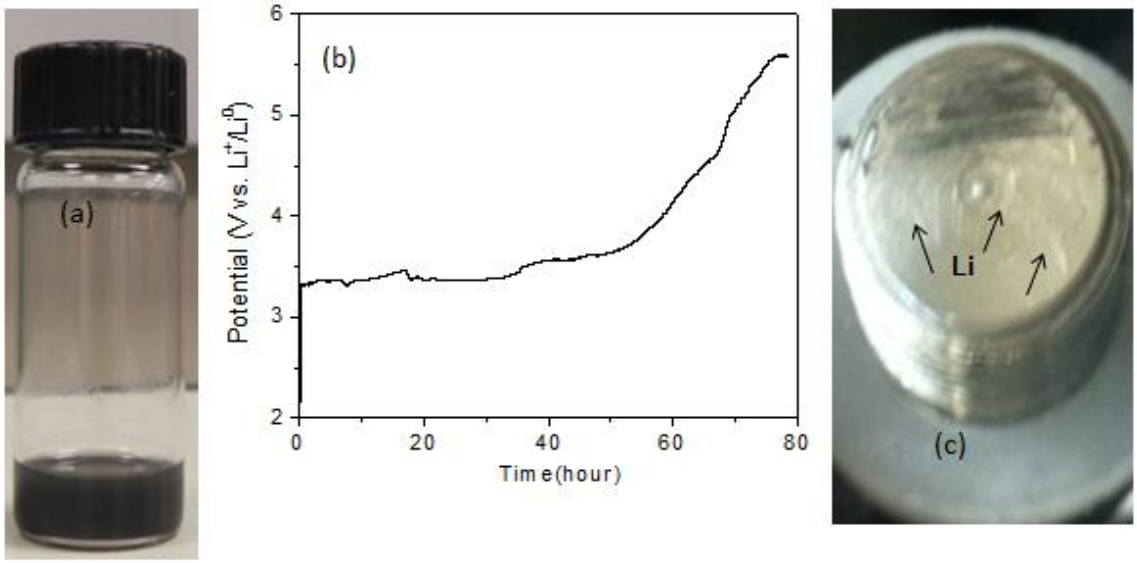


Figure 4.7 (a) Waste Li-ion battery materials in water, including $Li_xC_6$, $Li_xFePO_4$, and $LiPF_6$ in EC:DEC. (b) Charge voltage curve at $0.1mA/cm^2$ of the liquid solution shown in (a). (c) Li metal observed on the surface of a stainless steel (SS) electrode; the bare SS electrode was used before charging the battery.

Also confirming the formation of Li metal on the SS electrode, the charged cell (which collected Li metal from waste battery materials) was discharged when pure DI water was used as the cathode. Figure 4.8 shows the discharge voltage curve of the pure DI water versus Li metal harvested from the waste batteries. The mean discharge voltage appears to be about 2.7 V vs. $Li^+/Li^0$ at 0.1 mA/cm$^2$, which is similar to the voltage found when fresh Li metal was used in the cell. The following chemical reaction occurs during discharge of the Li-water cell [148].

$$2Li\ (s) + 2H_2O\ (l) \rightarrow 2LiOH\ (aq) + H_2\ (g)$$

The discharged products are LiOH dissolved in water and $H_2$ gas. The LiOH (aq) can be used as the cathode. Figure 4.5 (b) shows that the 0.1M LiOH liquid solution was charged at 4.0 V vs. $Li^+/Li^0$. However, it was reported that the solid electrolyte $Li_{1+x+y}Ti_{2-x}Al_xP_{3-y}Si_yO_{12}$ is not stable with a strong alkali and acidic aqueous solutions for a long time period [54, 139, 141, 149]. The solid electrolyte $Li_{1+x+y}Ti_{2-x}Al_xP_{3-y}Si_yO_{12}$ is currently the only commercially available glass ceramic plate for now. This plate allows one to test many new liquid solutions as the potential cathodes for the Li-liquid battery [132, 134-138]. However, the discovery of a solid electrolyte that is chemically stable with both Li metal and aqueous solutions is required for the further development of the Li-liquid battery based on the concept of the multilayer electrolyte strategy.

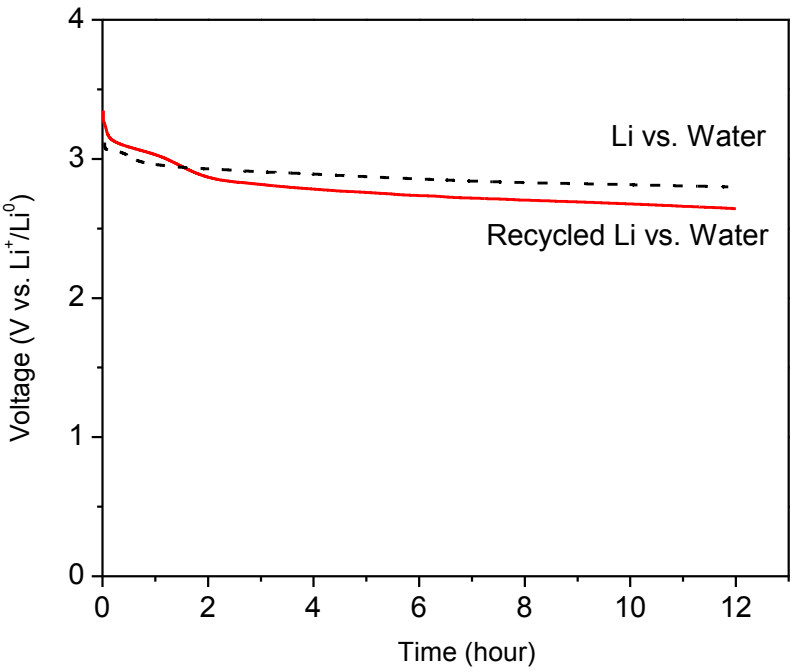


Figure 4.8 Discharge voltage curves at 0.1 mA/cm$^2$ when using a cathode of pure DI water and an anode of Li metal harvested from waste Li-ion batteries, compared to the discharge voltage curve when using an anode of fresh Li metal.

The electrochemical performance of the Li-liquid flow battery including discharge-charge voltage, voltage efficiency, and rate capability could be improved by increasing the electronic and Li-ion conductivities of the liquid solutions. As an electronic conductive powder, Super P carbon black (TIMCAL Ltd.), with 62 m$^2$/g of the specific BET surface area, was used in this experiment, but other carbon powders with different sizes and physical properties will be tested in the future. Since functionalized carbon powders are reported to have a good dispersion character in water [150], this approach may improve the charge efficiency of the battery by providing better electronic conductivity between waste materials in water. Li-ion conductivity in the liquid solution could also be improved by adding lithium salts such as $LiNO_3$, $LiClO_4$, and $Li_2SO_4$. The

addition of more waste organic liquid electrolyte may be another good strategy for improving the Li-ion conductivity in the liquid solution because it contains lithium salts such as $LiPF_6$ or $LiBF_4$.

## 4.4. Conclusion

The purpose of this study was to demonstrate the feasibility of developing a Li-liquid battery system that uses waste Li-ion batteries as a source of Li metal and that discharges with water, producing electricity. The use of the multilayer electrolyte strategy in this battery system made it possible to collect Li metal electrochemically from solid and liquid phase lithium compounds found in waste Li-ion batteries. This study further demonstrated that the harvested Li metal from waste Li-ion batteries could be used to form the anode in the battery system, producing 2.7 V at 0.1 $mA/cm^2$ when water was used as the cathode.

Although this study is in its early stages, the concept of using waste Li-ion batteries and water for the electrodes in a battery system is attractive for a large size energy storage application because it dramatically decreases the cost of electrode materials. With further development of the other parts of the system including the solid electrolyte, current collector, and overall system design, the Li-liquid flow battery system is a promising strategy for stationary energy storage of renewable energy sources.

# 5. CONCLUSION

To use lithium ion rechargeable batteries in transportation applications, further development is required; current batteries are too valuable to be wasted and also hundred pounds of batteries need to be employed to store the energy produced by a gallon of gas. Increment of the energy density of the lithium based energy storage devices is required for the advance development of future devices. Higher operation voltage of electrodes is one of the approaches which lead us to develop the batteries with higher energy density. Before any further improvement in this aspect, the properties of liquid electrolytes needed to be improved. The electrolyte required to provide stable and safe environment with both electrodes at the same time and be able to deliver high ionic conductivity for faster movement of lithium ions. Also, to employ higher voltages electrodes, electrolytes with wider electrochemical windows should be developed.

According to the literature review provided in the first chapter of this thesis, there is no reported single electrolyte by now which can satisfy all these properties. Although solid electrolytes have better performance over liquid electrolytes used for commercial lithium ion batteries, they are suffering from lower rate capability, low ionic conductivity, interfacial instability, and low loading of active materials; efforts to improve the interface resistance between solid electrode and solid electrolyte is quite challenging for investigators.

To understand if the performance degradation of all-solid-state batteries is resulted from the interface resistance, they were performed in second chapter. Initially, all-solid-state cell was assembled and cycling degradation was observed. Then a very

small amount of liquid electrolyte, just enough to make good contact between the solid electrolyte and the solid electrode, was added within the interface points to adjust the volume change during cycling of the cells. The constructed hybrid cell provided better performance and higher lithium ion conductivity in compare with the pure solid one. In compared with the pure liquid electrolyte cells, hybrid cell provided larger first charge capacity and small amount of its capacity fades in the following cycles. Finally, the self-safety behavior of the device was observed when sudden, higher temperatures were applied to it. Based on this study many types of hybrid electrolytes can be chosen from a combination of lithium ion conducting inorganic solids and liquids, which could be an alternative strategy to the one-phase electrolyte that struggles to enhance the electrochemical performance of current Li battery technology.

Penetration of dissolved electrode components in liquid electrolyte and observed results from the first study leads to develop a multilayer electrolyte cells. The cell was designed to hold electrodes separated and sealed from each other with a ceramic solid electrolyte. The designed cell went through few experiments to demonstrate their compatibility with current common devices for lithium ion batteries. Also, the same performance of the same electrodes was observed with different multilayer electrolyte loaded into the cell. Moreover, the high voltage cathode material of $LiNi_{0.5}Mn_{1.5}O_4$ as an example for next generation rechargeable batteries for electric vehicles was tested in the cell and significant improvement in cycle life was observed. These results prove that the performance degradation of this material is resulted from the dissolution of electrode components in the liquid electrolyte. The Multilayer electrolyte strategy is the alternative solution to overcome existence electrolytes problems.

The multilayer electrolyte strategy made it possible to develop new application in this industry to recycle lithium. The Li-liquid battery system is the unique strategy that uses waste Li-ion batteries as a source of Li metal and that discharges with water, producing electricity. Although this study is in its early stages, the concept of using waste Li-ion batteries and water for the electrodes in a battery system is attractive for next

generation rechargeable batteries and a large size energy storage application because it dramatically decreases the cost of electrode materials.

# LIST OF REFERENCES

# LIST OF REFERENCES


[1] J. B. Goodenough and Y. Kim, "Challenges for Rechargeable Li Batteries†," *Chemistry of Materials,* vol. 22, pp. 587-603, 2009.

[2] B. Garcia, S. Lavallée, G. Perron, C. Michot, and M. Armand, "Room temperature molten salts as lithium battery electrolyte," *Electrochimica Acta,* vol. 49, pp. 4583-4588, 2004.

[3] R. Moshtev and B. Johnson, "State of the art of commercial Li ion batteries," *Journal of Power Sources,* vol. 91, pp. 86-91, 2000.

[4] P. G. Bruce, B. Scrosati, and J.-M. Tarascon, "Nanomaterials for Rechargeable Lithium Batteries," *Angewandte Chemie International Edition,* vol. 47, pp. 2930-2946, 2008.

[5] D. H. Jang, Y. J. Shin, and S. M. Oh, "Dissolution of Spinel Oxides and Capacity Losses in 4 V Li/LixMn2O4 Cells," *Journal of The Electrochemical Society,* vol. 143, pp. 2204-2211, 1996.

[6] I. Stassen and G. Hambitzer, "Metallic lithium batteries for high power applications," *Journal of Power Sources,* vol. 105, pp. 145-150, 2002.

[7] G. Halpert, "Past development and the future of nickel electrode cell technology," *Journal of Power Sources,* vol. 12, pp. 177-192, 1984.

[8] E. Markevich, V. Baranchugov, and D. Aurbach, "On the possibility of using ionic liquids as electrolyte solutions for rechargeable 5V Li ion batteries," *Electrochemistry Communications,* vol. 8, pp. 1331-1334, 2006.

[9] M. S. Whittingham, "Lithium batteries and cathode materials," *Chem Rev,* vol. 104, pp. 4271-301, 2004.

[10] A. Nishimoto, M. Watanabe, Y. Ikeda, and S. Kohjiya, "High ionic conductivity of new polymer electrolytes based on high molecular weight polyether comb polymers," *Electrochimica Acta,* vol. 43, pp. 1177-1184, 1998.

[11] T. Ohzuku, Y. Iwakoshi, and K. Sawai, "Formation of Lithium-Graphite Intercalation Compounds in Nonaqueous Electrolytes and Their Application as a Negative Electrode for a Lithium Ion (Shuttlecock) Cell," *Journal of The Electrochemical Society,* vol. 140, pp. 2490-2498, 1993.

[12] Y. Koyama, N. Yabuuchi, I. Tanaka, H. Adachi, and T. Ohzuku, "Solid-State Chemistry and Electrochemistry of LiCo1/3Ni1/3Mn1/3O2 for Advanced Lithium-Ion Batteries: I. First-Principles Calculation on the Crystal and Electronic Structures," *Journal of The Electrochemical Society,* vol. 151, pp. A1545-A1551, 2004.

[13] T. Ohzuku and R. J. Brodd, "An overview of positive-electrode materials for advanced lithium-ion batteries," *Journal of Power Sources,* vol. 174, pp. 449-456, 2007.

[14] G. Amatucci and J.-M. Tarascon, "Optimization of Insertion Compounds Such as LiMn2 O 4 for Li-Ion Batteries," *Journal of The Electrochemical Society,* vol. 149, pp. K31-K46, 2002.

[15] K. Ariyoshi, Y. Iwakoshi, N. Nakayama, and T. Ohzuku, "Topotactic Two-Phase Reactions of Li [ Ni1 / 2Mn3 / 2 ] O 4 ( P4332 ) in Nonaqueous Lithium Cells," *Journal of The Electrochemical Society,* vol. 151, pp. A296-A303, 2004.

[16] A. K. Padhi, K. S. Nanjundaswamy, and J. B. Goodenough, "Phospho-olivines as Positive-Electrode Materials for Rechargeable Lithium Batteries," *Journal of The Electrochemical Society,* vol. 144, pp. 1188-1194, 1997.

[17] H. Huang, S.-C. Yin, and L. F. Nazar, "Approaching Theoretical Capacity of LiFePO4 at Room Temperature at High Rates," *Electrochemical and Solid-State Letters,* vol. 4, pp. A170-A172, 2001.

[18] N. Ravet, J. Goodenough, S. Besner, M. Simoneau, P. Hovington, and M. Armand, "Abstract# 127," in *196th Meeting of the Electrochem. Soc*, 1999.

[19] F. Croce, R. Curini, A. Martinelli, L. Persi, F. Ronci, B. Scrosati, *et al.*, "Physical and chemical properties of nanocomposite polymer electrolytes," *The Journal of Physical Chemistry B,* vol. 103, pp. 10632-10638, 1999.

[20] A. Pradel and M. Ribes, "Lithium chalcogenide conductive glasses," *Materials Chemistry and Physics,* vol. 23, pp. 121-142, 1989.

[21] L. Persi, F. Croce, and B. Scrosati, "A LiTi2O4–LiFePO4 novel lithium-ion polymer battery," *Electrochemistry Communications,* vol. 4, pp. 92-95, 2002.

[22] A. N. Dey and B. P. Sullivan, "The Electrochemical Decomposition of Propylene Carbonate on Graphite," *Journal of The Electrochemical Society,* vol. 117, pp. 222-224, 1970.

[23] C. K. Chan, H. Peng, G. Liu, K. McIlwrath, X. F. Zhang, R. A. Huggins, *et al.*, "High-performance lithium battery anodes using silicon nanowires," *Nat Nanotechnol,* vol. 3, pp. 31-5, 2008.

[24] F. Ronci, P. Reale, B. Scrosati, S. Panero, V. Rossi Albertini, P. Perfetti, *et al.*, "High-Resolution In-Situ Structural Measurements of the Li4/3Ti5/3O4 “Zero-Strain” Insertion Material," *The Journal of Physical Chemistry B,* vol. 106, pp. 3082-3086, 2002.

[25] W.-J. Zhang, "A review of the electrochemical performance of alloy anodes for lithium-ion batteries," *Journal of Power Sources,* vol. 196, pp. 13-24, 2011.

[26] M. Egashira, H. Takahashi, S. Okada, and J.-i. Yamaki, "Measurement of the electrochemical oxidation of organic electrolytes used in lithium batteries by microelectrode," *Journal of Power Sources,* vol. 92, pp. 267-271, 2001.

[27] K. Hayashi, Y. Nemoto, S.-i. Tobishima, and J.-i. Yamaki, "Mixed solvent electrolyte for high voltage lithium metal secondary cells," *Electrochimica Acta,* vol. 44, pp. 2337-2344, 1999.

[28] X. Zhang, R. Kostecki, T. J. Richardson, J. K. Pugh, and P. N. Ross, "Electrochemical and Infrared Studies of the Reduction of Organic Carbonates," *Journal of The Electrochemical Society,* vol. 148, pp. A1341-A1345, 2001.

[29] H. Ye, J. Huang, J. J. Xu, A. Khalfan, and S. G. Greenbaum, "Li ion conducting polymer gel electrolytes based on ionic liquid/PVDF-HFP blends," *Journal of the Electrochemical Society,* vol. 154, pp. A1048-A1057, 2007.

[30] C. Sirisopanaporn, A. Fernicola, and B. Scrosati, "New ionic liquid-based membranes for lithium battery application," *Journal of Power Sources,* vol. 186, pp. 490-495, 2009.

[31] J. Cho and M. Liu, "Preparation and electrochemical properties of glass-polymer composite electrolytes for lithium batteries," *Electrochimica Acta,* vol. 42, pp. 1481-1488, 1997.

[32] K. Xu, "Nonaqueous Liquid Electrolytes for Lithium-Based Rechargeable Batteries," *Chemical Reviews,* vol. 104, pp. 4303-4418, 2004.

[33] R. Imhof and P. Novák, "Oxidative Electrolyte Solvent Degradation in Lithium-Ion Batteries: An In Situ Differential Electrochemical Mass Spectrometry Investigation," *Journal of The Electrochemical Society,* vol. 146, pp. 1702-1706, 1999.

[34] R. Fong, U. von Sacken, and J. R. Dahn, "Studies of Lithium Intercalation into Carbons Using Nonaqueous Electrochemical Cells," *Journal of The Electrochemical Society,* vol. 137, pp. 2009-2013, 1990.

[35] R. Yazami, "Surface chemistry and lithium storage capability of the graphite–lithium electrode," *Electrochimica Acta,* vol. 45, pp. 87-97, 1999.

[36] M. C. Smart, K. A. Smith, R. V. Bugga, and L. D. Whitcanack, *Electrolytes for Wide Operating Temperature Range Li-Ion Cells,* 2008.

[37] V. R. Koch, L. A. Dominey, C. Nanjundiah, and M. J. Ondrechen, "The Intrinsic Anodic Stability of Several Anions Comprising Solvent-Free Ionic Liquids," *Journal of The Electrochemical Society,* vol. 143, pp. 798-803, 1996.

[38] Y. Wang, K. Zaghib, A. Guerfi, F. F. C. Bazito, R. M. Torresi, and J. R. Dahn, "Accelerating rate calorimetry studies of the reactions between ionic liquids and charged lithium ion battery electrode materials," *Electrochimica Acta,* vol. 52, pp. 6346-6352, 2007.

[39] L. Zinck, M. Borck, C. Ripp, and G. Hambitzer, "Purification process for an inorganic rechargeable lithium battery and new safety concepts," *Journal of Applied Electrochemistry,* vol. 36, pp. 1291-1295, 2006.

[40] J. B. Bates, N. J. Dudney, B. Neudecker, A. Ueda, and C. D. Evans, "Thin-film lithium and lithium-ion batteries," *Solid State Ionics,* vol. 135, pp. 33-45, 2000.

[41] J. Trevey, J. S. Jang, Y. S. Jung, C. R. Stoldt, and S.-H. Lee, "Glass–ceramic Li2S–P2S5 electrolytes prepared by a single step ball billing process and their application for all-solid-state lithium–ion batteries," *Electrochemistry Communications,* vol. 11, pp. 1830-1833, 2009.

[42] A. Hayashi, "Development of new glassy materials for all-solid-state lithium secondary batteries: a review," *Glass Technology - European Journal of Glass Science and Technology Part A,* vol. 49, pp. 213-220, 2008.

[43] T. Minami, A. Hayashi, and M. Tatsumisago, "Recent progress of glass and glass-ceramics as solid electrolytes for lithium secondary batteries," *Solid State Ionics,* vol. 177, pp. 2715-2720, 2006.

[44] Y. Wang, Z. Liu, F. Huang, J. Yang, and J. Sun, "A Strategy to Improve the Overall Performance of the Lithium Ion-Conducting Solid Electrolyte Li0.36La0.56-0.08Ti0.97Al0.03O3," *European Journal of Inorganic Chemistry,* vol. 2008, pp. 5599-5602, 2008.

[45] Z. Liu, F. Huang, J. Yang, B. Wang, and J. Sun, "New lithium ion conductor, thio-LISICON lithium zirconium sulfide system," *Solid State Ionics,* vol. 179, pp. 1714-1716, 2008.

[46] J. Ibarra, A. Várez, C. León, J. Santamaría, L. M. Torres-Martínez, and J. Sanz, "Influence of composition on the structure and conductivity of the fast ionic conductors La2/3−xLi3xTiO3 (0.03≤x≤0.167)," *Solid State Ionics,* vol. 134, pp. 219-228, 2000.

[47] Y. Maruyama, H. Ogawa, M. Kamimura, S. Ono, and M. Kobayashi, "Dynamical properties and electronic structure of (LaLi)TiO3; conductors," *Ionics,* vol. 14, pp. 357-361, 2008.

[48] O. Bohnke, "The fast lithium-ion conducting oxides Li3xLa2/3−xTiO3 from fundamentals to application," *Solid State Ionics,* vol. 179, pp. 9-15, 2008.

[49] R. Jimenez, A. Varez, and J. Sanz, "Influence of octahedral tilting and composition on electrical properties of the Li0.2−xNaxLa0.6TiO3 (0≤x≤0.2) series," *Solid State Ionics,* vol. 179, pp. 495-502, 2008.

[50] J. Percival, D. Apperley, and P. R. Slater, "Synthesis and structural characterisation of the Li ion conducting garnet-related systems, Li6ALa2Nb2O12 (A=Ca, Sr)," *Solid State Ionics,* vol. 179, pp. 1693-1696, 2008.

[51] Y. Zou, N. Inoue, K. Ohara, V. Thangaduri, and W. Weppner, "Structure and lithium ionic conduction of B-site Al-ion substitution in La4/3-yLi3yTi2O6," *Ionics,* vol. 10, pp. 463-468, 2004.

[52] B. Kumar, D. Thomas, and J. Kumar, "Space-Charge-Mediated Superionic Transport in Lithium Ion Conducting Glass–Ceramics," *Journal of The Electrochemical Society,* vol. 156, pp. A506-A513, 2009.

[53] J. S. Thokchom and B. Kumar, "The effects of crystallization parameters on the ionic conductivity of a lithium aluminum germanium phosphate glass–ceramic," *Journal of Power Sources,* vol. 195, pp. 2870-2876, 2010.

[54] S. Hasegawa, N. Imanishi, T. Zhang, J. Xie, A. Hirano, Y. Takeda, *et al.*, "Study on lithium/air secondary batteries—Stability of NASICON-type lithium ion conducting glass–ceramics with water," *Journal of Power Sources,* vol. 189, pp. 371-377, 2009.

[55] M. Marzantowicz, J. R. Dygas, F. Krok, A. Tomaszewska, Z. Florjańczyk, E. Zygadło-Monikowska, *et al.*, "Star-branched poly(ethylene oxide) LiN(CF3SO2)2: A promising polymer electrolyte," *Journal of Power Sources,* vol. 194, pp. 51-57, 2009.

[56] X. Yu, J. B. Bates, G. E. Jellison, and F. X. Hart, "A Stable Thin-Film Lithium Electrolyte: Lithium Phosphorus Oxynitride," *Journal of The Electrochemical Society,* vol. 144, pp. 524-532, 1997.

[57] K. Takada, T. Inada, A. Kajiyama, H. Sasaki, S. Kondo, M. Watanabe, *et al.*, "Solid-state lithium battery with graphite anode," *Solid State Ionics,* vol. 158, pp. 269-274, 2003.

[58] M. Singh, O. Odusanya, G. M. Wilmes, H. B. Eitouni, E. D. Gomez, A. J. Patel, *et al.*, "Effect of Molecular Weight on the Mechanical and Electrical Properties of Block Copolymer Electrolytes," *Macromolecules,* vol. 40, pp. 4578-4585, 2007.

[59] E. D. Gomez, A. Panday, E. H. Feng, V. Chen, G. M. Stone, A. M. Minor, *et al.*, "Effect of Ion Distribution on Conductivity of Block Copolymer Electrolytes," *Nano Letters,* vol. 9, pp. 1212-1216, 2009.

[60] P. Raghavan, X. Zhao, J.-K. Kim, J. Manuel, G. S. Chauhan, J.-H. Ahn, *et al.*, "Ionic conductivity and electrochemical properties of nanocomposite polymer electrolytes based on electrospun poly(vinylidene fluoride-co-hexafluoropropylene) with nano-sized ceramic fillers," *Electrochimica Acta,* vol. 54, pp. 228-234, 2008.

[61] Z. Ren, Y. Liu, K. Sun, X. Zhou, and N. Zhang, "A microporous gel electrolyte based on poly(vinylidene fluoride-co-hexafluoropropylene)/fully cyanoethylated cellulose derivative blend for lithium-ion battery," *Electrochimica Acta,* vol. 54, pp. 1888-1892, 2009.

[62] Z.-Y. Cui, Y.-Y. Xu, L.-P. Zhu, J.-Y. Wang, and B.-K. Zhu, "Investigation on PVDF-HFP microporous membranes prepared by TIPS process and their application as polymer electrolytes for lithium ion batteries," *Ionics,* vol. 15, pp. 469-476, 2009.

[63] P. G. Bruce, "Energy storage beyond the horizon: Rechargeable lithium batteries," *Solid State Ionics,* vol. 179, pp. 752-760, 2008.

[64] C. Shen, J. Wang, Z. Tang, H. Wang, H. Lian, J. Zhang, *et al.*, "Physicochemical properties of poly(ethylene oxide)-based composite polymer electrolytes with a silane-modified mesoporous silica SBA-15," *Electrochimica Acta,* vol. 54, pp. 3490-3494, 2009.

[65] P. Raghavan, J.-W. Choi, J.-H. Ahn, G. Cheruvally, G. S. Chauhan, H.-J. Ahn, *et al.*, "Novel electrospun poly(vinylidene fluoride-co-hexafluoropropylene)–in situ SiO2 composite membrane-based polymer electrolyte for lithium batteries," *Journal of Power Sources,* vol. 184, pp. 437-443, 2008.

[66] S. Panero, B. Scrosati, H. H. Sumathipala, and W. Wieczorek, "Dual-composite polymer electrolytes with enhanced transport properties," *Journal of Power Sources,* vol. 167, pp. 510-514, 2007.

[67] F. Croce, L. Settimi, and B. Scrosati, "Superacid ZrO2-added, composite polymer electrolytes with improved transport properties," *Electrochemistry Communications,* vol. 8, pp. 364-368, 2006.

[68] H.-M. Kao and C.-L. Chen, "An Organic–Inorganic Hybrid Electrolyte Derived from Self-Assembly of a Poly(Ethylene Oxide)–Poly(Propylene Oxide)–Poly(Ethylene Oxide) Triblock Copolymer," *Angewandte Chemie International Edition,* vol. 43, pp. 980-984, 2004.

[69] P. Agarwal, H. Qi, and L. A. Archer, "The Ages in a Self-Suspended Nanoparticle Liquid," *Nano Letters,* vol. 10, pp. 111-115, 2009.

[70] P. Agarwal, M. Chopra, and L. A. Archer, "Nanoparticle Netpoints for Shape-Memory Polymers," *Angewandte Chemie International Edition,* vol. 50, pp. 8670-8673, 2011.

[71] K.-S. Liao, T. E. Sutto, E. Andreoli, P. Ajayan, K. A. McGrady, and S. A. Curran, "Nano-sponge ionic liquid–polymer composite electrolytes for solid-state lithium power sources," *Journal of Power Sources,* vol. 195, pp. 867-871, 2010.

[72] Y. Ding, W. Di, Y. Jiang, F. Xu, Z. Long, F. Ren, *et al.*, "The morphological evolution, mechanical properties and ionic conductivities of electrospinning P(VDF-HFP) membranes at various temperatures," *Ionics,* vol. 15, pp. 731-734, 2009.

[73] A. Lewandowski and A. Świderska-Mocek, "Ionic liquids as electrolytes for Li-ion batteries—An overview of electrochemical studies," *Journal of Power Sources,* vol. 194, pp. 601-609, 2009.

[74] J. Fuller, R. T. Carlin, and R. A. Osteryoung, "The Room Temperature Ionic Liquid 1-Ethyl-3-methylimidazolium Tetrafluoroborate: Electrochemical Couples and Physical Properties," *Journal of The Electrochemical Society,* vol. 144, pp. 3881-3886, 1997.

[75] B. Bae, B. H. Chun, and D. Kim, "Surface characterization of microporous polypropylene membranes modified by plasma treatment," *Polymer,* vol. 42, pp. 7879-7885, 2001.

[76] F. C. Laman, M. A. Gee, and J. Denovan, "Impedance Studies for Separators in Rechargeable Lithium Batteries," *Journal of The Electrochemical Society,* vol. 140, pp. L51-L53, 1993.

[77] G. Venugopal, J. Moore, J. Howard, and S. Pendalwar, "Characterization of microporous separators for lithium-ion batteries," *Journal of Power Sources,* vol. 77, pp. 34-41, 1999.

[78] P. Knauth, "Inorganic solid Li ion conductors: An overview," *Solid State Ionics,* vol. 180, pp. 911-916, 2009.

[79] K. Takada, N. Aotani, K. Iwamoto, and S. Kondo, "Solid state lithium battery with oxysulfide glass," *Solid State Ionics,* vol. 86–88, Part 2, pp. 877-882, 1996.

[80] M. Tatsumisago, "Glassy materials based on Li2S for all-solid-state lithium secondary batteries," *Solid State Ionics,* vol. 175, pp. 13-18, 2004.

[81] K. Takada, S. Nakano, T. Inada, A. Kajiyama, H. Sasaki, S. Kondo, *et al.*, "Compatibility of Lithium Ion Conductive Sulfide Glass with Carbon-Lithium Electrode," *Journal of The Electrochemical Society,* vol. 150, pp. A274-A277, 2003.

[82] F. Mizuno, A. Hayashi, K. Tadanaga, and M. Tatsumisago, "New, Highly Ion-Conductive Crystals Precipitated from Li2S–P2S5 Glasses," *Advanced Materials,* vol. 17, pp. 918-921, 2005.

[83] R. Kanno and M. Murayama "Lithium Ionic Conductor Thio-LISICON: The Li2 S - GeS2 - P 2 S 5 System," *Journal of The Electrochemical Society,* vol. 148, pp. A742-A746, 2001.

[84] J. Saienga, Y. Kim, B. Campbell, and S. W. Martin, "Preparation and characterization of glasses in the LiI+Li2S+GeS2+Ga2S3 system," *Solid State Ionics,* vol. 176, pp. 1229-1236, 2005.

[85] H. Aono, N. Imanaka, and G.-y. Adachi, "High Li+ Conducting Ceramics," *Accounts of Chemical Research,* vol. 27, pp. 265-270, 1994.

[86] G.-y. Adachi, N. Imanaka, and H. Aono, "Fast Li⊕ Conducting Ceramic Electrolytes," *Advanced Materials,* vol. 8, pp. 127-135, 1996.

[87] R. Murugan, V. Thangadurai, and W. Weppner, "Fast Lithium Ion Conduction in Garnet-Type Li7La3Zr2O12," *Angewandte Chemie International Edition,* vol. 46, pp. 7778-7781, 2007.

[88] H. Takahara, T. Takeuchi, M. Tabuchi, H. Kageyama, Y. Kobayashi, Y. Kurisu, *et al.*, "All-Solid-State Lithium Secondary Battery Using Oxysulfide Glass: Addition and Coating of Carbon to Positive Electrode," *Journal of The Electrochemical Society,* vol. 151, pp. A1539-A1544, 2004.

[89] K. Takada, S. Nakano, T. Inada, A. Kajiyama, M. Kouguchi, H. Sasaki, *et al.*, "Solid-state lithium batteries with sulfide-based solid electrolytes," in *BVR Chowdari Solid State Ionics: The Science and Technology of Ions in Motion, Proceedings of the Asian Conference, 9th, Jeju Island, Republic of Korea, June 6-11, 2004, Publisher: World Scientific Publishing Co. Pte. Ltd., Singapore,* pp. 425-436, 2004.

[90] F. Mizuno, A. Hayashi, K. Tadanaga, and M. Tatsumisago, "Design of composite positive electrode in all-solid-state secondary batteries with Li2S-P2S5 glass-ceramic electrolytes," *Journal of Power Sources,* vol. 146, pp. 711-714, 2005.

[91] Y. Seino, K. Takada, B.-C. Kim, L. Zhang, N. Ohta, H. Wada, *et al.*, "Synthesis of phosphorous sulfide solid electrolyte and all-solid-state lithium batteries with graphite electrode," *Solid State Ionics,* vol. 176, pp. 2389-2393, 2005.

[92] T. Kobayashi, Y. Imade, D. Shishihara, K. Homma, M. Nagao, R. Watanabe, *et al.*, "All solid-state battery with sulfur electrode and thio-LISICON electrolyte," *Journal of Power Sources,* vol. 182, pp. 621-625, 2008.

[93] J. E. Trevey, Y. S. Jung, and S.-H. Lee, "Preparation of Li2S–GeSe2–P2S5 electrolytes by a single step ball milling for all-solid-state lithium secondary batteries," *Journal of Power Sources,* vol. 195, pp. 4984-4989, 2010.

[94] T. Kobayashi, A. Yamada, and R. Kanno, "Interfacial reactions at electrode/electrolyte boundary in all solid-state lithium battery using inorganic solid electrolyte, thio-LISICON," *Electrochimica Acta,* vol. 53, pp. 5045-5050, 2008.

[95] N. Ohta, K. Takada, L. Zhang, R. Ma, M. Osada, and T. Sasaki, "Enhancement of the High-Rate Capability of Solid-State Lithium Batteries by Nanoscale Interfacial Modification," *Advanced Materials,* vol. 18, pp. 2226-2229, 2006.

[96] A. Sakuda, H. Kitaura, A. Hayashi, K. Tadanaga, and M. Tatsumisago, "Modification of Interface Between LiCoO2 Electrode and Li2S – P2S5 Solid Electrolyte Using Li2O – SiO2 Glassy Layers," *Journal of The Electrochemical Society,* vol. 156, pp. A27-A32, 2009.

[97] K. Takada, N. Ohta, L. Zhang, K. Fukuda, I. Sakaguchi, R. Ma, *et al.*, "Interfacial modification for high-power solid-state lithium batteries," *Solid State Ionics,* vol. 179, pp. 1333-1337, 2008.

[98] H. Kitaura, A. Hayashi, K. Tadanaga, and M. Tatsumisago, "Improvement of electrochemical performance of all-solid-state lithium secondary batteries by surface modification of LiMn2O4 positive electrode," *Solid State Ionics,* vol. 192, pp. 304-307, 2011.

[99] J. Kim, S. Lee, and D. Shin, "Preparation of a hybrid solid glass electrolyte using a nano-porous sodium borosilicate glass membrane for lithium batteries," *Journal of Ceramic Processing Research,* vol. 8, p. 208, 2007.

[100] H. Aono, E. Sugimoto, Y. Sadaoka, N. Imanaka, and G. y. Adachi, "Ionic Conductivity of Solid Electrolytes Based on Lithium Titanium Phosphate," *Journal of The Electrochemical Society,* vol. 137, pp. 1023-1027, 1990.

[101] J. M. Tarascon and D. Guyomard, "Li Metal-Free Rechargeable Batteries Based on $Li1+x\ Mn2\ O\ 4$ Cathodes $(0 \le x \le 1)$ and Carbon Anodes," *Journal of The Electrochemical Society,* vol. 138, pp. 2864-2868, 1991.

[102] H. Aono, E. Sugimoto, Y. Sadaoka, N. Imanaka, and G. y. Adachi, "The Electrical Properties of Ceramic Electrolytes for $LiM\ x\ Ti2-x\ (\ PO\ 4\ )\ 3+yLi2\ O\ ,\ M=Ge\ ,\ Sn\ ,\ Hf\ ,\ and\ Zr$ Systems," *Journal of The Electrochemical Society,* vol. 140, pp. 1827-1833, 1993.

[103] J. Fu, "Fast Li+ ion conducting glass-ceramics in the system Li2O–Al2O3–GeO2–P2O5," *Solid State Ionics,* vol. 104, pp. 191-194, 1997.

[104] X. Xu, Z. Wen, Z. Gu, X. Xu, and Z. Lin, "Lithium ion conductive glass ceramics in the system Li1.4Al0.4(Ge1−xTix)1.6(PO4)3 (x=0–1.0)," *Solid State Ionics,* vol. 171, pp. 207-213, 2004.

[105] J. C. Hunter, "Preparation of a new crystal form of manganese dioxide: λ-MnO2," *Journal of Solid State Chemistry,* vol. 39, pp. 142-147, 1981.

[106] A. Mosbah, A. Verbaere, and M. Tournoux, "Phases LixMnO2λ rattachees au type spinelle," *Materials Research Bulletin,* vol. 18, pp. 1375-1381, 1983.

[107] R. J. Gummow, A. de Kock, and M. M. Thackeray, "Improved capacity retention in rechargeable 4 V lithium/lithium-manganese oxide (spinel) cells," *Solid State Ionics,* vol. 69, pp. 59-67, 1994.

[108] A. Blyr, C. Sigala, G. Amatucci, D. Guyomard, Y. Chabre, and J. M. Tarascon, "Self-Discharge of LiMn2 O 4/C Li-Ion Cells in Their Discharged State: Understanding by Means of Three-Electrode Measurements," *Journal of The Electrochemical Society,* vol. 145, pp. 194-209, 1998.

[109] D. H. Jang, Y. J. Shin, and S. M. Oh, "Dissolution of Spinel Oxides and Capacity Losses in 4 V Li / Li x Mn2 O 4 Cells," *Journal of The Electrochemical Society,* vol. 143, pp. 2204-2211, 1996.

[110] T. Inoue and M. Sano, "An Investigation of Capacity Fading of Manganese Spinels Stored at Elevated Temperature," *Journal of The Electrochemical Society,* vol. 145, pp. 3704-3707, 1998.

[111] G. Pistoia, A. Antonini, R. Rosati, and D. Zane, "Storage characteristics of cathodes for Li-ion batteries," *Electrochimica Acta,* vol. 41, pp. 2683-2689, 1996.

[112] N. Kamaya, K. Homma, Y. Yamakawa, M. Hirayama, R. Kanno, M. Yonemura, *et al.*, "A lithium superionic conductor," *Nat Mater,* vol. 10, pp. 682-6, 2011.

[113] J.-H. Kim, N. P. W. Pieczonka, Z. Li, Y. Wu, S. Harris, and B. R. Powell, "Understanding the capacity fading mechanism in LiNi0.5Mn1.5O4/graphite Li-ion batteries," *Electrochimica Acta,* vol. 90, pp. 556-562, 2013.

[114] A. Du Pasquier, A. Blyr, P. Courjal, D. Larcher, G. Amatucci, B. Gérand, *et al.*, "Mechanism for Limited 55°C Storage Performance of Li1.05Mn1.95 O 4 Electrodes," *Journal of The Electrochemical Society,* vol. 146, pp. 428-436, 1999.

[115] H. Tsunekawa, S. Tanimoto, R. Marubayashi, M. Fujita, K. Kifune, and M. Sano, "Capacity fading of graphite electrodes due to the deposition of manganese ions on them in Li-ion batteries," *Journal of The Electrochemical Society,* vol. 149, pp. A1326-A1331, 2002.

[116] S. Komaba, N. Kumagai, and Y. Kataoka, "Influence of manganese (II), cobalt (II), and nickel (II) additives in electrolyte on performance of graphite anode for lithium-ion batteries," *Electrochimica Acta,* vol. 47, pp. 1229-1239, 2002.

[117] J. Shim and K. A. Striebel, "Cycling performance of low-cost lithium ion batteries with natural graphite and LiFePO4," *Journal of Power Sources,* vol. 119–121, pp. 955-958, 2003.

[118] A. Yamada, S.-C. Chung, and K. Hinokuma, "Optimized LiFePO4 for lithium battery cathodes," *Journal of the Electrochemical Society,* vol. 148, pp. A224-A229, 2001.

[119] Y. Talyosef, B. Markovsky, G. Salitra, D. Aurbach, H. J. Kim, and S. Choi, "The study of LiNi0.5Mn1.5O4 5-V cathodes for Li-ion batteries," *Journal of Power Sources,* vol. 146, pp. 664-669, 2005.

[120] X. Fang, N. Ding, X. Y. Feng, Y. Lu, and C. H. Chen, "Study of LiNi0.5Mn1.5O4 synthesized via a chloride-ammonia co-precipitation method: Electrochemical performance, diffusion coefficient and capacity loss mechanism," *Electrochimica Acta,* vol. 54, pp. 7471-7475, 2009.

[121] R. N. Methekar, P. W. C. Northrop, K. Chen, R. D. Braatz, and V. R. Subramanian, "Kinetic Monte Carlo simulation of surface heterogeneity in graphite anodes for lithium-ion batteries: Passive layer formation," *Journal of the Electrochemical Society,* vol. 158, pp. A363-A370, 2011.

[122] K. Amine, J. Liu, S. Kang, I. Belharouak, Y. Hyung, D. Vissers, *et al.*, "Improved lithium manganese oxide spinel/graphite Li-ion cells for high-power applications," *Journal of Power Sources,* vol. 129, pp. 14-19, 2004.

[123] P. B. Balbuena and Y. Wang, *Lithium-ion batteries*. World Scientific, 2004.

[124] T. Robinson, "Metabolism and function of alkaloids in plants," *Science,* vol. 184, pp. 430-435, 1974.

[125] H. Ibrahim, A. Ilinca, and J. Perron, "Energy storage systems-Characteristics and comparisons," *Renewable and Sustainable Energy Reviews,* vol. 12, pp. 1221-1250, 2008.

[126] H. Chen, T. N. Cong, W. Yang, C. Tan, Y. Li, and Y. Ding, "Progress in electrical energy storage system: A critical review," *Progress in Natural Science,* vol. 19, pp. 291-312, 2009.

[127] C. S. P.E., "Altairnano Charging the Energy Revolution," in *IBM Almaden Conference "Lithium Ion Battery - Truth in Advertising",* 2009.

[128] R. Okuyama and E. Nomura, "Relationship between the total energy efficiency of a sodium–sulfur battery system and the heat dissipation of the battery case," *Journal of Power Sources,* vol. 77, pp. 164-169, 1999.

[129] L. Li, S. Kim, W. Wang, M. Vijayakumar, Z. Nie, B. Chen, *et al.*, "Large-Scale Energy Storage: A Stable Vanadium Redox-Flow Battery with High Energy Density for Large-Scale Energy Storage," *Advanced Energy Materials,* vol. 1, pp. 306-306, 2011.

[130] R. Crowe, "Energy Storage Industry Grows to Integrate Wind, Solar," in *Renewable Energy News Article,* ed, 2011.

[131] I. Kowalczk, J. Read, and M. Salomon, "Li-air batteries: A classic example of limitations owing to solubilities," *Pure Appl. Chem,* vol. 79, pp. 851-860, 2007.

[132] S. J. Visco, Y. S. Nimon, L. C. De Jonghe, B. D. Katz, and A. Petrov, "Compliant seal structures for protected active metal anodes," ed: Google Patents, 2010.

[133] H. Li, Y. Wang, H. Na, H. Liu, and H. Zhou, "Rechargeable Ni-Li Battery Integrated Aqueous/Nonaqueous System," *Journal of the American Chemical Society,* vol. 131, pp. 15098-15099, 2009.

[134] Y. Wang and H. Zhou, "A new type rechargeable lithium battery based on a Cu-cathode," *Electrochemistry Communications,* vol. 11, pp. 1834-1837, 2009.

[135] Y. Wang, H. Li, P. He, and H. Zhou, "Controllable Hydrogen Generation from Water," *ChemSusChem,* vol. 3, pp. 571-574, 2010.

[136] Y. Lu, J. B. Goodenough, and Y. Kim, "Aqueous cathode for next-generation alkali-ion batteries," *J Am Chem Soc,* vol. 133, pp. 5756-9, 2011.

[137] Y. Wang, Y. Wang, and H. Zhou, "A Li-liquid cathode battery based on a hybrid electrolyte," *ChemSusChem,* vol. 4, pp. 1087-90, 2011.

[138] Y. Lu and J. B. Goodenough, "Rechargeable alkali-ion cathode-flow battery," *Journal of Materials Chemistry,* vol. 21, pp. 10113-10117, 2011.

[139] T. Zhang, N. Imanishi, Y. Shimonishi, A. Hirano, J. Xie, Y. Takeda, *et al.*, "Stability of a Water-Stable Lithium Metal Anode for a Lithium–Air Battery with Acetic Acid–Water Solutions," *Journal of The Electrochemical Society,* vol. 157, pp. A214-A218, 2010.

[140] L. Li, X. Zhao, and A. Manthiram, "A dual-electrolyte rechargeable Li-air battery with phosphate buffer catholyte," *Electrochemistry Communications,* vol. 14, pp. 78-81, 2012.

[141] T. Zhang, N. Imanishi, Y. Takeda, and O. Yamamoto, "Aqueous Lithium/Air Rechargeable Batteries," *Chemistry Letters,* vol. 40, pp. 668-673, 2011.

[142] X.-H. Liu, T. Saito, T. Doi, S. Okada, and J.-i. Yamaki, "Electrochemical properties of rechargeable aqueous lithium ion batteries with an olivine-type cathode and a Nasicon-type anode," *Journal of Power Sources,* vol. 189, pp. 706-710, 2009.

[143] K. Kanamura, S. Shiraishi, H. Takezawa, and Z.-i. Takehara, "XPS Analysis of the Surface of a Carbon Electrode Intercalated by Lithium Ions," *Chemistry of Materials,* vol. 9, pp. 1797-1804, 1997.

[144] K. Izutsu, *Electrochemistry in nonaqueous solutions.* Wiley-VCH, 2010.

[145] U. Heider, R. Oesten, and M. Jungnitz, "Challenge in manufacturing electrolyte solutions for lithium and lithium ion batteries quality control and minimizing contamination level," *Journal of Power Sources,* vol. 81–82, pp. 119-122, 1999.

[146] D. Aurbach, A. Zaban, Y. Ein-Eli, I. Weissman, O. Chusid, B. Markovsky, *et al.*, "Recent studies on the correlation between surface chemistry, morphology, three-dimensional structures and performance of Li and Li-C intercalation anodes in several important electrolyte systems," *Journal of Power Sources,* vol. 68, pp. 91-98, 1997.

[147] T. Kawamura, S. Okada, and J.-i. Yamaki, "Decomposition reaction of LiPF6-based electrolytes for lithium ion cells," *Journal of Power Sources,* vol. 156, pp. 547-554, 2006.

[148] M. Urquidi-Macdonald, J. Flores, D. D. Macdonald, O. Pensado-Rodriguez, and D. Vanvoorhis, "Lithium/water system: primary batteries," *Electrochimica Acta,* vol. 43, pp. 3069-3077, 1998.

[149] T. Zhang, N. Imanishi, S. Hasegawa, A. Hirano, J. Xie, Y. Takeda, *et al.*, "Li/Polymer Electrolyte/Water Stable Lithium-Conducting Glass Ceramics Composite for Lithium–Air Secondary Batteries with an Aqueous Electrolyte," *Journal of The Electrochemical Society,* vol. 155, pp. A965-A969, 2008.

[150] M. Weissmann, S. Baranton, J.-M. Clacens, and C. Coutanceau, "Modification of hydrophobic/hydrophilic properties of Vulcan XC72 carbon powder by grafting of trifluoromethylphenyl and phenylsulfonic acid groups," *Carbon,* vol. 48, pp. 2755-2764, 2010.